nanomaterials

MDPI

Review

A Review on Carbon Dots: Synthesis, Characterization and Its Application in Optical Sensor for Environmental Monitoring

Nur Alia Sheh Omar [1,2], Yap Wing Fen [1,2,*], Ramli Irmawati [1], Hazwani Suhaila Hashim [1], Nur Syahira Md Ramdzan [1] and Nurul Illya Muhamad Fauzi [2]

[1] Faculty of Science, Universiti Putra Malaysia (UPM), Serdang 43400, Selangor, Malaysia; nuralia.upm@gmail.com (N.A.S.O.); irmawati@upm.edu.my (R.I.); hazwanisuhaila@gmail.com (H.S.H.); nursyahira.upm@gmail.com (N.S.M.R.)

[2] Institute of Nanoscience and Nanotechnology, Universiti Putra Malaysia (UPM), Serdang 43400, Selangor, Malaysia; illyafauzi97@gmail.com

* Correspondence: yapwingfen@upm.edu.my

Abstract: The development of carbon dots (CDs), either using green or chemical precursors, has inevitably led to their wide range application, from bioimaging to optoelectronic devices. The reported precursors and properties of these CDs have opened new opportunities for the future development of high-quality CDs and applications. Green precursors were classified into fruits, vegetables, flowers, leaves, seeds, stem, crop residues, fungi/bacteria species, and waste products, while the chemical precursors were classified into acid reagents and non-acid reagents. This paper quickly reviews ten years of the synthesis of CDs using green and chemical precursors. The application of CDs as sensing materials in optical sensor techniques for environmental monitoring, including the detection of heavy metal ions, phenol, pesticides, and nitroaromatic explosives, was also discussed in this review. This profound review will offer knowledge for the upcoming community of researchers interested in synthesizing high-quality CDs for various applications.

Keywords: carbon dots; green synthesis; chemical synthesis; optical sensor; environmental pollution

Citation: Omar, N.A.S.; Fen, Y.W.; Irmawati, R.; Hashim, H.S.; Ramdzan, N.S.M.; Fauzi, N.I.M. A Review on Carbon Dots: Synthesis, Characterization and Its Application in Optical Sensor for Environmental Monitoring. *Nanomaterials* **2022**, *12*, 2365. https://doi.org/10.3390/nano12142365

Academic Editor: Hideya Kawasaki

Received: 9 May 2022
Accepted: 15 June 2022
Published: 11 July 2022

1. Introduction

Fluorescent carbon dots (CDs), also known as carbon quantum dots (CQDs) or carbon nanodots (CNs), have drawn a great deal of attention in recent years, owing to their high photostability, excellent water solubility, tuneable fluorescence and optical properties, low toxicity, good biocompatibility, and environmental friendliness [1]. To date, a variety of precursors have been utilized to prepare CDs through "bottom-up" or "top-down" approaches [2]. Among these approaches, hydrothermal/carbonization treatment is frequently applied for the preparation CDs because of the outstanding advantages, such as high yield, simple manipulation, easy control, uniform products, lower air pollution, low energy consumption and so on [3]. Despite these advantages, CDs cannot be produced without the presence of starting materials, also known as precursors. In this regard, the development of green and chemical synthesis methods for producing high fluorescent CDs has gathered the focus of researchers. The green synthesis methods by means of green precursors of synthesis involves the usage of inexpensive or recycled materials, while the chemical synthesis methods involve toxic chemical reagents or organic solvents as precursors. CDs synthesized using these methods usually contain a certain amount of oxygen, hydrogen, and nitrogen. With all these options to prepare CDs under certain experimental conditions, it is no surprise that differential fluorescence properties of CDs were easily acquired. In addition, surface passivation (generally involves functional groups such as amine groups and hydroxyl groups) and the heteroatom doping (n-type doping: nitrogen, phosphorus, sulfur, and chlorine or p-type doping: boron) approach is another factor that paves the way to efficiently improve the fluorescent properties, quantum yield,

and other physicochemical properties of CDs [4]. Such intriguing properties have triggered new capabilities in the field of sensing and bioimaging.

To date, many review articles on the preparation of CDs, heteroatom doped CDs, and their applications have been published [5–8]. However, there is no comprehensive review exploring various green and chemical precursors as the carbon source in CDs and their application in environmental monitoring. The purpose of this review is, therefore, to update and organize the green and chemical precursors used in CD preparation. The final section will give a concise overview of their application in the optical sensing of heavy metal ions, phenol, pesticides, and nitroaromatic explosives.

2. CDs Synthesized from Green Precursors

Carbon dots (CDs) can be synthesized using two precursors, either from green or chemical sources. As of now, researchers focus more on simple, low-cost, and greenway synthesis for the large-scale production of high-quality CDs. Numerous green sources, such as fruits, vegetables, flowers, leaves, seeds, stems, crop residues, fungi/bacteria species and waste products, have been used as a carbon source for the preparation of CDs. In this section, all green sources used for the synthesis of CDs are briefly arranged and compared.

2.1. Fruits

Orange juice and watermelon peels were among the very first precursors used as a carbon source to synthesize CDs. The studies reveal the as-prepared CDs have different fluorescence properties, due to the presence of different chemical groups in the raw materials and synthesis method. The synthesized CDs from orange juice showed the quantum yield of 26% at an emission of 441 nm, whereas a 7.1% quantum yield was demonstrated by watermelon peel-derived CDs at an emission of 490–580 nm [9,10]. In 2014, Du et al. reported renewable wastes of sugar cane bagasse as a new precursor for fluorescent CDs [11]. It, thus, demonstrated that such bagasse-derived CDs could function as highly effective fluorescent sensing probes for labeling and imaging in biomedical applications.

Lemon peels, prunus avium extract, cornstalk, corn bract, dried lemon peels, pulp-free lemon juice, citrus lemon peels, citrus sinensis peels, etc. are another precursor that have been used in the development of CDs, as shown in Table 1 [12–41]. Among these precursors, acidic fruits, such as lemon peels, lemon juice, and citrus sinensis, were frequently chosen. This is because the juice extract is rich in sucrose, glucose, fructose, citric acid, and ascorbic acid, while the peels are mainly composed of proteins, fibers, and less of oils and antioxidants. Consequently, CDs from juice extract exhibit higher fluorescence properties than peels, due to the high acid and sugar contents that provide a considerable amount of carbon and hydrogen elements. A comparison study of the different precursors used in hydrothermal synthesis was then carried out to understand the role of citric acid [30]. It was found that lemon juice has higher photoluminescence (PL) emission than ripe lemon juice and orange juice. This result is because lemon juices have higher concentrations of citric acid than orange juices. Moreover, the decrease in PL emission of ripe lemon juice was due to a significant decrease in the grade of constituents and destroyed their surface structure.

Instead of just relying on carbon sources to produce high quantum yields of CDs, it has been found that by passivating CDs with amine-containing molecules, such as ethylenediamine, one can increase the quantum yield and selectively sensing analytes. Figure 1 shows the hydrothermal reaction of CDs from citrus lemon juice in the presence of ethylenediamine to produce nitrogen-doped CDs. The results showed that the prepared nitrogen-doped CDs had the quantum yield of 31% under bright blue emission [28]. However, there are limits to these blue emissive CDs, especially in the field of bioimaging because of strong tissue autofluorescence at low wavelength emissions. Herein, Ding et al. (2017) have heated an ethanol solution of pulp-free lemon juice to produce very high red-luminescent CDs, which hold the promise for in vitro and in vivo bio-imaging [17].

Table 1. Summary of the synthesis CDs from fruits.

Precursor		Technique	Properties			Year	Reference
Carbon Source	Passivation/Solvent		Particle Size	Fluorescence	Quantum Yield		
Orange juice	-	Hydrothermal	TEM- 2.5 nm	λ_{em}- 441 nm λ_{ex}- 360 nm	26%	2012	[9]
Watermelon peels	-	Carbonization	TEM- 2.0 nm	λ_{em}- 490–580 nm	7.1%	2012	[10]
Sugar cane bagasse	Sodium hydroxide solution	Hydrothermal carbonization	HRTEM- 1.8 nm	λ_{em}- 475 nm λ_{ex}- 370 nm	12.3%	2014	[11]
Lemon peels	Sulfuric acid	Hydrothermal carbonization	TEM- 1 to 3 nm	λ_{em}- 441 nm λ_{ex}- 360 nm	14%	2016	[12]
Prunus avium extract	Ammonia	Hydrothermal carbonization	HRTEM- 7 nm	λ_{em}- 411 nm λ_{ex}- 310 nm	13%	2016	[13]
Cornstalk	Distilled water	Hydrothermal	TEM- 5.2 nm	λ_{em}- 500 nm λ_{ex}- 420 nm	7.6%	2017	[14]
Corn bract	Anhydrous ethanol	Solvothermal	TEM- 1.8–3.4 nm	λ_{em}- 470 nm and 678 nm λ_{ex}- 406 nm	6.9%	2017	[15]
Dried lemon peel	Deionized water	Hydrothermal	TEM- 9.5 nm	λ_{em}- 505 nm λ_{ex}- 425 nm	11%	2017	[16]
Pulp-free lemon juice	Ethanol	Solvothermal	AFM- 1.5 nm TEM- 4.6 nm	λ_{em}- 631 nm λ_{ex}- 540 nm	28%	2017	[17]
Citrus lemon peels	-	Carbonization	TEM- 4.5 nm	λ_{em}- 435 nm λ_{ex}- 330 nm	16.8%	2017	[18]
Citrus sinensis peels			TEM- 6.5 nm	λ_{em}- 455 nm λ_{ex}- 365 nm	15.5%		
Lemon juice	-	Thermal decomposition	-	λ_{em}- 400 nm λ_{ex}- 320 nm	7%	2018	[19]
Lemon juice	Poly(ethylenimine)	Carbonization	TEM- 5.7 nm	λ_{em}- 540 nm λ_{ex}- 420 nm	-	2018	[20]
Citrus lemon juice	-	Hydrothermal	TEM- 5.8 nm	λ_{em}- 450 nm λ_{ex}- 360 nm	10.20%	2018	[21]
Watermelon juice	Ethanol	Hydrothermal	TEM- 3–7 nm	λ_{em}- 439 nm λ_{ex}- 355 nm	10.6%	2018	[22]
Jackfruit juice	Ethanol and distilled water	Hydrothermal	HRTEM- <2.5 nm	λ_{em}- 485 nm λ_{ex}- 395 nm	14.6%	2018	[23]
Lemon Grapefruit	Ethylenediamine	Hydrothermal	TEM- 20 nm	-	20%	2018	[24]
Durian juice	Water and ethanol	Carbonization	-	-	-	2018	[25]
Acerola fruit	Water	Hydrothermal	-	λ_{em}- 504 nm λ_{ex}- 360 nm	-	2019	[26]
Bitter orange juice	-	Hydrothermal	AFM- 2–4 nm DLS- 1–2 nm	λ_{em}- 390 nm λ_{ex}- 325 nm	19.9%	2019	[27]
Citrus lemon juice	Ethylenediamine	Hydrothermal	HRTEM- 3 nm	λ_{em}- 452 nm λ_{ex}- 360 nm	31%	2019	[28]
Lemon and onion juices	Ammonium hydroxide solution	Microwave assisted carbonization	TEM- 6.15 nm	λ_{em}- 425 nm λ_{ex}- 340 nm	23.6%	2019	[29]
Lemon juice	-	Hydrothermal	HRTEM- 3–15 nm	λ_{em}- 524 nm λ_{ex}- 420 nm	21.37%	2019	[30]
Durian shell	Tris base and deionized water	Hydrothermal carbonization	TEM- 6.5 nm	λ_{em}- 414 nm λ_{ex}- 340 nm	12.93%	2019	[31]
Lemon	Hydroxylamine	Hydrothermal	HRTEM- 2 nm	λ_{em}- 430–470 nm λ_{ex}- 360 nm	5%	2020	[32]
Pomegranate	Sodium hydroxide and polyethylene glycol	Microwave	HRTEM- 1 to 5 nm	λ_{em}- 532 nm	-	2020	[33]
Watermelon peels				λ_{em}- 515 nm			
Rosa roxburghii fruits	Water	Hydrothermal	TEM- 2.5 nm	λ_{em}- 450 nm λ_{ex}- 360 nm	24.8%	2020	[34]
Citrus fruit peels	Deionized water	Sand bath	TEM- 4.6 nm	λ_{em}- 510 nm λ_{ex}- 420 nm	-	2021	[35]
Banana peel	Deionized water	Hydrothermal	TEM- 5 nm	λ_{ex}- 355 nm	20%	2021	[36]
Elaeagnus angustifolia	Ultrapure water	Hydrothermal	TEM- <10 nm	λ_{em}- 410 nm λ_{ex}- 330 nm	16.8%	2021	[37]

Table 1. *Cont.*

Precursor		Technique	Properties			Year	Reference
Carbon Source	Passivation/Solvent		Particle Size	Fluorescence	Quantum Yield		
Kiwi (Actinidia deliciosa) fruit peels	-	Hydrothermal carbonization	TEM- 5.6 nm	λ_{em}- 432 nm λ_{ex}- 360 nm	14%	2021	[1]
	Ammonium hydroxide		TEM- 5.1 nm		19%		
Canon ball fruit	Distilled water	Hydrothermal	TEM- <15 nm	λ_{em}- ~500 nm λ_{ex}- 380 nm	7.24%	2022	[38]
Indian *Bael patra*- hard shell-pulp-pulp and gum	-	Hydrothermal carbonization	TEM- 3 nm TEM- 6 nm TEM- 8 nm		59.39% 59.07% 55.25%	2022	[39]
Morus nigra (black mulberry)	Deionized water	Hydrothermal	TEM- 4.5 nm	λ_{em}- 427 nm λ_{ex}- 360 nm	24%	2022	[40]
Jatropha	Distilled water	Hydrothermal	TEM- 3.2 nm	λ_{em}- 462 nm λ_{ex}- 370 nm	13.7%	2022	[41]

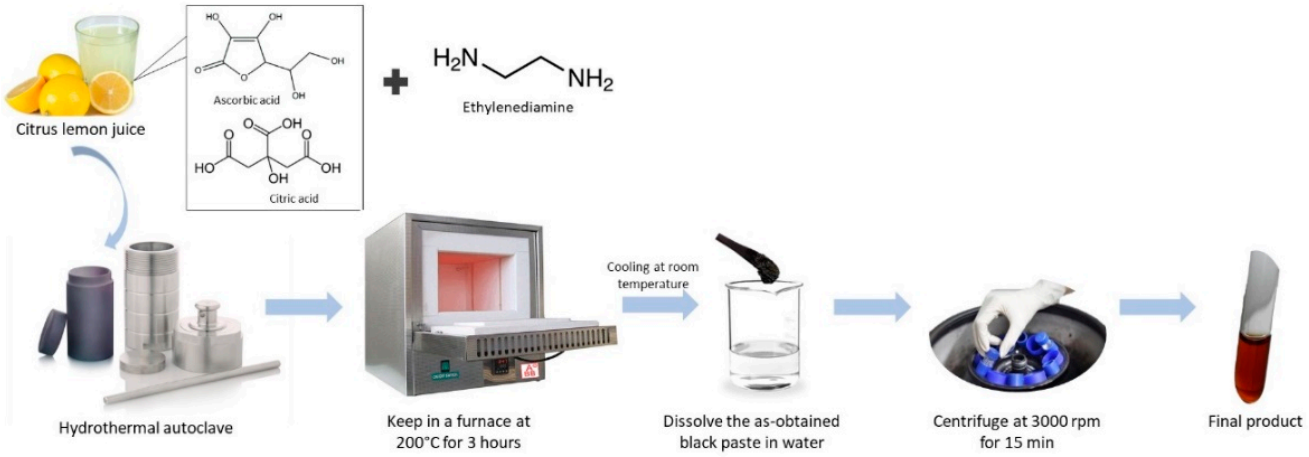

Figure 1. Schematic of hydrothermal reaction of CDs from citrus lemon juice and ethylenediamine.

At present, Bael patra fruit-derived CDs turned out to be an excellent carbon source without the need of chemical additives [39]. Typically, three different components of Bael patra fruit, i.e., hard shell, edible pulp, and a mixture of pulp and gum were reported for the successful synthesis of emissive CDs, and it was found that CDs derived from the hard shell had the highest quantum yield of 59.39%. This is because the synthesized CDs via the carbonization approach resulted in more production of carbon content and micropores over its surface. These micropores can provide a higher ratio of surface-active sites for the adsorption of toxins from wastewater samples, thus significantly improving the sensing performance.

2.2. Vegetables

The exploration of new carbon sources that possess abundant reserve, green, simple and high quality CDs has drawn tremendous attention in the area of kitchen waste, such as vegetables. Various green and non-green vegetables, such as celery leaves, sweet pepper, lemon grass, tomato, carrot, rose-heart radish, turmeric, cinnamon, red chili, black pepper, hongcaitai, cauliflower, kelp, tomato, crown daisy leaves, cabbage, cherry tomatoes, scallion leaves, and red beet, have been reported, as shown in Table 2 [42–58]. Both green and non-green vegetables have many properties and their own advantages. For instance, the family of green vegetables, such as celery leaves, lemon grass, hongcaitai, kelp, cabbage, crown daisy leaf, and scallion, often contain many organic compounds, such as organic acids, amides, amino acids, proteins, saccharides, carbohydrates, chlorophyll, etc., which can bring good physical and chemical properties to CDs. Meanwhile, non-green vegetables, such as tomato, red chili, turmeric, black pepper, cinnamon, and red beet, are plants rich in various bioactive compounds of lycopene, capsaicin, curcumin, piperine,

and cinnamaldehyde, respectively, which enable their application in the biomedical field. It was reported that bioactive compounds will partially remain inside or at the surface of the CDs after the hydrothermal process, leading to different photoluminescent and biomedical properties. Vasimalai et al. (2018) have demonstrated the uses of cinnamon, red chili, turmeric, and black pepper as CD precursors for biomedical applications [48]. They found that black pepper CDs have the highest quantum yield of 43.6% due to the various functional groups present in the sample, namely O–H, C–H, C–O–N, C=O, C–O, and C–N vibrational stretching peaks. All in all, the CDs prepared using celery leaves have contributed to the highest quantum yield of 53%. It was discovered that celery leaves contain abundant folic acid with affluent -COOH and the addition of L-glutathione as N, S-dopant has enriched their surface groups, which are beneficial for improving the quantum yield of CDs [42].

2.3. Flowers

Flowers such as *Selenicereus grandifloras*, water hyacinth, *Osmanthus fragrans*, rose flowers, and *Tagetes erecta* have also shown promise as carbon precursors, which were subsequently used to bind pesticides and metal ions. From Table 3, we can observe that there is an increase in quantum yield from 3.8% in 2019 to 63.7% in 2021. This significant improvement was attained by the presence of surface-active organic groups of C–N, –NH, and –OH, as shown in the FTIR analyses [59–63].

Table 2. Summary of the synthesis of CDs from vegetables.

Precursor		Technique	Properties			Year	Reference
Carbon Source	Passivation/Solvent		Particle Size	Fluorescence	Quantum Yield		
Celery leaves	Glutathione and double distilled water	Hydrothermal	TEM- 2.08 nm	λ_{em}- 415 nm λ_{ex}- 340 nm	53%	2013	[42]
Sweet pepper	Water	Carbonization	TEM- 4.6 nm	λ_{em}- 450 nm λ_{ex}- 360 nm	19.3%	2013	[43]
Lemon grass	Water	Hydrothermal	-	λ_{em}- 440 nm λ_{ex}- 320 nm	23.3%	2016	[44]
Tomato juice	-	Hydrothermal	HRTEM- 3 nm DLS- 3 nm	λ_{em}- 440 nm λ_{ex}- 367 nm	13.9%	2016	[45]
Carrot juice	-	Hydrothermal	TEM- 5.5 nm	λ_{em}- 442–565 nm λ_{ex}- 360–520 nm	5.16%	2017	[46]
Rose-heart radish	Ultrapure water	Hydrothermal	TEM- 3.6 nm	λ_{em}- 420 nm λ_{ex}- 330 nm	13.6%	2017	[47]
Turmeric	Ethylenediamine	Hydrothermal	TEM- 20 nm	-	20%	2018	[24]
Cinnamon	Ultrapure water	Hydrothermal	TEM- 3.4 nm	λ_{em}- 465 nm λ_{ex}- 370 nm	35.7%	2018	[48]
Red chili			TEM- 3.1 nm	λ_{em}- 477 nm λ_{ex}- 380 nm	26.8%		
Turmeric			TEM- 4.3 nm	λ_{em}- 460 nm λ_{ex}- 370 nm	38.3%		
Black pepper			TEM- 3.5 nm	λ_{em}- 489 nm λ_{ex}- 390 nm	43.6%		
Hongcaitai	Ultrapure water	Hydrothermal	TEM- 1.9 nm	λ_{em}- 410 nm λ_{ex}- 330 nm	21.0%	2018	[49]
Cauliflower	-	Hydrothermal	AFM- 4 nm DLS- 1.54 nm	λ_{em}- 380 nm λ_{ex}- 325 nm	43%	2019	[50]
Kelp	Ethylenediamine	Microwave irradiation	TEM- 3.7 nm	λ_{em}- 450 nm λ_{ex}- 370 nm	23.5%	2019	[51]
Tomato	Sulfuric acid	Chemical oxidation	HRTEM- 5–10 nm	λ_{em}- 450 λ_{ex}- 360 nm	12.70%	2019	[52]
	Phosphoric acid			λ_{em}- 520 λ_{ex}- 420 nm	4.21%		
	Phosphoric acid			λ_{em}- 560 nm λ_{ex}- 460 nm	2.76%		
Crown daisy leaf waste	Ultrapure water and urea	Hydrothermal	TEM- 5–10 nm	λ_{em}- 380 nm λ_{ex}- 300 nm	-	2019	[53]

Table 2. *Cont.*

Precursor		Technique	Properties			Year	Reference
Carbon Source	**Passivation/Solvent**		**Particle Size**	**Fluorescence**	**Quantum Yield**		
Cabbage	Anhydrous ethanol	Solvothermal	TEM- 3.4 nm	λ_{em}- 500 nm and 678 nm λ_{ex}- 410 nm	12.4%	2020	[54]
Cherry tomatoes	-	Hydrothermal	TEM- 7 nm	λ_{em}- 430 nm λ_{ex}- 340 nm	9.7%	2020	[55]
Tomato	Hydroxylamine	Hydrothermal	HRTEM- 3 nm	λ_{em}- 430–470 nm λ_{ex}- 360 nm	3.38%	2020	[32]
Scallion leaves	Water	Hydrothermal	TEM- 3.5 nm	λ_{em}- 418 nm λ_{ex}- 320 nm	3.2%	2020	[56]
Tomato	-	Hydrothermal	HRTEM- 9 nm	λ_{em}- 430 nm λ_{ex}- 344 nm	1.24%	2021	[57]
Red beet	Water	Hydrothermal	TEM- 4.66 nm	λ_{em}- 438 nm λ_{ex}- 350 nm	8.17%	2022	[58]

Table 3. Summary of the synthesis of CDs from flowers.

Precursor		Technique	Properties			Year	Reference
Carbon Source	**Passivation/Solvent**		**Particle Size**	**Fluorescence**	**Quantum Yield**		
Selenicereus grandiflorus	-	Boiling	HRTEM- 2.5 nm	λ_{em}- 440 and 365 nm	3.8%	2019	[59]
Water hyacinth	Phosphoric acid	Carbonization	SEM- $\leq$10 nm DLS- $\leq$10 nm TEM- 5.22 nm	λ_{em}- 370 nm λ_{ex}- 300 nm	17.02%	2019	[60]
Osmanthus fragrans	Ultrapure water	Hydrothermal	TEM- 2.23 nm	λ_{em}- 410 nm λ_{ex}- 340 nm	18.53%	2019	[61]
Rose flowers: Blue Red Yellow	Water	Hydrothermal	TEM- 37 nm TEM- 39 nm TEM- 33 nm	λ_{ex}- 335 nm λ_{ex}- 330 nm λ_{ex}- 340 nm	46% 44% 48%	2020	[62]
	Ethanol		TEM- 30 nm TEM- 27 nm TEM- 26 nm	λ_{ex}- 420 nm λ_{ex}- 410 nm λ_{ex}- 425 nm	43% 46% 47%		
Tagetes erecta	Deionized water	Solvo(hydro)-thermal carbonization	FESEM- 3.41 nm	λ_{em}- 495 nm λ_{ex}- 420 nm	63.7%	2021	[63]

In another study, Shekarbeygi et al. (2020) evaluated the effect of rose pigments (blue, red, and yellow) and the effect of their extraction methods (aqueous and alcohol) on optical properties of the synthesized CDs [62]. The results indicated that the quantum yields obtained for all the CDs were not affected by the rose pigments and extraction methods, as the yields were almost the same. However, such rose pigments and extraction methods affected the CDs' thermal stability and emission wavelengths. In the case of thermal stability, the fluorescence intensities were reduced in both aqueous and alcoholic CDs, with an increase in temperature ranging from 17 to 57 °C, yet aqueous CDs showed a higher decreasing rate than alcoholic CDs. As for the emission wavelengths, the alcohol extract had a larger wavelength than the aqueous extract, which may be due to the change in dielectric constant of solvent and the presence of more phenolic groups in the alcoholic extract. Thus, this work showed that CDs prepared with alcoholic extract with yellow petals has higher stability and a longer emission wavelength with better quantum yield than the others.

2.4. Leaves, Seeds, and Stems

In this section, we focused on the parts of plant-derived CDs, namely leaves (such as *Ocimum sanctum* leaves, bamboo leaves, gingko leaves, *Gynostemma* leaves, betel leaves, *Calotropis procera* leaves, *Elettaria cardamomum* leaves, Cornus walteri leaves, tea leaves, Kentucky bluegrass), seeds (such as *Acacia concinna* seeds, fennel seeds, *Pearl millet* seeds), and stem (lotus root), as presented in Table 4 [64–78]. Most of them have excellent healing properties, such as anti-inflammatory, antioxidant, antimicrobial, and antidote properties.

Due to those health benefits, the synthesized CDs could serve simultaneously in the fluorescent sensing of metal ions and as contrast agents for live cells [64–66]. Nonetheless, more efforts are still needed to explore the effect of reaction temperature, time, and pH, despite the remarkable use of carbon precursors. The work of Dager et al. (2019) witnessed complete carbonization of fennel seeds (hydrocarbon converted to the graphitic structure) when the reaction temperature increased to the highest temperature at 500 °C for 3 h [70]. It was also found that by heating the sample longer (for 5 h) did not result in any significant change in either PL or crystallinity. Furthermore, when the synthesized CDs were dispersed in water at different pHs ranging from 3 to 13, the emission intensity gradually increased from acidic to basic media and eventually decreased when the reaction pH was higher than 9.

Table 4. Summary of the synthesis of CDs from leaves, seeds, and stems.

Precursor		Technique	Properties			Year	Reference
Carbon Source	Passivation/Solvent		Particle Size	Fluorescence	Quantum Yield		
Lotus root	-	Microwave	TEM- 9.41 nm	λ_{em}- 435 nm λ_{ex}- 360 nm	19.0%	2016	[64]
Ocimum sanctum leaves	Distilled water	Hydrothermal	TEM- 2.23 nm	λ_{em}- 410 nm λ_{ex}- 340 nm	9.3%	2017	[65]
Acacia concinna seeds	Methanol	Microwave treatment	HRTEM- 2.5 nm	λ_{em}- 468 nm λ_{ex}- 390 nm	10.20%	2018	[66]
	Acetonitrile				7.20%		
	Acetone				7.85%		
Bamboo leaves	Sodium hydroxide and sodium hypochlorite	Pyrolysis	AFM- 2 nm	λ_{em}- 425–475 nm	-	2018	[67]
Gingko leaves	-	Pyrolysis	TEM- 4.11 nm	λ_{em}- 427 nm λ_{ex}- 360 nm	21.7%	2018	[68]
Gynostemma	-	Calcination	TEM- 2.5 nm	λ_{em}- 400 nm λ_{ex}- 320 nm	5.7%	2019	[69]
Fennel seeds (*Foeniculum vulgare*)	-	Pyrolysis	TEM- 3.9 nm	λ_{em}- 417 nm λ_{ex}- 240 nm	9.5%	2019	[70]
Bamboo leaves	-	Calcination	TEM- 11 nm	λ_{em}- 419 nm λ_{ex}- 313 nm	5.18%	2020	[71]
Betel leaves	Ammonia	Hydrothermal	HRTEM- less 10 nm PSA-3.7 nm	λ_{em}- 402 nm λ_{ex}- 320 nm	4.21%	2021	[72]
Calotropis procera leaves	Deionized water	Hydrothermal carbonization	FETEM- 4.3 nm	λ_{em}- 416 nm λ_{ex}- 340 nm	71.95%	2021	[73]
Elettaria cardamomum leaves	Distilled water	Ultrasonication	-	λ_{em}- 520 and 850 nm λ_{ex}- 514 nm	-	2021	[74]
Pearl millet seeds	Double distilled water	Thermal treatment	HRTEM- 4–5 nm	λ_{em}- 415 nm λ_{ex}- 250 nm	52%	2021	[75]
Cornus walteri leaves	Maleic anhydride, hydrogen peroxide and water	Hydrothermal	TEM- 3.53 nm	λ_{em}- 550 nm λ_{ex}- 420 nm	18.34%	2022	[76]
Tea leaves	Urea and ultrapure water	Hydrothermal	TEM- 2.32 nm	λ_{em}- 455 nm λ_{ex}- 360 nm	-	2022	[77]
Kentucky bluegrass	Ethylenediamine	Hydrothermal	TEM- 9 nm	λ_{em}- 370–470 nm λ_{ex}- 280–400 nm	7%	2022	[78]

Leaves are recognized as the most excellent carbon precursors by reason of exhibiting higher quantum yields than seeds and stem. Most interestingly, the *Calotropis procera* leaf-derived CDs provided an excellent quantum yield (71.95%) without any toxic agents or surface passivation chemicals [73]. It is noteworthy that an excellent quantum yield resulted from the functional groups (OH, N–H, C=O, and C=N bond) derived from the carbon precursors itself. Furthermore, the synthesized CDs have a strong peak around 320 nm in the UV–Vis spectra of CDs (Figure 2), implying that it was spawned by the $n \rightarrow \pi^*$ transition of C=O bonds over the surface of CDs.

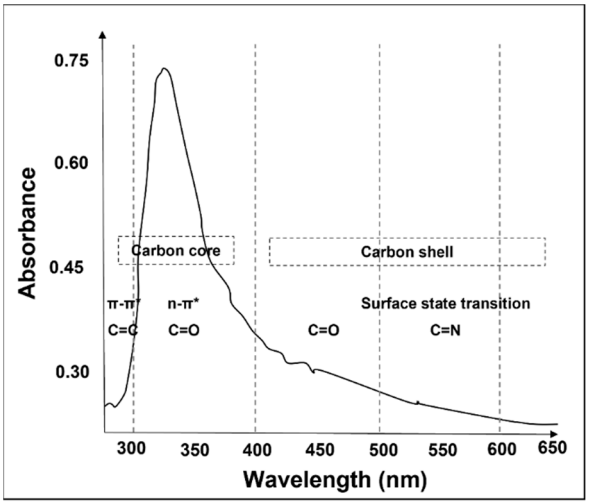

Figure 2. UV–Vis spectra of CDs from *Calotropis procera* leaves through hydrothermal method at 200 °C for 4 h. Reproduced with copyright permission of Elsevier [73].

2.5. Crop Residues

Crop residues, such as sago waste, palm kernel shell, and wheat straw, are another potential carbon source used in the green preparation of CDs (Table 5). In the year of 2014, Tan et al. successfully demonstrated the conversion of sago waste into fluorescent CDs via thermal pyrolysis without any surface passivation [79]. The heating temperature of pyrolysis was found to alter the degree of carbonization of bulk sago waste into carbonaceous residues. It was observed that heating treatments of lower than 400 °C can lead to incomplete carbonization, while higher temperatures can cause severe decomposition of the organic structures in sago waste into ashes, which leads to the loss of the fluorescing property. The optimum temperature of carbonization was found to be 400 °C. However, the synthesized CDs may suffer from low quantum yields due to the absence of solvent.

Table 5. Summary of the synthesis of CDs from crop residues.

Precursor		Technique	Properties			Year	Reference
Carbon Source	Passivation/Solvent		Particle Size	Fluorescence	Quantum Yield		
Sago waste	-	Thermal pyrolysis	SEM- 6–17 nm	λ_{em}- 390 nm λ_{ex}- 315 nm	-	2014	[79]
Palm kernel shell	Diethylene glycol	Microwave irradiation	TEM- 6.6 to 7 nm	λ_{em}- 438–459 nm λ_{ex}- 370 nm	44.0%	2020	[80]
Palm kernel shell	Ultrapure water and ethylenediamine	Hydrothermal	TEM-2 nm	λ_{em}- 430–450 nm λ_{ex}- 350–400 nm	13.7%	2021	[81]
	Ethanol and L-phenylalanine				8.6%		
Wheat straw	Deionized water	Hydrothermal	TEM- 2.1 nm DLS- 5.7 nm	λ_{em}- 470 nm λ_{ex}- 380 nm	7.5%	2021	[82]

Solvents, especially solvents with high boiling points, play an important role in providing better carbonization rates for the formation of CDs. Of these, controlling the reaction conditions by adding solvent is of particular importance. Thus, to date, diethylene glycol [80], ultrapure water and ethanol [81], and deionized water [82] have been used as solvents to improve carbonization efficiency. The results showed that the reaction of diethylene glycol (DEG) on palm kernel shell-derived CDs had the highest quantum yield of 44%. This advancement is due to the higher boiling point of DEG than the others, thus allowing a more complete reaction for the formation of CDs at higher temperatures.

2.6. Fungi/Bacteria Species

The conversion of fungi/bacteria species into a value-added product such as carbonaceous nanomaterials has contributed to the green and sustainable improvement. Algal blooms [83], yogurt [84], enokitake mushroom [85], microalgae biochar [86], mushroom [87], agarose waste [88], and *Shewanella oneidensis* [89] have been previously chosen as a carbon resource (Table 6). A study conducted by Pacquiao et al. (2018) demonstrated the increment of quantum yield of 11% to 39% upon passivation with tetraethylenepentamine in the presence of 5% *v/v* sulfuric acid [85]. The XPS spectrum revealed the presence of small signals of nitrogen and sulfur at 399 eV (N_{1s}) and 168 eV (S_{2p}), respectively, thus confirming the successful heteroatoms doping on CDs and sulfuric acid as a reagent. Furthermore, the effect of temperatures (180, 200, and 250 °C) and reaction times (4, 6, and 8 h) on the quantum yield was evaluated, yielding the optimum temperature and reaction time at 250 °C for 4 h. The research, thus, concluded that higher temperatures and shorter reaction times can produce higher quantum yields. Even so, CDs prepared from agarose waste-derived CDs without using other passivation chemicals exhibited the highest quantum yield of 62% [88]. This quantum efficiency can be attributed to the presence of different functional groups (–C=O, –OH, and N–H) on the surface of CDs, in addition to being related to the surface defects and the particle size of CDs.

Table 6. Summary of the synthesis of CDs from fungi/bacteria species.

Precursor		Technique	Properties			Year	Reference
Carbon Source	Passivation/Solvent		Particle Size	Fluorescence	Quantum Yield		
Algal blooms	Phosphoric acid	Microwave	TEM- 8.5 nm	λ_{em}- 438 nm λ_{ex}- 360 nm	13%	2016	[83]
Yogurt	Hydrochloric acid	Pyrolysis	TEM- 3.5 nm	λ_{em}- 420 nm λ_{ex}- 320 nm	2.4%	2018	[84]
Enokitake mushroom	Sulfuric acid	Hydrothermal	TEM- 4 nm	λ_{em}- 470 nm λ_{ex}- 360 nm	11%	2018	[85]
	Sulfuric acid and tetraethylenepentamine				39%		
Microalgae biochar	Potassium permanganate	Oxidizing agent and autoclave	AFM- 68 nm	λ_{ex}- 398 nm λ_{ex}- 280 nm	-	2019	[86]
Mushroom	Ultrapure water	Hydrothermal	TEM- 5.8 nm	λ_{em}- 440 nm λ_{ex}- 360 nm	11.5%	2020	[87]
Agarose waste	-	Thermal treatment	HRTEM- 2–10 nm	λ_{em}- 420 nm λ_{ex}- 300 nm	62%	2021	[88]
Shewanella oneidensis	Luria-Bertani	Hydrothermal	-	λ_{em}- 410 nm λ_{ex}- 320 nm	7%	2022	[89]

2.7. Waste Products

There are ongoing efforts to improve the photoluminescent properties while reducing the production cost and protecting the environment. Of the different plant and fungi sources, the reuse of waste (Table 7), such as frying oil [90], biocrude oil [91], polystyrene [92], tea powders [93], expired milk [94], coal powder [95], papers [96], polyolefin [97], polypropylene plastic waste [98], bike soot [99], etc. [100–111], has become one of the hottest scientific research topics nowadays for the development of CDs. Among these materials, plastic waste and heavy oil products offer a promising precursor, as they have produced high quantum yields of more than 60%. In the case of plastic waste, cup-derived CDs have displayed the highest quantum yield value of 65% at 310 nm compared to bottles (64%) and polybags (62%) [108]. The high quantum yield of CDs is highly dependent on the carbonyl groups in CDs, revealing the presence of NH_2. Furthermore, all the three prepared CDs displayed a slight red shift in the emission peak, with respect to the excitation wavelength. These behavioral variations were mainly due to the presence of epoxy and hydroxyl functional groups in the CDs prepared from the plastic waste, which resulted in creating new energy levels between n-π^* gaps. Due to this reason, the energy gaps of the CDs between the lowest unoccupied molecular orbital (LUMO) and the highest occupied

molecular orbital (HOMO) became reduced with the increasing degree of surface oxidation, thereby contributing to the enhanced fluorescence property (Figure 3).

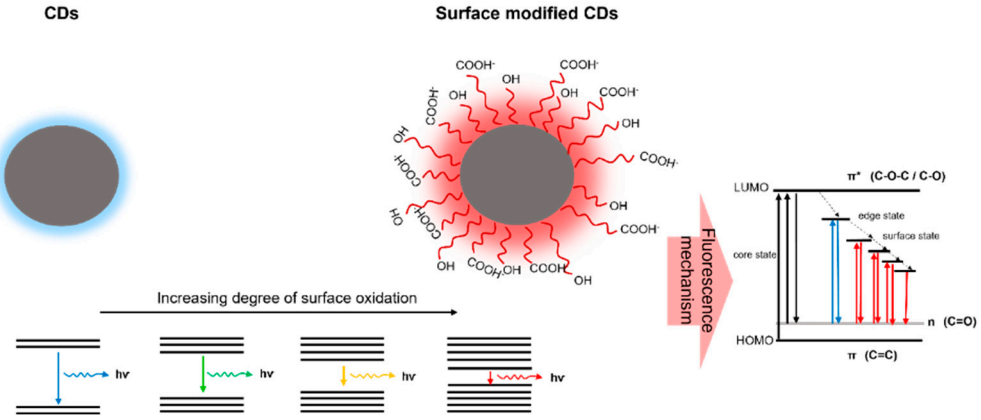

Figure 3. Scheme illustration of tunable PL of CDs with different degrees of oxidation.

Recently, the precursors with higher molecular weight, higher heteroatoms and higher aromatic structures were shown to be more conducive to the production of CDs. Ma et al. (2021) observed that CDs synthesized with asphalt as the precursor have the highest fluorescence quantum yield compared to heavy oil, light deasphalted oil (LDAO), and heavy deasphalted oil (HDAO) [110]. The reason is that the CDs from asphalt had the highest aromatic carbon ratio and the lowest naphthenic carbon ratio and alkyl carbon ratio. In addition, the asphalt had higher molecular weight, more oxygen, nitrogen and sulfur contents, and higher carbon/hydrogen atomic ratio than the other precursors. This result was further confirmed by the presence of the doublet γ peak and (002) peak in the X-ray diffraction pattern of asphalt, which indicated that the asphalt had a great quantity of graphite-like ordered structures.

Table 7. Summary of the synthesis of CDs from waste products.

Precursor		Technique	Properties			Year	Reference
Carbon Source	Passivation/Solvent		Particle Size	Fluorescence	Quantum Yield		
Waste frying oil	Sulfuric acid	Carbonization	HRTEM- 2.6 nm	λ_{em}- 378 nm λ_{ex}- 300 nm	3.66%	2014	[90]
Nannochloropsis biocrude oil	Sulfuric acid	Hydrothermal liquefaction	TEM- 4 nm	λ_{em}- 280–560 nm λ_{ex}- 400–550 nm	13.71%	2017	[91]
Polystyrene	Ethylenediamine	Solvothermal	TEM- 4 nm	λ_{em}- 456 nm λ_{ex}- 380 nm	~20%	2017	[92]
Assam CTC tea	Acetic acid	Carbonization	TEM- <10 nm	λ_{ex}- 380–500 nm	-	2017	[93]
Expired milk	Water	Subcritical water	TEM- <5 nm	λ_{em}- 440 nm λ_{ex}- 360 nm	8.64%	2018	[94]
Long flame coal powder	Deionized water	Ozone oxidation	DLS- 4.2 nm	λ_{em}- 530 nm λ_{ex}- 470 nm	8.4%	2018	[95]
Paper waste	Sodium hydroxide and distilled water	Hydrothermal	TEM- 2–4 nm	λ_{em}- 420 nm λ_{ex}- 320 nm	20%	2018	[96]
Waste polyolefin	Sulfuric acid and nitric acid	Ultrasonic-assisted chemical oxidation	TEM- 2.5 nm	λ_{em}- 540 nm λ_{ex}- 490 nm	4.84%	2018	[97]
Polypropylene plastic waste	Ethanol	Heating process	TEM- <20 nm	λ_{em}- 410–465 nm λ_{ex}- 365 nm	-	2018	[98]
Bike soot	Deionized water	Hydrothermal	TEM- 4.2 nm	λ_{em}- 396 nm λ_{ex}- 240 nm	~5.63%	2018	[99]
	Nitric acid		TEM- 5.6 nm	λ_{em}- λ_{ex}-	3.25%		
	Phosphoric acid			λ_{em}- 560 nm λ_{ex}- 460 nm	2.76%		

Table 7. *Cont.*

Precursor		Technique	Properties			Year	Reference
Carbon Source	**Passivation/Solvent**		**Particle Size**	**Fluorescence**	**Quantum Yield**		
Coke powder	Hydrogen peroxide	Chemical oxidation	TEM- 6.5 nm	λ_{em}- 410 nm λ_{ex}- 330 nm	9.2%	2019	[100]
Waste plastic bottles	Hydrogen peroxide	Air oxidation and hydrothermal	TEM- 3–10 nm	λ_{em}- 434 nm λ_{ex}- 340 nm	5.2%	2019	[101]
Waste tea powder	Nitric acid	Chemical oxidation	TEM- 3.2 nm	λ_{em}- 430 nm λ_{ex}- 310 nm	2.47%	2019	[102]
Waste tea powder	-	Carbonization	TEM- 5 nm	λ_{em}- 415 nm λ_{ex}- 315 nm	4.76%	2019	[103]
Waste green tea powder	Deionized water and manganese chloride	Hydrothermal	TEM- 5 nm	λ_{em}- 410–440 nm λ_{ex}- 360 nm	12%	2019	[104]
Tieguanyin Tea leaves	Acetic acid	Hydrothermal	TEM- 7–9 nm	λ_{em}- blue λ_{ex}- 325 nm	-	2019	[105]
Peanut shell				λ_{em}- blue λ_{ex}- 335 nm			
Kerosene soot	Nitric acid	Oxidative acid treatment	HRTEM- 5 nm	λ_{em}- 510 nm λ_{ex}- 300–360 nm	~3%	2019	[106]
Paper waste	Deionized water	Hydro-/solvothermal	TEM- 2.6 nm	λ_{em}- blue λ_{ex}- 360 nm	12%	2020	[107]
	Ethanol		TEM- 4.0 nm	λ_{em}- 435 nm (cyan) λ_{ex}- 360 nm	27%		
	2-propanol		TEM- 4.4 nm	λ_{em}- 435 nm (cyan) λ_{ex}- 360 nm	10%		
Polybags	-	Hydrothermal carbonization	HRTEM- 5–10 nm	λ_{em}- 420–425 nm λ_{ex}- 310 nm	62%	2021	[108]
Cups				λ_{em}- 420–425 nm λ_{ex}- 310 nm	65%		
Bottles				λ_{em}- 420–425 nm λ_{ex}- 310 nm	64%		
Polymeric waste	-	Hydrothermal	TEM- 3 nm	λ_{em}- 400 nm λ_{ex}- 310 nm	-	2021	[109]
	4,7,10-trioxa-1,13-tridecanediamine			λ_{em}- 440 nm λ_{ex}- 365 nm			
Heavy oil	-	Hydrothermal	-	-	-	2021	[110]
Light deasphalted oil (LDAO)			-	-	~64%		
Heavy deasphalted oil (HDAO)			-	-	23.5%		
Asphalt			TEM- 2.39 nm	λ_{em}- 610 nm λ_{ex}- 475 nm	11.5%		
			TEM- 1.77 nm	λ_{em}- 560 nm λ_{ex}- 420 nm	17.7%		
			TEM- 1.21 nm	λ_{em}- 510 nm λ_{ex}- 410 nm	28.3%		
			TEM- 1.18 nm	λ_{em}- 440 nm λ_{ex}- 350 nm	64%		
Waste tobacco leaves	Ethylenediamine and ultrapure water	Hydrothermal	TEM- 6.30 nm	λ_{em}- 430 nm λ_{ex}- 360 nm	13.7%	2022	[111]

3. CDs Synthesized from Chemical Precursors

Although many natural precursors have been used in the preparation of low-cost CDs, chemical precursors are still being explored to this day to produce high quantum yields of CDs. This section reviews two types of reaction chemical precursors used in CD preparation, namely acid and non-acid reagents, which were briefly summarized in Tables 8 and 9.

3.1. Acid Reagents

Since 2012, carbon sources based on acid reagents, such as citric acid, phosphoric acid, acetic acid, folic acid, ascorbic acid, sodium citrate, ascorbic acid, glutamic acid, malonic

acid, maleic anhydride, boric acid, pyrogallic acid, phthalic acid, 3-aminobenzeneboronic acid, succinic acid, p-aminosalicylic acid, diethylenetriamine-pentacetate acid, maleic anhydride, DL-thioctic acid, sulfamic acid, tartaric acid, 2-aminoterephthalic acid, trans-aconitic acid, dehydroabietic acid, dithiosalicylic acid, etc., have been intensively employed in the production of CDs [112–197].

Dong et al. (2013) first compared the fluorescence properties of the following three types of CDs: (i) O-CDs synthesized from citric acid only, (ii) N-CDs synthesized from citric acid and glycine, and (iii) N,S-CDs synthesized from citric acid and L-cysteine [113]. It was observed that the doping of nitrogen into O-CDs can introduce a new kind of surface state (labelled as the N-state). Electrons trapped by the new formed surface states are able to facilitate a high yield of radiative recombination. Although the quantum yield of N-CDs was found to be higher than that of O-CDs, the fluorescence spectra were still broad and excitation-dependent. In such cases, the introduction of sulfur atoms into CDs could lead to more significant enhancement, offering higher yields and excitation-independent emission. The introduced sulfur atoms seem to be able to eliminate the O-states and enhance the N-state, meaning that the original surface states are almost neglected in the N,S-CDs. However, when the authors tuned the ratio of L-cysteine into citric acid, from 1 g:2 g into 0.125 g:2 g, the quantum yield of N,S-CDs decreased from 73% to 37% and the emission wavelength was dependent on excitation and yielded a red-shift from 415 to 540 nm under the excitation wavelength of 375 to 480 nm. Interestingly, when the excitation wavelength was set lower than 375 nm, the emission wavelength was excitation independent. Although the aforementioned CDs were highly enhanced by nitrogen and sulfur co-doping, the chemistry involved therein is extremely challenging due to the involvement of oxygen, let alone the interference from defects. Therefore, until single nitrogen doping-sources, such as urea, ethylenediamine, PEG diamine, melamine, etc., have been widely reported, as shown in Table 8.

On the other hand, citric acid as the carbon source was commonly used in the chemical synthesis of CDs. Citric acid has considerable advantages over other acid reagents, such as being relatively cheap, more sour, less harmful to the environment, and readily available in large commercial quantities. Consequently, two highest fluorescence quantum yields were attributed to the reflux reaction of citric acid and diethylenetriamine [133] and hydrothermal reaction of citric acid and ethylenediamine [176] at 82.40% and 85.69%, respectively. As expected, ethylenediamine as N-doping agents plays a major role in improving the fluorescence properties in CDs. By way of example, Wang et al. (2015) have reported the influence of three different polyethylenic amine molecules, i.e., ethylenediamine (EDA), diethylenetriamine (DETA), and tetraethylenepentamine (TEPA) with a combination of citric acid on photoluminescence performance [129]. The results showed that the CDs-EDA has the highest PL quantum yield at 69.3%, followed by CDs-DETA (68%) and CDs-TEPA (33.4%). The results imply that the increasing presence of cyclic imines (C=N) with the enhancement of conjugated π-domains in CDs imparts superior PL efficiency.

There is another study that reported the fabrication of CDs from different nitrogen sources, such as ethylenediamine (e), hexamethylenetetramine (h), and triethanolamine (t) [130]. From the X-ray photoelectron spectroscopy analyses, the ratios of carbon to nitrogen in these CDs were determined, namely, 83:17 for e-CDs, 86.14 for h-CDs, and 96:4 for t-CDs. Because of the high nitrogen content in e-CDs, the quantum yield was found to be highest at 53%. The amount of nitrogen can be typically correlated with a high photoluminescence quantum yield and confirms similar features in the absorption spectra (a shoulder at 234 nm and a broad peak at 340 nm) between e-CDs and pure citrazinic acid, the basic unit from the presumed class of fluorophores. However, at wavelengths longer than 400 nm, pure citrazinic acid has no absorption characteristic, unlike e, h and t-CDs, as shown in Figure 4a. The presence of broad absorption in this energy is commonly assigned to surface states related to the functional surface groups in CDs, which form low-energy sub-band gaps within the $n-\pi^*$ band gap.

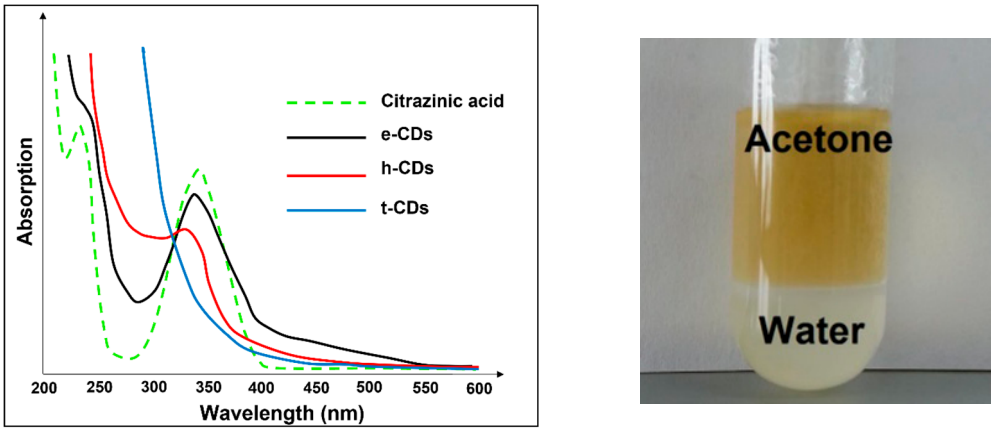

(**a**) (**b**)

Figure 4. (**a**) Absorption spectra of three CD species and pure citrazinic acid. Adapted with permission from ref. [130]. Copyright 2017 American Chemical Society; (**b**) the salt-induced phase separation using acetone. Reproduced with copyright permission of Elsevier [137].

Furthermore, Chang et al. (2017) reported that the phosphoric acid (H_3PO_4) or sucrose solution alone could not produce a significant fluorescence emission under the excitation of 423 nm [137]. However, when H_3PO_4 and sucrose solutions were mixed and incubated in the oven, the fluorescence light was emitted at the excitation wavelength of 423 nm. It is thought that the mild heating of H_3PO_4 has the power to hydrolyze sugar into simple carbon-rich molecules. Of note, to deactivate the carbonization process, the authors then added sodium hydroxide into CDs, but this appeared to cause a high salt content that was not favourable to many applications. Hence, acetone with a 1:1 volume-to-volume ratio was used to overcome this problem, resulting in two phases, as shown in Figure 4b. The highly ionic salt species remained in the water mother-liquor, while the CDs that were less ionic were partitioned into the acetone phase. The removal of CDs from acetone can be easily achieved via evaporation, since acetone is quite volatile. Based on this, the fluorescence signal of CDs was found to be increased by approximately 10%.

Recently, other carbon sources derived from amino acids, namely arginine, lysine, histidine, cysteine, and methionine have been reported [168,193–195]. This is because of their several advantages, for instance, non-toxic, biocompatible, and eco-friendly nature. Most importantly, each of the amino acids have different numbers of -COOH, -NH, and -SH functional groups, which can effectively improve the optical and chemical properties of CDs. Upon mixing these amino acids with citric acid via the microwave method, N and/or S-doped CDs were successfully synthesized in a very short time for the first time, which only took 1–4 min [168]. The reaction mechanism was proposed to include the following two steps: (i) reaction of carboxylic acid of citric acid with the -NH and –SH groups of amino acids via condensation polymerization and then the esterification of citric acid with amino acids, (ii) carbonization of these polymer clusters during irradiation by total dehydration to generate N and/or S doped CDs under microwave exposure. The research concluded that only cysteine-CDs were found to possess the highest quantum yield of 89.5% upon the N and S atom containing CDs.

The highest quantum yield of 93% was achieved when sodium citrate dihydrate and urea were used as precursors [179]. Sodium citrate dihydrate plays an important role as a self-assembly trigger for a carbon-based structure, due to the intermolecular H-bonding, while urea acts as nitrogen-doping precursors, which both are responsible for the increase in quantum yield. In another study, instead of using common synthesis methods such as oxidation, combustion, and hydrothermal, Ji et al. (2021) established another method, which is simpler and timesaving. Briefly, 0.34 g of L-cysteine, 0.15 g of urea, and 8.5 g of diphosphorus pentoxide were mixed, followed by the addition of 6 mL of water with a rapid stirring process [193]. These CDs were then embedded in in polyvinyl alcohol

(PVA) gel substrate to form a smooth and high fluorescent CD/PVA film for further use in hexavalent chromium detection.

Table 8. Summary of the synthesis of CDs from acid reagents.

Precursor		Technique	Properties			Year	Reference
Carbon Source	Passivation/Solvent		Particle Size	Fluorescence	Quantum Yield		
Citric acid	Terbium (III) nitrate pentahydrate	Carbonization	TEM- 3 nm	λ_{em}- 450 nm λ_{ex}- 320 nm	-	2012	[112]
Citric acid monohydrate	L-cysteine	Hydrothermal treatment	HRTEM- 7 nm	λ_{em}- 415 nm λ_{ex}- 345 nm	73%	2013	[113]
	-		-	λ_{em}- 435 nm λ_{ex}- 345 nm	5.3%		
	Glycine		-	λ_{em}- 415 nm λ_{ex}- 345 nm	16.9%		
Citric acid	Urea	Microwave	TEM- 4 to 6 nm	λ_{em}- 460 nm λ_{ex}- 360 nm	0.13%	2013	[114]
Ethyleneglycol bis-(2-aminoethyl ether)-N,N,N′,N′-tetraacetic acid	Tris(hydroxymethyl) aminomethane	Thermal carbonization	TEM- 5 nm	λ_{em}- 425 nm λ_{ex}- 310 nm	28%	2014	[115]
Citric acid	PEG-diamine	Solid-phase	TEM- 1.7 nm	λ_{em}- 435 nm λ_{ex}- 360 nm	31%	2014	[116]
Citric acid	Poly(ethylenimine)	Pyrolysis	HRTEM- 3.5–4.5 nm	-	42.5%	2014	[117]
Folic acid	Ethylene glycol and nanopure water	Hydrothermal	TEM- 4.5 nm	λ_{em}- 470 nm λ_{ex}- 395 nm	15.7%	2014	[118]
Poly(ethylene glycol) and ascorbic acid	Distilled water	Microwave	TEM- 2.3 nm	λ_{em}- 450 nm λ_{ex}- 373 nm	-	2014	[119]
Citric acid	Ethylenediamine	Microwave-assisted pyrolysis	TEM- 3 nm	λ_{em}- 455 nm λ_{ex}- 280 nm	-	2015	[120]
Citric acid	L-Tyrosine methyl ester hydrochloride	Hydrothermal	TEM- 3.7 nm	λ_{em}- 433 nm λ_{ex}- 348 nm	3.8%	2015	[121]
Citric acid	Ethylenediamine and double distilled water	Hydrothermal	-	-	75.0%	2015	[122]
Citric acid	1-Aminopropyl-3-methy-imidazolium bromide	Pyrolysis	HRTEM- 0.6–1.6 nm	λ_{em}- 440 nm λ_{ex}- 380 nm	2.03–27.66%	2015	[123]
Glacial acetic acid	N-Acetyl-L-cysteine, diphosphorus pentoxide and distilled deionized water	Simple mixing	TEM- 2.51–3.44 nm	λ_{em}- 480 nm λ_{ex}- 300 nm	4.65%	2015	[124]
Citric acid	L-cysteine, urea and ultrapure water	Microwave	TEM- 1.1 nm	λ_{em}- 450 nm λ_{ex}- 353 nm	25.2%	2015	[125]
Citric acid	Dithiooxamide and distilled water	Microwave-assisted hydrothermal	STEM- 2 nm	λ_{em}- 448 nm λ_{ex}- 360 nm	17.6%	2015	[126]
Citric acid monohydrate	Ammonia and double distilled water	Hydrothermal	TEM- 3.7 nm	λ_{em}- 442 nm λ_{ex}- 350 nm	40.5%	2015	[127]
Sodium citrate	Urea and ultrapure water	Electrochemical carbonization	TEM- 2.4 nm	λ_{em}- 433 nm λ_{ex}- 351 nm	11.9%	2015	[128]
Citric acid anhydrous	Ethelendiamine	Condensation carbonization	TEM- 3.9 nm	λ_{em}- 445 nm λ_{ex}- 365 nm	69.3%	2015	[129]
	Diethylenetriamine		TEM- 3.7 nm		68%		
	Tetraethylenepentamine		TEM- 4.1 nm		33.4%		
Citric acid anhydrous	Ethylenediamine and deionized water	Hydrothermal	-	λ_{em}- 440 nm λ_{ex}- 320 nm	53%	2016	[130]
	Hexamethylenetetramine and deionized water			λ_{em}- 420 nm λ_{ex}- 320 nm	17%		
	Triethanol-amine and deionized water			λ_{em}- 420 nm λ_{ex}- 320 nm	7%		

Table 8. *Cont.*

Precursor		Technique	Properties			Year	Reference
Carbon Source	Passivation/Solvent		Particle Size	Fluorescence	Quantum Yield		
Citric acid	Ethylenediamine and deionized water	Hydrothermal	TEM- 5 to 7 nm	λ_{em}- 443 nm λ_{ex}- 365 nm	-	2016	[131]
Citric acid	Branched polyethylenimine	Condensation	DLS- 1.9 nm	λ_{em}- 450 nm λ_{ex}- 350 nm	-	2016	[132]
Citric acid	Diethylenetriamine	Reflux treatment	TEM- 5 -7 nm	-	82.40%	2016	[133]
Ascorbic acid and valine	Ethanol and distilled water	Hydrothermal	TEM- 4 nm	λ_{em}- 430 nm λ_{ex}- 352 nm	4.8%	2016	[134]
L-glutamic acid	Silica gel powders and water	Microwave	TEM- 1.64 nm	λ_{em}- 450 nm λ_{ex}- 370 nm	41.2%	2016	[135]
Malonic acid	Urea and ultrapure water	Hydrothermal	TEM- 2.5 nm	λ_{em}- 397 nm λ_{ex}- 320 nm	12.6%	2017	[136]
Sucrose and phosphoric acid	Sodium hydroxide	Carbonization	SEM- 10 nm	λ_{em}- 524 nm λ_{ex}- 423 nm	-	2017	[137]
Citric acid	Sodium phosphate	Solid-phase	TEM- 1.7 nm	λ_{em}- 435 nm λ_{ex}- 360 nm	-	2017	[138]
Citric acid	Ethylenediamine and ultrapure water	Hydrothermal	TEM- <10 nm	λ_{em}- 431 nm λ_{ex}- 337 nm	32.25%	2017	[139]
Citric acid monohydrate	Thiourea	Microwave solid-phase pyrolysis	TEM- 2 nm	λ_{em}- 436 nm λ_{ex}- 358 nm	23.6%	2017	[140]
Citric acid	Silk	Hydrothermal	TEM- 5.6 nm	λ_{em}- 425 nm λ_{ex}- 360 nm	61.1%	2017	[141]
Citric acid	Melamine	Hydrothermal	TEM- 1.8 nm	λ_{em}- 422 nm λ_{ex}- 320 nm	8.11%	2017	[142]
Citric acid	Tartaric acid, ethanediamine and oleic acid	Solvothermal	TEM- 2.66 nm	λ_{em}- 460 nm λ_{ex}- 360 nm	42.2%	2017	[143]
Citric acid and urea	Water	Solvothermal	TEM- 1.7 nm	λ_{em}- 448–638 nm λ_{ex}- 375 nm	-	2017	[144]
	Glycerol		TEM- 2.8 nm				
	Dimethylformamide		TEM- 4.5 nm				
Maleic anhy- dride and tetraethylenepentamine	Sulfuric acid and deionized water	Pyrolysis	TEM- 20 nm DLS- 8 nm	λ_{em}- 450 nm λ_{ex}- 360 nm	21%	2017	[145]
D-(+)-maltose monohydrate, boric acid and thiocarbamide	-	Hydrothermal	TEM- 2.0 nm	λ_{em}- 415 nm λ_{ex}- 326 nm	8.9%	2017	[146]
Pyrogallic acid	N-N-dumethylformamide	Solvothermal	TEM- 11.9 nm	λ_{em}- 520 nm λ_{ex}- 360–450 nm	16.8%	2018	[147]
L-histidine and citric acid	Ethylene glycol	Polyol microwave	TEM- 19 nm	λ_{em}- 430–511 nm λ_{ex}- 350 nm	-	2018	[148]
Phthalic acid and triethylenediamine hexahydrate	Deionized water	Microwave	TEM- 2–6 nm	λ_{em}- 520–542 nm λ_{ex}- 360–440 nm	16.1%	2018	[149]
Citric acid	Urea	Solvothermal	TEM- 1.87 nm	λ_{em}- 590 nm λ_{ex}- 540 nm	43%	2018	[150]
Citric acid	Lysine and ultrapure water	Hydrothermal	TEM- 10 nm	-	-	2018	[151]
Citric acid monohydrate	-	Thermal treatment	TEM- 3.5 nm	λ_{em}- 450 nm λ_{ex}- 360 nm	3.54%	2018	[152]
Citric acid	Ammonium thiocyanate and deionized water	Microwave-assisted	HRTEM- 30 nm	λ_{em}- 490 nm λ_{ex}- 410 nm	-	2018	[153]
Folic acid and p-phenylenediamine	Sodium hydroxide	Hydrothermal	TEM- 2 nm	λ_{em}- 505 nm λ_{ex}- 420 nm	8.4%	2018	[154]
3-Aminobenzeneboronic acid	Deionized water	Hydrothermal	TEM- 3 nm	λ_{em}- 504 nm λ_{ex}- 400 nm	-	2018	[155]
Succinic acid	Deionized water and glycerol	Hydrothermal	TEM- 2.3 nm	λ_{em}- 410 nm λ_{ex}- 280 nm	11%	2018	[156]
			TEM- 4.6 nm	λ_{em}- 525 nm λ_{ex}- 480 nm	7%		

Table 8. *Cont.*

Precursor		Technique	Properties			Year	Reference
Carbon Source	**Passivation/Solvent**		**Particle Size**	**Fluorescence**	**Quantum Yield**		
Phosphoric acid	Ethylenediamine	Simple heating (180 °C, 2 h)	TEM- 3.2 nm	λ_{em}- 430 nm λ_{ex}- 340 nm	5.17%	2018	[157]
		Simple heating (280 °C, 2 h)	TEM- 6.4 nm	λ_{em}- 413 nm λ_{ex}- 340 nm	21.8%		
Phosphoric acid and ethanolamine	Water	Microwave irradiation	TEM- 3.4 nm	λ_{em}- 417 nm λ_{ex}- 340 nm	20.52%	2018	[158]
P-aminosalicylic acid	Ethyleneglycol dimethacrylate and double distilled water	Hydrothermal	TEM- 3 nm AFM- 1.6 nm DLS- 11.7 nm	λ_{em}- 520 nm λ_{ex}- 390 nm	27.2%	2018	[159]
Sodium citrate	Urea and dimethylformamide	Solvothermal	TEM- 3.52 nm	λ_{em}- 446 nm λ_{ex}- 370 nm	67%	2018	[160]
Citric acid monohydrate	3-(Aminopropyl)triethoxysilane (APTES)	Thermal decomposition	TEM- 5–15 nm	λ_{em}- 416 and 480 nm	-	2019	[161]
Citric acid	Urea and deionized water	Hydrothermal	-	-	-	2019	[162]
	Glycine and deionized water		-				
	Citric acid, deionized water, ethylene glycol, N,N′- bis(2-aminoethyl)-1,3-propanediamine		HRTEM- 5–6 nm				
Citric acid and urea	N,N-dimethylformamide	Solvothermal	-	λ_{em}- 450, 550, 630 nm λ_{ex}- 400–450 nm	-	2019	[163]
	N,N-dimethylformamide, NaOH and HCl		TEM- 3.7 nm	λ_{em}- 630 nm λ_{ex}- 550 nm	-		
	N,N-dimethylformamide, NaOH and water		TEM- 2.1 nm	-	-		
Procaine hydrochloride and citric acid	Double distilled water and ethylenediamine	Hydrothermal	TEM- 3.3 nm	λ_{em}- 440 nm λ_{ex}- 360 nm	47.1%	2019	[164]
Anhydrous citric acid	N-(β-aminoethyl)-γ-aminopropyl-methyldimethoxysilane	Hydrothermal	TEM- 2.22 nm	λ_{em}- 460 nm λ_{ex}- 370 nm	51.8%	2019	[165]
Citric acid	Thiourea and deionized water	Microwave-assisted pyrolysis	TEM- 3.3 nm	-	-	2019	[166]
Sodium citrate and aminopyrazine	Ultrapure water	Hydrothermal	TEM- 2.38 nm	λ_{em}- 389 nm λ_{ex}- 310 nm	11.8%	2019	[167]
Citric acid	Deionized water and arginine	Microwave	TEM- 11 ± 4 nm	λ_{em}- 330 nm λ_{ex}- 430 nm	3.9 ± 0.4%	2019	[168]
	Deionized water and lysine		TEM- 17 ± 2 nm	λ_{em}- 330 nm λ_{ex}- 430 nm	4.2 ± 1.9%		
	Deionized water and histidine		TEM- 6 ± 5 nm	λ_{em}- 330 nm λ_{ex}- 433 nm	2.8 ± 0.2%		
	Deionized water and cysteine		TEM- 10 ± 7 nm	λ_{em}- 330 nm λ_{ex}- 420 nm	89.5 ± 2.3%		
	Deionized water and methionine		TEM- 9 ± 5 nm	λ_{em}- 330 nm λ_{ex}- 407 nm	2.5 ± 0.6%		
Citric acid and phenylalanine	Ultrapure water	Hydrothermal	TEM- 2–3 nm	λ_{em}- 330 nm λ_{ex}- 310 nm	-	2020	[169]
Polyacrylamide and citric acid	Ultrapure water	Hydrothermal	TEM- 4.1 nm	λ_{em}- 330 nm λ_{ex}- 310 nm	12.6%	2020	[170]
Citric acid and urea	-	Infrared carbonization	TEM- 5–10 nm	λ_{em}- 475 nm λ_{ex}- 360 nm	22.2%	2020	[171]
Citric acid and urea	-	Hydrothermal (180 °C, 20 min)	TEM- 2–7 nm	-	46% 26% 4%	2020	[172]
		(230 °C, 20 min)		λ_{em}- 394, 440, 523 nm λ_{ex}- 350 nm	23% 35% 36%		

Table 8. *Cont.*

Precursor		Technique	Properties			Year	Reference
Carbon Source	Passivation/Solvent		Particle Size	Fluorescence	Quantum Yield		
Citric acid	Melamine and formaldehyde	Hydrothermal	TEM- 3.7 nm	λ_{em}- 425 nm λ_{ex}- 350 nm	63.7%	2020	[173]
Citric acid monohydrate	Urea	Microwave irradiation	TEM- 6 nm	λ_{em}- 536 and 532 nm λ_{ex}- 350 nm	-	2020	[174]
Citric acid	Phenylalanine	Hydrothermal	TEM- 11.9 nm	λ_{em}- 413 nm λ_{ex}- 350 nm	65%	2020	[175]
Citric acid monohydrate	Ethylenediamine	Hydrothermal	TEM- 5–10 nm	λ_{em}- blue λ_{ex}- 305–395 nm	85.69%	2020	[176]
Citric acid	Ethylenediamine and ultrapure water	Hydrothermal	TEM- 5 nm	λ_{em}- 444 nm λ_{ex}- 360 nm	-	2020	[177]
Ascorbic acid	Urea and deionized water	Microwave irradiation	TEM- 2 nm	λ_{em}- 415 nm λ_{ex}- 340 nm	7%	2020	[178]
Sodium citrate dihydrate	Urea and deionized water	Thermal pyrolysis	TEM- 2.75 nm	λ_{em}- 525 nm λ_{ex}- 400 nm	93%	2020	[179]
Citric acid and 3-aminobenzeneboronic	Dimethylformamide	Hydrothermal	HRTEM- 3.4 nm	-	-	2020	[180]
Diethylenetriamine-pentacetate acid	Ultrapure water	Carbonization	HRTEM- 2.85 nm	-	-	2020	[181]
Maleic anhydride and triethylenetetramine	Deionized water and nitric acid	Pyrolysis	TEM- 5.9 nm	λ_{em}- 400 nm λ_{ex}- 320 nm	6.3%	2021	[182]
DL-thioctic acid	Dimethylformamide, trisodium citrate dihydrate, sodium hydroxide, double deionized water	Hydrothermal	HRTEM- 2.52 nm	λ_{em}- 438 nm λ_{ex}- 340 nm	-	2021	[183]
Citric acid and sulfamic acid	Polyethyleneimine	Two-step hydrothermal	TEM- 5.1 nm	λ_{em}- 460 nm λ_{ex}- 355 nm	29.1%	2021	[184]
Tartaric acid	Urea	Solid-phase thermal	TEM- 4.13 nm	λ_{em}- 537 nm λ_{ex}- 460 nm	10.5%	2021	[185]
2-aminoterephthalic acid and polyethylene glycol	Orthophosphoric acid	Microwave-assisted pyrolysis	TEM- 3–10 nm	λ_{em}- 470 nm λ_{ex}- 410 nm	67%	2021	[186]
Citric acid	Ultrapure water and ethylenediamine	Hydrothermal	TEM- 3.1 nm	λ_{em}- 445 nm λ_{ex}- 356 nm	-	2021	[187]
Citric acid	Ethylenediamine and water	Microwave	TEM- 2.3 nm	λ_{em}- 450 nm λ_{ex}- 360 nm	-	2021	[188]
Trans-aconitic acid	Diethylenetriamine and distilled water	Hydrothermal	HRTEM- 2–8 nm	λ_{em}- 435 nm λ_{ex}- 345 nm	81%	2021	[189]
Dehydroabietic acid	Ethanolamine	Hydrothermal	TEM- 3.2 nm	λ_{em}- 433 nm λ_{ex}- 365 nm	10%	2021	[190]
Citric acid	L-glutamine	Hydrothermal	TEM- 3.5 nm	λ_{em}- 450 nm λ_{ex}- 360 nm	-	2021	[191]
	D-glutamine		TEM- 3–4 nm				
Dithiosalicylic acid	Acetic acid and o-phenylenediamine	Solvothermal	TEM- 4.5 nm	λ_{em}- 620 nm λ_{ex}- 560 nm	4.05%	2021	[192]
	Acetic acid and m-phenylenediamine		TEM- 4.0 nm	λ_{em}- 560 nm λ_{ex}- 460 nm	20.77%		
	Acetic acid and p-phenylenediamine		TEM- 3.5 nm	λ_{em}- 478 nm λ_{ex}- 460 nm	1.76%		
L-cysteine and urea	Diphosphorus pentoxide and water	One-pot synthesis	TEM- 4.5 nm	λ_{em}- 445 nm λ_{ex}- 362 nm	17%	2021	[193]
Methyl cellulose and L-cysteine	Ethylenediamine	Hydrothermal	TEM-19 nm	λ_{em}- 370 nm λ_{ex}- 330 nm	12.3%	2021	[194]
Ce $(NO_3)_3 \cdot 6H_2O$ and L-histidine	Sodium hydroxide and deionized water	One-pot hydrothermal	SEM- 46 nm	-	-	2021	[195]
Polyethylenimine and citric acid	Hot water	Microwave-assisted	STEM- 12 nm	λ_{em}- 442 nm λ_{ex}- 354 nm	54%	2022	[196]
Citric acid and urea	Ultrapure water	Solvothermal	HRTEM- 3.18 nm	λ_{em}- 470 nm λ_{ex}- 330 nm	20.1%	2022	[197]
	20 mL dimethylformamide		HRTEM- 3.25 nm	λ_{em}- 500 nm λ_{ex}- 330 nm	22.1%		

Table 8. *Cont.*

Precursor		Technique	Properties			Year	Reference
Carbon Source	Passivation/Solvent		Particle Size	Fluorescence	Quantum Yield		
Citric acid and urea	10 mL dimethylformamide and ethanol	Solvothermal	HRTEM- 3.47 nm	λ_{em}- 539 nm λ_{ex}- 330 nm	21.9%	2022	[197]
	10 mL dimethylformamide and acetic acid		HRTEM- 3.68 nm	λ_{em}- 595 nm λ_{ex}- 330 nm	24.2%		

3.2. Non-Acid Reagents

Carbon sources based on non-acid reagents, namely graphite oxide [198], poly(ethylene glycol) [199,200], 3-(3,4-dihydroxyphenyl)-L-alanine [201], ethanolamine [202], polyimide [203], polyethyleneglycol bis(3-aminopropyl) [204], ethanol [205], 3-bromophenol [206], azidoimidizole [207], activated carbon [208], glucose [209], N-methylethanolammonium thioglycolate [209], chitosan [210], chlorophyll [211], microcrystalline cellulose [212], o-phenylenediamine [213], carbon paper [214], papain [215], dextrose solution [216], etc. [217–230], have also been reviewed, as shown in Table 9. 3-Bromophenol is the first insecticide adopted to be a potential precursor, thus suggesting that carbon sources are not limited in typical chemical reagents with high purity or low toxicity [206]. In this study, the effect of mixed solvent of ethanol and water ratio (v/v) such as 1:9, 3:7, 5:5, 7:3 and 9:1 and the effect of temperatures such as 150, 160, 170 °C were evaluated. The results indicate that both much thicker organic solvents and much higher carbonized temperatures are in favour of the formation of C-dots featuring monodispersion, high yield, and smaller size. The proposed mechanism behind the fabrication of insecticide-based CDs was verified by the occurrence of aromatic C-Br and Br anion, Csp2 C-C peak and Csp3 C-C peak found on the XPS spectrum. The three possible main classes of the reaction that happened among the 3-bromophenol molecules are given in Figure 5.

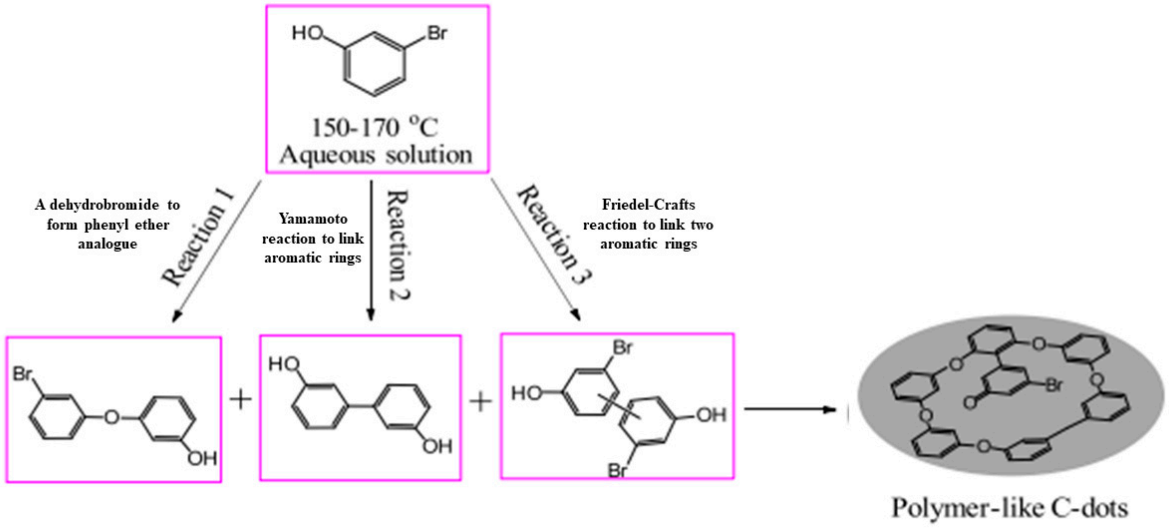

Figure 5. Proposed possible mechanisms for the formation CDs using 3–bromophenol. Reproduced with copyright permission of Elsevier [206].

Efforts to develop and improve the fluorescence of the CDs have been made toward polymer compounds, including synthetic and natural polymers. Thanks to the toxicity of synthetic polymers, natural polymers extracted from plants have been used as a carbon source with the characteristics of being environment-friendly, non-toxic, low price, good biocompatibility, and stable chemical properties. For this reason, Wu et al. (2017) reported microcrystalline cellulose as a carbon precursor to prepare a facile and low-cost one-step hydrothermal treatment of CQDs [212]. The modification of these CQDs with

ethylenediamine not only allowed nitrogen atoms on its surface but also introduced them into the carbon nuclear lattice to obtain better optical properties and higher quantum yield than CQDs. Fortunately, nitrogen doped CQDs (NCQDs) have a fluorescence emission intensity of 7.1 times stronger than the CQDs, and it can be explained by the reduction of epoxy, ether, and carboxyl groups on the surface of NCQDs via nucleophilic reactions with amidogen, thus forming a few non-radiative recombination centers in NCQDs. The amination and/or amidation also create radiative recombination centers, such as amine (–C–N–) and amide groups (R_2-NCOR), which belong to electron-donating groups. These electron-donating groups and π-electrons that existed in the –C=N group have contributed to the improvement of the fluorescence intensity of a substance. All in all, these NCQDs successfully provided the highest quantum yield of 55%.

The synthesis of CDs using non-acid reagents can be further explored by attempting to use three different aniline compounds, i.e., 1,2,4,5-benzenetetramine tetrahydrochloride, 1,2,4-benzenetriamine dihydrochloride, and o-phenylenediamine, as carbon sources and ethanol as a solvent [217]. In an approach where more amino groups and a high nitrogen content are present in CDs-benzenetetramine tetrahydrochloride, the excitation and emission wavelengths all exhibited a redshift with an increase in the CD particle size. The quantum yield also greatly increased up to 30.2%. Additionally, the fluorescence intensity of the CDs was observed to gradually increase with the increasing amount of raw material from 0.005 g to 0.025 g. It is important to note that the number of amino groups and particle size of CDs have a great influence on the emission wavelength, while the amount of raw material influences the color and intensity of the fluorescence. In another study, the CDs were synthesized using three types of aldehydes, such as glutaraldehyde, nitrobenzaldehyde and benzaldehyde, via the solvothermal method [225]. The resulting CDs were then composited with chitosan, functionalized by a DNA probe and utilized as a detecting platform for rapid detection of microRNA-21. The function of CDs is further classified as a cross-linking agent and fluorescent donor, while chitosan plays an important role in the preparation of three-dimensional hydrogel frames.

Table 9. Summary of the synthesis of CDs from non-acid reagents.

Precursor		Technique	Properties			Year	Reference
Carbon Source	Passivation/Solvent		Particle Size	Fluorescence	Quantum Yield		
Graphite oxide	Nitric acid	Microwave-hydrothermal	TEM- 4 nm	λ_{em}- 520 nm λ_{ex}- 470 nm	2.72%	2011	[198]
Poly(ethylene glycol)	Sodium hydroxide and distilled water	Reflux method	TEM- 5 nm	λ_{em}- bright blue λ_{ex}- 350 nm λ_{em}- cyan λ_{ex}- 390 nm λ_{em}- yellow λ_{ex}- 470 nm λ_{em}- red λ_{ex}- 540 nm	-	2013	[199]
Polyethylene glycol 1500	Serine and glycerin	Microwave pyrolysis	-	-	-	2013	[200]
3-(3,4-dihydroxyphenyl)-L-alanine	-	Carbonization-oxidation	TEM- 3.64 nm	λ_{em}- 500 nm λ_{ex}- 400 nm	6.3%	2013	[201]
	Nitric acid		TEM- 4.31 nm	λ_{em}- 475 nm λ_{ex}- 360 nm	1%		
Ethanolamine	-	Pyrolysis	TEM- 2.7 nm	λ_{em}- 450 nm λ_{ex}- 365 nm	7%	2014	[202]
	Hydrogen peroxide		TEM- 8.3 nm		10.3%		
Polyimide	-	Hydrothermal	TEM- 4 nm	λ_{em}- 490 nm λ_{ex}- 365 nm	20.9%	2015	[203]
Polyethyleneglycol bis(3-aminopropyl)	6-Bromohexylboronic acid	Thermal carbonization	TEM- 5 nm	λ_{em}- 440 nm λ_{ex}- 362 nm	0.3%	2015	[204]
Ethanol	Hydrogen peroxide and deionized water	Hydrothermal	TEM- 4.8 nm	λ_{em}- 456 nm λ_{ex}- 400 nm	38.7%	2015	[205]
3-Bromophenol	Ethanol and deionized water	Carbonization	TEM- 5.2 nm	λ_{em}- 440 nm λ_{ex}- 367 nm	19.6%	2016	[206]

Table 9. *Cont.*

Precursor		Technique	Properties			Year	Reference
Carbon Source	**Passivation/Solvent**		**Particle Size**	**Fluorescence**	**Quantum Yield**		
Azidoimidizole	Ethanol	-	AFM- 5–10 nm	λ_{em}- 515 nm λ_{ex}- 460 nm	-	2016	[207]
Activated carbon	Potassium permanganate, sulfuric acid, deionized water, hydrogen peroxide	Exhausted oxidation	TEM- 12 nm	λ_{em}- 465 nm λ_{ex}- 350 nm	3.94%	2016	[208]
	Potassium permanganate, sulfuric acid, deionized water, hydrogen peroxide, PAMAM-NH_2		TEM- 65 nm		6.93%		
Glucose	Water and sodium hydroxide	Ultrasonic	-		7%	2016	[209]
N-Methylethanolammonium thioglycolate	Water and hydrogen peroxide		HRTEM- 3–8 nm		12.5%		
Chitosan	-	Carbonization	TEM- 1–6 nm	λ_{em}- 390 nm λ_{ex}- 310 nm	4.34%	2016	[210]
Chlorophyll	Water	Hydrothermal	DLS- 18 nm	λ_{em}- 520 nm λ_{ex}- 440 nm	-	2017	[211]
Microcrystalline cellulose	Ethylenediamine	Hydrothermal	TEM- 3.2 nm	λ_{em}- 426–436 nm λ_{ex}- 360 nm	55%	2017	[212]
o-Phenylenediamine	Ethanol	Hydrothermal	TEM- 1–2 nm	λ_{em}- 400–600 nm λ_{ex}- 350–500 nm	20%	2018	[213]
Carbon paper	Nitric acid	Hydrothermal	TEM- 4.8 nm	λ_{em}- 450 nm λ_{ex}- 350 nm	5.1%	2018	[214]
Papain and PEG6000	Ultrapure water	Hydrothermal	TEM- 2–3 nm	λ_{em}- 420 nm λ_{ex}- 320 nm	9.45%	2018	[215]
Dextrose solution	Hydrochloric acid	Mechano-chemical	TEM- 10 nm	λ_{em}- 456 nm λ_{ex}- 390 nm	40%	2018	[216]
1,2,4,5-Benzenetetramine tetrahydrochloride	Ethanol	Solvothermal	TEM- 9.39 nm	λ_{em}- 605 nm λ_{ex}- 540 nm	30.2%	2019	[217]
1,2,4-Benzenetriamine dihydrochloride			TEM- 8.60 nm	λ_{em}- 598 nm λ_{ex}- 510 nm	13.4%		
o-Phenylenediamine			TEM- 6.50 nm	λ_{em}- 538 nm λ_{ex}- 420 nm	16.7%		
Copper (II) chloride dihydrate	Ethanediamine	Hydrothermal	TEM- 1.8 nm	λ_{em}- 380 nm λ_{ex}- 320 nm	7.8%	2019	[218]
Glucose and taurine	Distilled water	Hydrothermal	TEM- 3 nm	λ_{em}- 410 nm λ_{ex}- 340 nm	11%	2019	[219]
Polyethylene glycol	-	Pyrolysis	DLS- 10 nm	λ_{em}- ~380 nm λ_{ex}- 340 nm	16%	2020	[220]
m-Phenylenediamine	Deionized water	Hydrothermal	TEM- 5.1 nm	λ_{em}- 420 nm λ_{ex}- 340 nm	12%	2020	[221]
Glucosamine	Ethylenediamine and water	Microwave digestion	TEM- 4.45 nm	λ_{em}- 466 nm λ_{ex}- 384 nm	25.38%	2020	[222]
Lactose	Hydrochloric acid	Hydrothermal	TEM- 7 to 8 nm	-	-	2021	[223]
Selenourea and o-phenylenediamine	Hydrochloric acid	Hydrothermal	TEM- 3 nm	λ_{em}- 625 nm λ_{ex}- 564 nm	23.6%	2021	[224]
Glutaraldehyde	Ethanol	Solvothermal	TEM- 1 nm	λ_{em}- 453 nm λ_{ex}- 360 nm	-	2021	[225]
Nitrobenzaldehyde			TEM- 5 nm	λ_{em}- 421 nm λ_{ex}- 360 nm			
Benzaldehyde			-	λ_{em}- 430 nm λ_{ex}- 360 nm			
Diphenyl ether	p-Phenylenediamine		TEM- 2.8 nm	λ_{em}- ultraviolet λ_{ex}- 285 nm	8%	2021	[226]
	p-Phenylenediamine, dopamine and tris (hydroxymethylaminomethane)		TEM- 10–18 nm	λ_{em}- red λ_{ex}- 285 nm	15.5%		

Table 9. *Cont.*

Precursor		Technique	Properties			Year	Reference
Carbon Source	Passivation/Solvent		Particle Size	Fluorescence	Quantum Yield		
o-Phenylenediamine	Ethanol	Two separate solutions mixed in one-pot hydrothermal	TEM- 5 nm	λ_{em}- ~570 nm λ_{ex}- 430 nm	-	2022	[227]
Ammonium sulfate	Deionized water						
Glucose	Deionized water	Hydrothermal	TEM- 8.9 nm	λ_{em}- 450 nm λ_{ex}- 350 nm	-	2022	[228]
	Boric acid		TEM- 6.2 nm	λ_{em}- 400 nm λ_{ex}- 320 nm			
	Sodium persulfate		TEM- 6.9 nm	λ_{em}- 400 nm λ_{ex}- 320 nm			
	Urea		TEM- 5.6 nm	λ_{em}- 450 nm λ_{ex}- 390 nm			
p-Phenylenediamine and thylenediamine	Anhydrous ethanol	Hydrothermal	TEM- 2.76 nm	-	-	2022	[229]
m-Phenylenediamine	Ethanol	Solvothermal	TEM- 6.9 nm	λ_{em}- 440 nm λ_{ex}- 380 nm	11%	2022	[230]
o-Phenylenediamine			TEM- 7.8 nm	λ_{em}- 550 nm λ_{ex}- 380 nm	17%		

4. Application of CD-Based Optical Sensor for Environmental Monitoring

The incorporation of CDs in optical sensors for environmental monitoring, including the detection of heavy metal ions, phenol, pesticides, and nitroaromatic explosives, are reviewed below (Figure 6). This review aims to survey state-of-the-art CD-based optical sensors with their sensing performance, namely range of detection, limit of detection, and linear correlation coefficient.

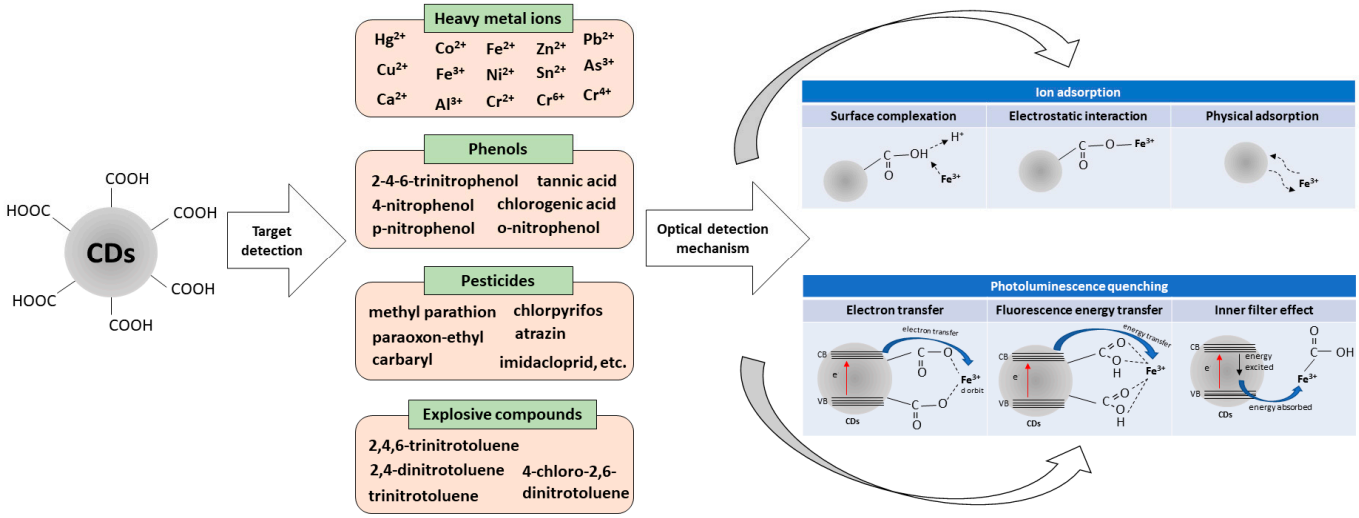

Figure 6. Schematic diagram of target detection and possible detection mechanism.

4.1. Heavy Metal Ions

Environmental pollutions caused by toxic heavy metal ions (HMI) have resulted in the development of different optical sensors using nanoscale materials [231–237]. Of late, CD-based optical sensors have garnered tremendous research interest, which is summarized chronologically in Table 10. Herein, an optical fibre sensor for Hg^{2+} and Cu^{2+} detection was developed using CDs functionalized with poly(ethylene glycol) and N-acetyl-l-cysteine [238]. This sensor has quite interesting analytical potential, as it allows for higher linear coefficients when detecting Hg^{2+} in aqueous solutions. Furthermore, the concentration range of Hg^{2+} was successfully lowered to femtomolar detection using a fluorescent sensor [199]. The outstanding nature of the sensing performance can be probably attributed

to the Hg^{2+} ions, which have stronger affinity toward carboxylic groups on the surface of CDs and stronger quenching effect on the PL of the prepared CDs.

On the other hand, Co^{2+} and Cu^{2+} ions have been detected using CD-based composites. In the presence of CTAB to PEG-passivated CDs, a long fluorescence lifetime with higher emission efficiency was noticed due to the rapid production of •OH radicals from the Co(II)-H_2O_2-OH^- system, which is responsible for the highly selective response of the present chemiluminescence system towards Co^{2+} ions [200]. On the other hand, the electrochemiluminescence of the oxidized CDs/$K_2S_2O_8$ system resulted in higher quenching to 20 nM of Cu^{2+} compared to 1 μM of Pb^{2+}, Ni^{2+}, Mn^{2+}, Fe^{2+}, and Co^{2+} [201]. Another HMI of interest is Fe^{3+}, which have been detected three times in a row in the year of 2014 using diverse optical sensors [116,117,119]. Among them, the phenolic hydroxyl of N-doped CDs exhibited higher sensitivity toward Fe^{3+} quenching, with the linearity range of 0.01−500 μM and detection limit of 2.5 nM [116]. The reason is that the hydroxyl group has a good binding affinity for Fe^{3+}, leading to the splitting of d orbital of Fe^{3+} and consequently causing significant fluorescent quenching. Similarly, nitrogen-doped CQDs were used as an effective fluorescent sensing platform for label-free sensitive detection of Hg^{2+} ions in an ultrapure water solution with a detection limit of 0.23 μM [118]. Due to the excellent sensitivity and selectivity of the Hg^{2+} sensor, this sensor was further applied to the determination of Hg^{2+} in tap water and real lake water samples. The results showed that the PL intensity (excited at 360 nm) decreased gradually with the increasing concentration of Hg^{2+} in both tap water and lake water from 5 to 50 μM.

In other work, the sensing potential of fluorescent CDs synthesized through the pyrolysis method was evaluated for Cu (II), Cr (II), Co (II), Ni (II), Al (III), Ca (II), Pb (II), Zn (II), Sn (II) and Hg (II) ions [79]. Among all the metal ions tested, Cu (II) and Pb (II) have the highest sensitivity, while Zn (II), Hg (II) and Ca (II) have the lowest sensitivity. The reason for this relatively low sensitivity might be due to the diamagnetic properties of Zn (II), Hg (II) and Ca (II) ions, which eliminate the paramagnetic quenching mechanism with the CDs.

With the accelerating demand of mercury in the skin lightening industry, a high number of optical techniques for Hg^{2+} have been reported [15,23,54,65,89,122,124–128,133,142,143,152,153,160,178,207]. Notably, fluorescence techniques are the most employed. Altogether, there are several phenomena about the quenching effect of CDs to Hg^{2+}, which are as follows: (i) electron transfer from excited nitrogen and sulfur atoms in CDs to Hg^{2+} (nonradiative recombination); (ii) strong binding between Hg^{2+} and S atoms or carboxylate or hydroxyl groups from CDs; and (iii) Hg^{2+} has a larger ionic radius and polarization; therefore, deformation happened more easily when it interacted with the nitrogen and sulfur atoms. Fortunately, the Hg^{2+} can be detected as low as 2.6 nM using CD-labeled oligodeoxyribonucleotide (ODN) and quenched by graphene oxide [122]. In this study, CD-ODN acted as the energy donor and molecular recognition probe and GO served as the fluorescence resonance energy transfer acceptor.

Due to the concerns about improving and protecting living organisms, more optical detection methods that utilize CDs as a sensing element have been developed to detect $Fe^{2+/3+}$ [13,22,38,40,72,78,87,124,135,142,151,159,166,169,219,226], Cu^{2+} [53,66,97,141,227,239], Pb^{2+} [65,87,181,240], $Cr^{6+/4+}$ [23,85,193,241], and Co^{2+} [51]. For instance, Shamsipur et al. (2018) prepared green-emitting CDs instead of common blue-emitting CDs for selective and sensitive detection of Fe^{3+} [159]. This green CDs approach could detect Fe^{3+} in the range of 0.05–10.0 μM, with a detection limit of 0.0137 μM. The detection limit was found to be significantly lower than the maximum level of Fe^{3+} (0.54 μM) allowed in drinking water by the U.S. Environmental Protection Agency.

Li et al. (2021) invested in interesting research to detect low concentrations of Pb^{2+} ions [181]. An electrochemiluminescence (ECL) aptasensor was prepared by modifying a glassy carbon electrode (GCE)/NCQDs with amino aptamers by NHS/EDC linkage for selective and sensitive detection of Pb^{2+}. As shown in Figure 7, the binding of the hairpin aptamer with Pb^{2+} forms the G-quadruplex, and thus exposes the amino group

to the NCQDs, causing significant changes in ECL intensity. The results revealed that the GCE/NCQDs/aptamer sensor can detect Pb^{2+} quickly and accurately, providing the lowest detection limit of 18.9 pM. Importantly, the proposed aptasensor did not suffer from interference and it had excellent stability.

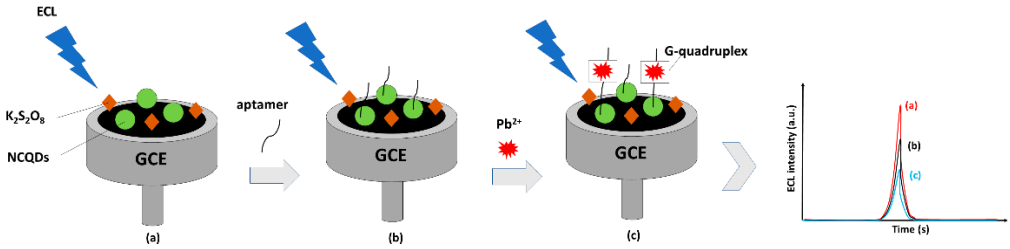

Figure 7. Surface functionalization of (**a**) GCE/NCQDs, (**b**) GCE/NCQDs/aptamer, and (**c**) GCE/NCQDs/aptamer/Pb^{2+}.

The fabrication of CDs with industrial/agricultural waste has proven to be useful as a detection probe for metal ions. A study conducted by Yan et al. (2020) demonstrated that the synthesized N-CDs from crown daisy leaves had abundant surface functional groups that could selectively and sensitively detect Cu^{2+} at a very low detection limit of 1.0 nM by the fluorescent quenching effect [53]. This result is due to the selective complexation interaction between Cu^{2+} and carboxyl and amino groups of the N-CDs.

On the other hand, improving the detection performance of hexavalent chromium (Cr^{6+}) even at the nanomolar level has become an enduring concern of researchers. Rajendran and Rajendiran (2018) reported that the CQDs can be effectively used as fluorescent probes for the detection of Cr^{6+} at the nanomolar level [23]. This research reported strong fluorescence quenching with increasing Cr^{6+} concentration, resulting in an improved detection limit of 10 nm. Nevertheless, the detection limit of Co^{2+} was found to be higher at the micromolar level despite using CD-based optical sensors [51]. The proposed sensor was then applied in the analysis of real river water samples with a recovery value of 95.0–106.8% and a relative standard deviation below 5.3%, indicating that the synthesized CDs had great application prospects in Co^{2+} detection.

4.2. Phenols

The existence of different forms of phenolic in petrochemical engineering, printing, food processing, and dyeing has been continuously reported as the most harmful pollutant due to its high toxicity and low biodegradability [242]. Table 11 summarizes the chronological order of the detection of phenolic compounds using optical sensors. Among the reported studies, 2-4-6-trinitrophenol, also called picric acid, is the most common pollutant monitored by means of fluorescent sensor [72,112,114,134,136,150,170,221]. It is well known that 2-4-6-trinitrophenol is a representative electron-deficient nitroaromatic, due to the electron-withdrawing nature of the three nitro groups. From the perspective of the sensor performance, Niu et al. (2013) explored the feasibility of using amine-capped CDs for the detection of 2-4-6-trinitrophenol in aqueous and ethanol solutions [114]. For the detection of 2-4-6-trinitrophenol in ethanol, the amine-capped CDs demonstrated obvious fluorescent quenching and superior sensitivity to 2-4-6-trinitrophenol in aqueous solution. Since water is much more polar than ethanol, the detection is, therefore, driven by an electrostatic interaction between 2-4-6-trinitrophenol and CDs.

Generally, there are three possible mechanisms causing fluorescence quenching between the phenolic compounds and proposed CDs, which are as follows: (i) electron transfer; (ii) fluorescence energy transfer; and (iii) inner filter effect. Amid all the mechanisms, fluorescence energy transfer (FET) is a dominant quenching pathway due to the electron-rich nature of the CDs and the electron-deficient aromatic group of the phenol [115,134,243]. In contrast to FET, the electron transfer process became possible for phenol fluorescence quenching [112,150,204]. Notably, electron transfer in the excited state of CDs can occur

from the lowest unoccupied molecular orbital (LUMO) to the LUMO of phenols, if possible. In addition, there are certain rules that are required to fulfil FET quenching. The rules are as follows: (i) the absorption spectrum of the quencher (phenols) should overlap with the emission spectrum fluorophore and (ii) there is a change in the fluorescence lifetime of CDs before and after the addition of the quencher. Furthermore, the inner filter effect (IFE) is also considered important and has been applied as a developing novel fluorescent assay in recent studies [34,136,170,218,219,226]. This approach offers more simplicity and expediency because IFE-based sensors use fluorophore and the receptor directly rather than chemically interacting with each other.

In another study, Xue et al. (2018) found that phenol can form hydrogen bonds with the carboxyl group on the surface of the fluorescence CQDs, which will facilitate the fluorescence quenching of the CQDs in the excited state, leading to the high sensitivity and selectivity of CQDs for the detection of phenol [95]. In addition, the fluorescence quenching effect can be explained by either a dynamic or static process. Interestingly, a static quenching effect between N-CDs and tannic acid found in the works of [167] can be proved by several measurements, which are as follows: (i) a decrease in the fluorescence lifetime; (ii) a rate that is constant more than 1.0×10^{10} $M^{-1}s^{-1}$; and (iii) a blue-shift of the absorption peak of CDs. Wang et al. (2019) compared the selectivity of the CDs@MIP and CDs@MIP to 4-nitrophenol, which resulted in good selectivity of CDs@MIP on 4-nitrophenol, due to the hydrogen bonding interactions, leading to the charge transfer from CDs to 4-nitophenol [165]. There is still much room for further development of CD-based optical sensors for the detection of phenolic compounds, despite achieving a high quantum yield and good sensing performance. For instance, Saravanan et al. (2020) successfully synthesized N@CDs from m-phenylenediamine as a single source of carbon and nitrogen to detect 2-4-6-trinitrophenol [221]. The fluorescent N@CD probe showed high selectivity toward 2-4-6-trinitrophenol relative to other nitro explosives, such as 4-nitrophenol, 4-amino-3-nitrophenol, 2,5-dinitrophenol, phenol, 2-chlorophenol, 3-nitrophenol, and 4-amino-triphenol.

Table 10. Summary of the developed optical sensors for heavy metal ions detection.

Heavy Metal Ions	Material	Optical Sensor	Range of Detection	Limit of Detection	Linear Correlation Coefficient	Year	Reference
Hg^{2+}	CDs@PEG and N-acetyl-l-cysteine	Optical fibre	0–2.69 µM	-	0.977	2010	[238]
Cu^{2+}					0.975		
Hg^{2+}	CDs	Fluorescent	0–5 fM	1 fM	-	2013	[199]
Co^{2+}	CTAB@CDs	Chemiluminescent	1.0–1000 nM	0.67 nM	0.992	2013	[200]
Cu^{2+}	o-CDs/$K_2S_2O_8$	Electrochemiluminescent	0–4 nM	-	-	2013	[201]
Fe^{3+}	N-CDs	Chemiluminescent	1.0×10^{-7}–1.0×10^{-6} M	66.7 nM	0.993	2014	[117]
Fe^{3+}	N-doped CDs	Fluorescent	0.01–500 µM	2.5 nM	-	2014	[116]
Fe^{3+}	CDs	Electrochemiluminescent	5–80 µM	700 nM	0.993	2014	[119]
Hg^{2+}	N-CQDs	Fluorescent	0–25 µM	0.23 µM	0.994	2014	[118]
Pb^{2+}	CDs	Fluorescent	0–47.62 µM	7.49 µM	-	2014	[79]
Cu^{2+}				7.78 µM			
Al^{3+}				13.38 µM			
Ni^{2+}				13.90 µM			
Co^{2+}				18.07 µM			
Cr^{2+}				23.69 µM			
Sn^{2+}				31.51 µM			
Ca^{2+}				34.79 µM			
Hg^{2+}				38.02 µM			
Zn^{2+}				69.64 µM			

Table 10. *Cont.*

Heavy Metal Ions	Material	Optical Sensor	Range of Detection	Limit of Detection	Linear Correlation Coefficient	Year	Reference
Fe^{3+}	CDs	Fluorescent	0.10–10 μM	31.5 nM	0.9977	2015	[124]
Hg^{2+}			0.01–2.0 μM	15.3 nM	0.9977		
Hg^{2+}	CDs	Fluorescent	0.01–10 μM	3.3 nM	0.997	2015	[128]
Hg^{2+}	ODN-CDs	Fluorescent	5–200 nM	2.6 nM	0.974	2015	[122]
Hg^{2+}	N-S-CDs	Fluorescent	0–40 μM	2.0 μM	0.994	2015	[125]
Hg^{2+}	N-CDs	Fluorescent	0–8 μM	0.087 μM	0.9962	2015	[127]
Hg^{2+}	N,S-co-doped CDs	Fluorescent	0–20 μM	0.18 μM	0.9975	2015	[126]
Hg^{2+}	N-rich CDs	Fluorescent	0–20 μM	0.63 μM	0.989	2016	[207]
Fe^{3+}	N-doped CDs	Fluorescent	0–1000 μM	100 μM	-	2016	[135]
Fe^{3+}	N-CDs	Fluorescent	0–1000 μM	0.96 μM	-	2016	[13]
Hg^{2+}	LR-CDs	Fluorescent	0.1–1.5 μM	18.7 nM	0.9919	2016	[64]
			2.0–60.0 μM		0.994		
Hg^{2+}	CDs	Fluorescent	0–80 μM	0.201 μM	0.9982	2016	[133]
Pb^{2+}	CDs	Fluorescent	0.01–1.0 μM	0.59 nM	0.998	2017	[65]
Cu^{2+}	Nitrogen-doped CDs	Fluorescent	0.5–4 μM	0.38 μM	0.998	2017	[141]
Hg^{2+}	CDs	Fluorescent	0–0.5 mM	0.78 μM	0.9944	2017	[142]
Fe^{3+}			0–0.15 mM	1.17 μM	0.9977		
Hg^{2+}	Nitrogen-doped CQDs	Fluorescent	0–18 μM	83.5 nM	0.9979	2017	[143]
Hg^{2+}	CDs	Fluorescent	0–40 μM	9 nM	0.9896	2017	[15]
Fe^{3+}	N-CQDs	Fluorescent	0–300 μM	0.16 μM	0.9811	2018	[22]
Cr^{6+}	CDs	Fluorescent	0–100 μM	0.73 μM	0.9903	2018	[85]
Cu^{2+}	CQDs	Fluorescent	1–8 μM	6.33 nM	0.998	2018	[97]
Cu^{2+}	CDs	Fluorescent	0.01–500 μM	4.3 nM	0.9907	2018	[66]
Cu^{2+}	CQDs	Fluorescent	0–100 μM	31.5 μM	0.9897	2018	[239]
Fe^{3+}	CdSe@SiO_2-CDs	Fluorescent	9–120 μM	0.26 μM	0.995	2018	[151]
Fe^{3+}	CDs	Fluorescent	0.05–10.0 μM	13.7 nM	0.992	2018	[159]
Hg^{2+}	N-CDs	Fluorescent	0.001–5 μM	0.65 μM	0.985	2018	[160]
Hg^{2+}	CDs	Fluorescent	0–100 μM	2.47 μM	0.9892	2018	[152]
Hg^{2+}	N-S-CDs	Fluorescent	0.01–50 μM	0.008 μM	0.9622	2018	[153]
Hg^{2+}	CQDs	Fluorescent	5–70 nM	8 nM	0.9970	2018	[23]
Cr^{6+}				10 nM	0.9956		
Fe^{3+}	CDs	Fluorescent	1–700 μM	<1 μM	0.993	2019	[219]
Fe^{2+}	CDs	Optical microfiber	0–5.372 μM	0.179 μM	-	2019	[166]
Co^{2+}	CDs	Fluorescent	1–2 μM	0.39 μM	0.9912	2019	[51]
Pb^{2+}	VV-CDs	Fluorescent	1–100 μM	12 nM	0.99853	2020	[87]
Fe^{3+}				16 nM	0.99933		
Pb^{2+}	GCE/NCQDs/aptamers	Electrochemiluminescence	50–387.9 nM	0.0189 nM	0.998	2020	[181]
As^{3+}	CDs-MnO_2	Fluorescent	0–200 nM	16.8 nM	0.992	2020	[177]
Cu^{2+}	CDs	Fluorescent	0–120 nM	1.0 nM	0.997	2020	[53]
Fe^{3+}	Phe-CDs	Fluorescent	5–500 μM	0.720 μM	0.9959	2020	[169]
Hg^{2+}	N-CDs	Fluorescent	0.15–90 μM	0.20 μM	0.993	2020	[178]
Hg^{2+}	CDs	Fluorescent	0.01–5 μM	6.25 nM	0.991	2020	[54]
Cr^{4+}	S, N-CDs	Fluorescent	0.03–50 μM	21.14 nM	0.996	2021	[193]
Fe^{3+}	N-CDs	Fluorescent	0.3–3.3 μM	0.135 μM	0.9918	2021	[72]
Fe^{3+}	CDs@PDA	Fluorescent	2–27 μM	3.75 μM 5.82 μM	0.994 0.991	2021	[226]
Pb^{2+}	N-CDs/R-CDs@ZIF-8	Fluorescent	0.05–50 μM	4.78 nM	0.9952	2021	[240]
Cr^{6+}	BNCDs	Fluorescent	0–100 μM	0.41 μM	0.999	2021	[241]

Table 10. *Cont.*

Heavy Metal Ions	Material	Optical Sensor	Range of Detection	Limit of Detection	Linear Correlation Coefficient	Year	Reference
Fe^{3+}	KBNCDs	Fluorescent	0–25 μM	1.2 μM	0.997	2022	[78]
Mn^{2+}				1.4 μM	0.998		
Hg^{2+}	CDs	Fluorescent	0–46 μM	2 μM	0.997	2022	[89]
Fe^{3+}	CDs	Fluorescent	20–100 μM	0.07 μM	0.9977	2022	[38]
Fe^{3+}	M-CDs	Fluorescent	5–30 μM	0.47 μM	0.998	2022	[40]
Cu^{2+}	NS-CDs	Colorimetric	1–100 μM	200 nM	0.99481	2022	[227]

Where CDs@PEG: carbon dots functionalized poly(ethylene glycol), CTAB: cationic cetyltri-methylammonium bromide, o-CDs/$K_2S_2O_8$: oxidized carbon dots/potassium persulfate, N-CDs: nitrogen doped carbon dots, N-CQDs: nitrogen doped carbon quantum dots, ODN-CDs: carbon dots-labeled oligodeoxyribonucleotide, N,S-CDs: nitrogen and sulphur co-doped carbon dots, LR: lotus root, CdSe@SiO_2-CDs: silica coated cadmium selenide carbon dots, VV-CDs: *Volvariella volvacea*-carbon dots, GCE: glassy carbon electrode, MnO_2: manganese dioxide, Phe-CDs: phenylalanine-carbon dots, CDs@PDA: p-phenylenediamin-derived carbon dots, N-CDs/R-CDs@ZIF-8: nitrogen-doped carbon dots/red-carbon dots@zeolite imidazole, BNCDs: boron-nitrogen co-doped carbon dots, KBNCDs: Kentucky bluegrass nitrogen-doped carbon dots, M-CDs: *Morus nigra* carbon dots, Hg^{2+}: mercury ions, Cu^{2+}: copper ions, Co^{2+}: cobalt ions, $Fe^{3+}/^{2+}$: ferric ions, Pb^{2+}: lead ions, Al^{3+}: aluminum ions, Ni^{2+}: nickel ions, $Cr^{2+}/^{4+}/^{6+}$: chromium ions, Sn^{2+}: tin ions, Ca^{2+}: calcium ions, Zn^{2+}: zinc ions, As^{3+}: arsenic ions.

Table 11. Summary of the developed optical sensors for phenol detection.

Phenolic Compound	Material	Optical Sensor	Range of Detection	Limit of Detection	Linear Correlation Coefficient	Year	Reference
2-4-6-Trinitrophenol	Amine-capped CDs	Fluorescent	0–50 × 10^{-5} M	0.9996 μM	-	2013	[114]
2-4-6-Trinitrophenol	Tb-CDs	Fluorescent	500 nM–100 μM	200 nM	0.991	2013	[112]
4-Nitrophenol	CDs	Fluorescent	0.1–50 μM	28 nM	-	2014	[115]
Tannic acid	PEGA-CDs	Fluorescent	0.05–0.6 μM	0.01 μM	-	2015	[204]
2-4-6-Trinitrophenol	N-CQDs	Fluorescent	0.27–34.1 μM	50 nM	0.992	2016	[134]
2-4-6-Trinitrophenol	CDs	Fluorescent	0.1–26.5 μM	51 nM	0.995	2017	[136]
2-4-6-Trinitrophenol	CDs	Fluorescent	-	0.127 μM	-	2018	[150]
Phenol	CDs	Fluorescent	0–50 μM	0.076 μM	0.998	2018	[95]
Tannic acid	N-CDs	Fluorescent	0.4–9.0 μM	0.12 μM	0.9990	2019	[167]
4-Nitrophenol	CDs@MIPs	Fluorescent	0–0.03594 mM	35 nM	-	2019	[165]
p-Nitrophenol	Cu-doped carbon dots	Fluorescent	0.5–50 μM	0.08 μM	0.998	2019	[218]
2-4-6-Trinitrophenol	CDs	Fluorescent	0–305.54 μM	0.023 μM	-	2020	[170]
o-Nitrophenol	CQDs	Fluorescent	0.08–40 μM	15.2 nM	0.999	2020	[34]
4-Nitrophenol	N,CDs	Fluorescent	0.25–125 μM	0.05 μM	0.9919	2020	[222]
2-4-6-Trinitrophenol	N@CDs	Fluorescent	1–75 μM	2.45 μM	0.994	2020	[221]
Trinitrophenol	wsNP-CDs	Fluorescent	100–300 μM	23 μM	0.9861	2020	[243]
Tannic acid	Nitrogen-doped CDs	Chemiluminescence	0.2–10 μM	39.3 nM	0.9971	2020	[173]
Chlorogenic acid	N,S-CDs	Fluorescent	0.9314–83.82 μM	0.3387 μM	0.9970	2021	[184]
4-Nitrophenol	CDs@PDA	Fluorescent	2–34 μM	7.29 μM 3.44 μM	0.992 0.993	2021	[226]
2-4-6-Trinitrophenol	N-CDs	Fluorescent	0.3–3.3 μM	0.11 μM	0.9923	2021	[72]
p-Nitrophenol	G-CDs	Fluorescent	0–50 μM	0.0175 μM	0.9951	2022	[76]

Where Tb-CDs: terbium doped carbon dots, PEGA-CDs: polyethyleneglycol bis(3-aminopropyl)-carbon dots, CDs@MIPs: carbon dots fabricated with molecularly imprinted polymers, N@CDs: nitrogen doped carbon dots, wsNP-CDs: water soluble nitrogen and phosphorous doped carbon dots, CDs@PDA: polydopamine encapsulated carbon dots, G-CDs: green-emitting carbon dots.

In addition, ultra-weak chemiluminescent (CL) systems have become one of the focuses of the increasing attention on the determination of tannic acid [173]. Interestingly,

tannic acid could dramatically suppress the CL intensity of the FNCDs-H_2O_2-$K_3Fe(CN)_6$ system with an excellent linear response (R^2 = 0.9971) and was further applied for the determination of tannic acid in a red wine sample. The recovery of 98.9–102.1% was obtained, demonstrating its reliability and application potential in real sample analysis. Recently, the aggregated N,S-CDs as a dual-excitation ratiometric fluorescent probe have proven to be an effective approach for the quantitative determination of chlorogenic acid [184]. Apart from dual excitation, Liu et al. (2021) observed the dual-color fluorescence emission of ultraviolet and red light when detecting 4-nitrophenol using CDs@PDA [226]. The detection limits obtained for the ultraviolet and red-light emission were 3.44 μM and 7.29 μM, respectively. In addition, 2-4-6-trinitrophenol has been detected using the fluorescence method with a detection limit of 0.11 μM in the concentration range of 0.3–3.3 μM [72]. The possible mechanism for fluorescence quenching of N-CDs by 2-4-6-trinitrophenol is explained by the electrostatic interaction or hydrogen bonding that occurs between the nitrogen groups of CDs and phenolic group of 2-4-6-trinitrophenol. To be exact, the electrostatic interactions occur when a large number of nitro groups with electron-withdrawing characteristics on benzene interact with nitrogen-containing functional groups of CDs. Hence, it can be concluded that nitro groups play a vital role in fluorescent quenching.

4.3. Pesticides

Pesticides are chemical compounds that are used to kill pests. Generally, there are six classes of pesticides according to their target species, i.e., insecticides, herbicides, rodenticides, bactericides, fungicides, and larvicides. The largest and most widely used in crop protection are insecticides [244]; however, they are classified as an extremely toxic class of chemical compounds by the World Health Organization (WHO).

Organophosphorus (OP) compounds, such as methyl parathion [121,138], paraoxon-ethyl [137], dichlorvos [245], malathion [245], ethion [245], paraoxon [154,155,211], chlorpyrifos [63,96,246], methyl-paraoxon [180], diazinon [50,62], and quinalphos [247], [63], are widely reported insecticides in the development of CD-based optical sensors. Oddly, most OP pesticides are always selected as inhibitors for sensors based on enzyme activity. According to Hou et al. (2016), dichlorvos can inhibit the activity of acetyl cholinesterase (AChE), which can turn the fluorescence of CDs off again [245], which is similar to the detection of paraoxon [155]. However, in a study of Lin et al. (2017), only OP of chlorpyrifos effectively inhibited H_2O_2 production by destroying the acetylcholinesterase activity, thereby increasing the fluorescence of C-dots after being initially turned off by Fe^{3+} [96]. Moreover, the proposed sensor exhibits a low selectivity against OP. Therefore, a new facile fluorescence probing based on novel N-doped carbon dots and methyl parathion hydrolase (MPH) was developed to detect methyl parathion selectively [138]. The use of MPH in this study helps to degrade OP compounds and has many advantages over other enzymes, such as less background noise and high turnover number, which is favourable for sensitive detection.

Another class of insecticide is carbamates. Li and co-workers have been devoted to detecting carbaryl in the presence of acetylcholinesterase (ACh) and choline oxidase (ChOx) by using N-CQDs, S-CQDs, and co-doped N, S-CQD-based photoluminescence sensors [209]. The results demonstrated that high sensitivity originates from the N and S dopants, which offer stronger capacities to adsorb hydrogen peroxide (H_2O_2) and generate local states to trap hot electrons, promoting the electron transfer to H_2O_2, and thus resulting in the strong quenching of the CQD fluorescence.

Apart from the insecticide organophosphate, insecticides neonicotinoids and organochlorine have become a target pesticide. Mandal et al. (2019) have reported a simple fluorescence-based method using CDs for the detection of commonly used insecticides, such as imidacloprid and lindane [246]. The fluorescence emission of the CDs was found to be enhanced in the presence of the increasing concentration of imidacloprid; however, the emission was quenched in the presence of lindane. The interactions between CDs and insecticides were mainly driven by the high reactive -NO_2 and -NH groups in imidacloprid that directly bind

to the surface functionality amino groups of CDs and by the H-bond or week ionic interaction or covalent binding between the free surface groups of the CDs and lindane, followed by the substitution reaction. In addition, the researchers also expanded the potential of CDs in sensing unclassified pesticides, namely tetradifon [246]. The leaving groups (-Cl) of tetradifron were found to possessstrong covalent binding with the surface amine group of the CDs with a high affinity. Nonetheless, the results showed that tetradifron has a higher detection limit than imidacloprid, but offers a lower detection limit than lindane. This phenomenon can be attributed to the binding affinity of all the different target pesticides. Their binding affinity can be arranged in the following decreasing order: imidacloprid > tetradifron > lindane.

Until 2021, the fluorescence response of CDs towards herbicides [50,60,213,220,246] and fungicides [73,182,183] has also been explored. It is reported that with increasing concentrations of herbicides, i.e., atrazine [213], pretilachlor [60], glyphosate [50], and fungicide thiophanate methyl [183], this has resulted in an increase in PL emission intensity (turn-on). This fluorescence 'turn-on' model was dynamic quenching, whereas, when the concentrations of trifluralin [220], pyrimethanil [182], and isoprothiolane [73] were increased, the fluorescence emission of CDs was found to decrease, leading to static quenching. Supchocksoonthorn et al. (2021) suggested that the fluorescent quenching is closely related to the inner filter effect, due to the π-π interaction between the large aromatic core of the CDs and anilinopyrimidine unit of pyrimethanil and between their polar functional groups [182].

Furthermore, as an improvement to the method with a single fluorescence signal, Zhu et al. (2022) developed a new type of CD-functionalized core-shell nanospheres as a ratiometric fluorescence to detect λ-cyhalothrin (LC), a typical pyrethroid insecticide. Figure 8 shows the main binding reactions in the preparation of the CD-functionalized core-shell nanospheres. Here, silica nanoparticles play a role in preventing the contact between m-CDs and the dispersion solvent so the m-CDs could act as a reliable reference background; o-CDs act as a fluorescence signal; 3-aminopropyrtriethoxy silane (APTES) as a functional monomer to connect with LC through hydrogen bonding; ionic liquids (IL) as a cationic surfactant, which are attached to the system by electrostatic interaction to enhance the fluorescence of the core-shell nanospheres; and tetraethyl orthosilicate (TEOS) is used to form a layer of imprinted silicon shell on the surface of m-CDs@SiO_2. Inspired by the role of materials, these newly formed core-shell nanospheres managed to achieve lower detection limits, excellent reusability, and better precision than those of other methods reported in this work [230]. All the proposed CD-based optical sensors for the detection of pesticides are tabulated orderly in Table 12.

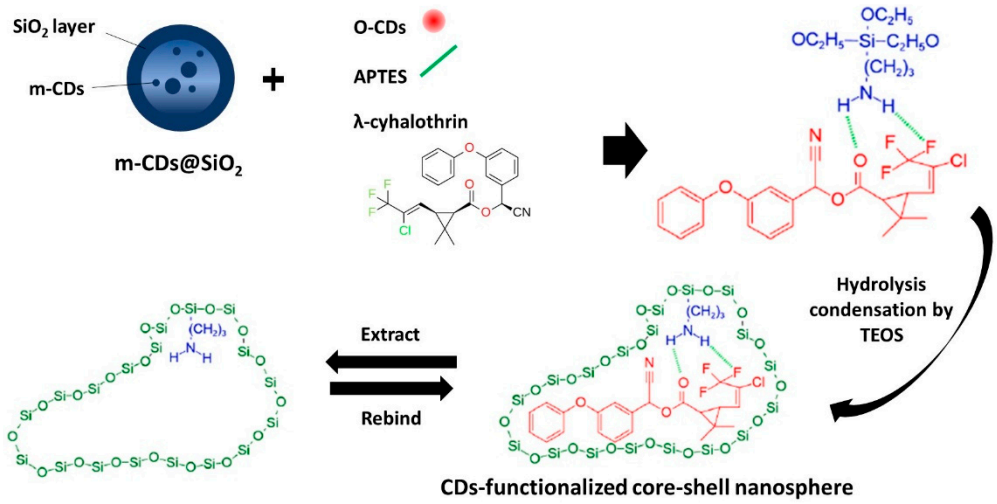

Figure 8. Schematic diagram of binding reactions of the prepared CD-functionalized core-shell nanospheres for detection of λ-cyhalothrin.

Table 12. Summary of the developed optical sensors for pesticides detection.

Pesticide	Material	Optical Sensor	Range of Detection	Limit of Detection	Linear Correlation Coefficient	Year	Reference
Methyl parathion	Tyr-CDs	Fluorescent	1.0×10^{-10}–1.0×10^{-4} M	4.8×10^{-11} M	0.997	2015	[121]
Paraoxon-ethyl	CDs	Fluorescent	0–5.80 mM	0.22 μM	0.9974	2016	[137]
Dichlorvos, malathion, ethion	CDs/Cu(II)/AChE/ATChCl	Fluorescent	6 nM–0.6 nM 6 nM–0.8 nM 8 nM–0.8 nM	3.8 nM 3.4 nM 4.2 nM	0.998 0.996 0.997	2016	[245]
Carbaryl	N,S co-doped CQDS	Photoluminescent	0.00003131–3.131 μM	0.02485 μM	-	2016	[209]
Paraoxon	CQDs	Fluorescent	0.1817–181.7 nM	0.1817 nM	0.994	2017	[211]
Paraoxon	BChE-ATCh-MnO_2-CDs	Fluorescent	0.1817–18.17 nM	0.05451 nM	0.9941	2017	[155]
Chlorpyrifos	Fe-modified CDs	Fluorescent	0.028523–2.8523 μM	0.008557 μM	-	2017	[96]
Methyl parathion	N-doped CDs-MPH	Fluorescent	2.38–73.78 μM	0.338 μM	0.9934	2017	[138]
Paraoxon	CDs	Fluorescent	0–1.817 μM	0.00145 μM	0.993	2018	[154]
Atrazine	N-CQDs	Fluorescent	0–1.0 nM	3 pM	0.9812	2018	[213]
Atrazine; chlorpyrifos; imidacloprid; lindane; tetradifon	CDs	Fluorescent	-	0.12 μM; 0.029 μM; 0.013 μM; 0.14 μM; 0.04 μM	-	2019	[246]
Pretilachlor	CDs	Fluorescent	5.7 μM–61.5 μM	2.9 μM	0.9847	2019	[60]
Diazinon	CDs	Fluorescent	0.8214 nM–16.43 μM	0.8214 nM	-	2020	[50]
Glyphosate			1.4787 nM–29.574 μM	0.01183 μM			
Amicarbazone			1.036 nM–20.72 μM	0.002072 μM			
Methyl-paraoxon	B,N-CDs	Fluorescent	0.1–15 μM	0.1 μM	0.9967	2020	[180]
Diazinon	CDs	Fluorescent	0.02–10 μM	0.01 μM	0.9727	2020	[62]
Trifluralin	Ca-modified CDs	Fluorescent	-	7.89 μM	0.96	2020	[220]
Quinalphos	OPCD@UiO-66-NH_2	Fluorescent	0–16 μM	0.3 nM	0.992	2021	[247]
Chlorpyrifos	TEF-CDs	Fluorescent	0.05–100.0 μM	0.00599 μM	0.9959	2021	[63]
Quinalphos			0.01–50.0 μM	0.0057 μM	0.9965		
Pyrimethanil	CDs	Fluorescent	0.5–75 μM	14 nM	0.9907	2021	[182]
Thiophanate methyl	SCDs/Hg^{2+}	Fluorescent	0.05–2.0 μM	7.6 nM	0.9998	2021	[183]
			2.0–5.0 μM		0.9983		
Isoprothiolane	CDs	Fluorescent	1 mM-0.05 μM	11.58 nM	0.9921	2021	[73]
λ-Cyhalothrin	CD-functionalized core-shell nanopsheres	Ratiometric fluorescent	3.045–456.8 nM	0.146 nM	0.988	2022	[230]
Chlorpyrifos	J-CQDs	Fluorescent	57.05–513.4 nM	7.701 nM	0.993	2022	[41]

Where Tyr-CDs: L- tyrosine methyl ester functionalized carbon dots, CDs/Cu(II)/AChE/ATChCl: carbon dots/copper ion/acetyl cholinesterase/acetylthiocholine, BChE-ATCh-MnO_2-CDs: butyrylcholinesterase-acetylthiocholine- manganese dioxide- carbon dots, N-doped CDs-MPH: nitrogen-doped carbon dots and methyl parathion hydrolase, B,N-CDs: boron and nitrogen-doped carbon dots, Ca-modified CDs: calcium-modified carbon dots, OPCD@UiO-66-NH_2: carbon dots derived from orthophenylenediamine incorporated UiO-66-NH_2, TEF-CDs: carbon dots from *Tagetes erecta* flower, SCDs/Hg^{2+}: sulfur-doped carbon dots/mercury ions, J-CQDs: Jatropha-carbon quantum dots.

4.4. Explosive Compounds

Military-grade explosives such as trinitroluene (TNT), dinitroaniline (DNT), are still a major worldwide concern in terms of terror threat and environmental impact. The only method that detects explosive compounds using CDs is a fluorescent sensor. For instance, Zhang et al. (2015) used N-rich CDs for 2,4,6-trinitrotoluene determination [120]. Apparently, TNT is a typical electron deficient nitro compound, which can selectively interact with amine group on CDs, leading to charge transfer from fluorescent CDs to the aromatic rings of TNT and consequently quenching the fluorescence emission of CDs strongly.

Dai and co-workers found that fluorescence sensors are well suited for detecting nitroaromatic compounds, such as 2,4-dinitrotoluene (DNT), as they can quench the emission

of the excited species [132]. In this work, static quenching occurred with an increasing concentration of DNT, as CDs formed stable charge-transfer complexes with DNT molecules. Considering that the selectivity of those sensors were relatively low because some metal ions or other structure analogy can quench those fluorescent nanoparticles, Xu et al. introduced molecularly imprinted polymers (MIPs) to improve the selectivity [131]. However, this causes poor sensitivity because of the highly cross-linked nature of MIPs. Therefore, a novel strategy using periodic mesoporous silica particles as the imprinting matrix and using amino-CDs directly as a "functional monomer" was proposed to improve the sensitivity of M-MIPs@CDs.

In addition, Campos et al. (2016) first demonstrated the fluorometric sensing of 4-chloro-2,6-dinitroaniline in an aqueous solution using carbon quantum dots coated with PAMAM-NH_2 [208]. The presence of amine groups in the PAMAM-NH_2 dendrimer results in the enhanced fluorescence intensity and quantum yield from 3.94% to 6.93%. Moreover, it is interesting that with an increase in pH starting from 2.25, the fluorescence intensity increases drastically and then become constant from pH 6 to 11. The reason for the constant fluorescence intensity may be due to the buffering effect of the surface groups (–COOH and $–NH_2$ mainly).

Next, a selective and sensitive detection of TNT explosive residues based on CD-modified optical sensors has been developed and rapidly elevating until 2022 [99,139,196,214,248]. The research concluded that the possible mechanism for TNT detection corresponds to the Jackson–Meisenheimer (JM) complex. Particularly, functionalizing CDs with amino groups can selectively form a JM complex with typical electron-deficient groups in TNT via charge transfer during a nucleophilic aromatic substitution reaction, which consequently causes fluorescence quenching. In addition, the selectivity of the sensor against TNT was investigated by Devi's group [214]. The proposed sensor showed high selectivity for TNT over other weaker Lewis acids, such as dinitrotoulene (DNT), 2,4-dinitrotoluic acid (TA), nitrobenzene (NB), and p-nitrophenol (NP). It can be concluded that the JM complex formed by TNT is more stabilized due to more resonance structures; more nitro groups on the TNT aromatic ring than that formed by DNT, TA, NB, and NP. All the proposed CD-based optical sensors for the detection of explosive compounds are tabulated orderly in Table 13.

Table 13. Summary of the developed optical sensors for explosive compound detection.

Explosive Compound	Material	Optical Sensor	Range of Detection	Limit of Detection	Linear Correlation Coefficient	Year	Reference
2,4,6-Trinitrotoluene	N-rich CNDs	Fluorescent	10 nM–1.5 µM	1 nM	-	2015	[120]
2,4-Dinitrotoluene	Amine-functionalized CDs	Fluorescent	1 mM–50 mM	1 mM	-	2016	[132]
Trinitrotoluene	M-MIPs@CDs	Fluorescent	-	17 nM	-	2016	[131]
4-Chloro-2,6-dinitroaniline	CQDs@PAMAM-NH_2	Fluorescent	1.0×10^{-5}–6.0×10^{-5} M	2 µM	0.994	2016	[208]
2,4,6-Trinitrotoluene	Ethylenediamine-modified CDs	Fluorescent	-	0.213 µM	0.997	2017	[139]
Trinitrotoluene	Nitrogen-doped CQD	Fluorescent	4.4 nM–26.4 µM	0.03258 µM	0.9993	2018	[214]
Trinitrotoluene	CDs capped with EDA	Fluorescent	44.03–220.14 nM	57.24 nM	0.95457	2018	[99]
	CDs (in the presence of nitric acid) capped with\EDA		44.03–220.14 nM	48.43 nM	0.9752		
			88.06–264.17 nM	21.88 nM	0.99602		
2,4,6-Trinitrotoluene	CDs and Fe@SiO_2-NH_2	Chemosensor	44.03–8806 nM	9.466 nM	-	2021	[248]
2,4,6-Trinitrotoluene	PEI-CQDs	Fluorescent	0–38.17 µM	0.4094 µM	0.9979	2022	[196]

Where N-rich CNDs: nitrogen-rich carbon nanodots, M-MIPs@CDs: mesoporous structured molecularly imprinted polymers capped carbon dots, CQDs@PAMAM-NH_2: carbon quantum dots functionalized with amine groups by PAMAM dendrimer, EDA: ethylenediamine, CDs and Fe@SiO_2-NH_2: carbon dots and the magnetism of amino-functionalized magnetic core-shell nanomaterial, PEI-CQDs: polythylenimine capped carbon quantum dots.

5. Concluding Remarks

An enormous research effort has been devoted to the development of CDs using green and chemical precursors. The reason behind the interest in this fabrication is its fluorescent properties that make it continuously competitive to produce bright and high-quality CDs. This paper has presented the recent progress in the field of CDs, focusing on the green and chemical precursors and fluorescent properties. To the best of our knowledge, this is the first review paper that highlights each of the precursors used in the CDs with the values of the fluorescence quantum yield.

Among the available green precursors, CDs produced by plants are the most popular source because it is a more stable and straightforward process to scale up. For instance, the CDs synthesized from leaves, i.e., *Calotropis procera* leaves, without any addition of surface passivation have the highest quantum yield of 71.95% under the hydrothermal carbonization process, as shown in Figure 9a. It can be observed that the leaves have shown great potential as carbon sources due to their carbon-, hydrogen-, oxygen-, nitrogen-rich composition, which can eliminate the need of surface-chemical passivating agents. Other factors that contributed to the excellent photoluminescence properties include (i) heteroatom doping, such as sulfur, nitrogen, phosphorus, and boron; (ii) heating temperature and time; (iii) type and ratio of solvent; and (iv) pH of media. Even so, the quantum yields obtained from the green precursors were still low compared to the chemical precursors, as depicted in Figure 9b. It was shown that the thermal pyrolysis treatment of sodium citrate dihydrate and urea led to green fluorescence CDs with a quantum yield as high as 93%. As expected, CDs synthesized from acid reagents possess higher quantum yields due to the existence of carboxyl groups. The greater the number of carboxyl groups in the carbon source, the more amino groups of urea that will conjugate onto the surface of CDs.

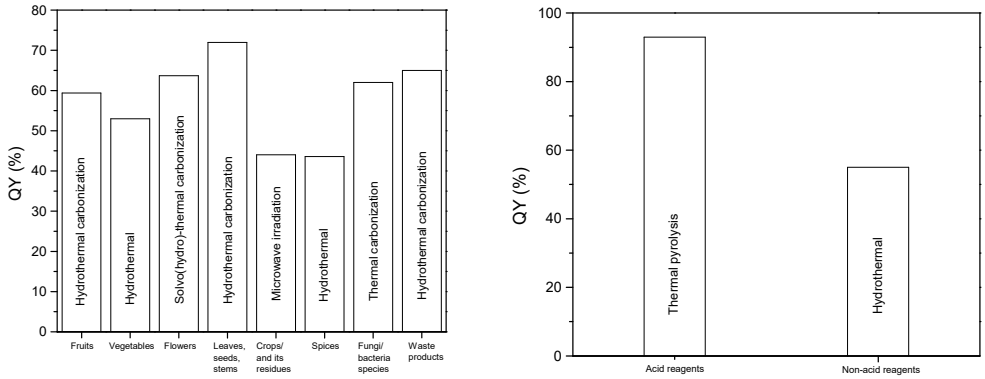

Figure 9. Quantum yields of the CDs based on (**a**) green precursors and (**b**) chemical precursors.

Although the highest quantum yield results have been achieved using chemical precursors (acid reagents), the high toxicity of this precursor may hinder their potential for diverse applications. Therefore, future development should firstly focus on synthesizing CDs from green precursors, particularly plant parts and waste products. In addition, it is highly necessary to fabricate green precursors consisting of hydroxyl, carboxyl and amino groups to avoid the use of toxic chemical passivating agents. Furthermore, this will allow for the development of high-quality and non-toxicity CDs, finally paving the way towards their practical application in various fields.

Author Contributions: Conceptualization and writing—original draft preparation, N.A.S.O.; supervision and funding acquisition, Y.W.F. and R.I.; writing—review and editing, H.S.H. and N.S.M.R.; visualization, N.I.M.F. All authors have read and agreed to the published version of the manuscript.

Funding: This research was funded by the Putra Grant Universiti Putra Malaysia (GP-IPB/2021/9700700).

Institutional Review Board Statement: Not applicable.

Informed Consent Statement: Not applicable.

Data Availability Statement: Not applicable.

Conflicts of Interest: The authors declare no conflict of interest.

References

1. Atchudan, R.; Edison, T.N.J.I.; Perumal, S.; Vinodh, R.; Sundramoorthy, A.K.; Babu, R.S.; Lee, Y.R. Leftover Kiwi Fruit Peel-Derived Carbon Dots as a Highly Selective Fluorescent Sensor for Detection of Ferric Ion. *Chemosensors* **2021**, *9*, 166. [CrossRef]
2. Carbonaro, C.M.; Corpino, R.; Salis, M.; Mocci, F.; Thakkar, S.V.; Olla, C.; Ricci, P.C. On the Emission Properties of Carbon Dots: Reviewing Data and Discussing Models. *C—J. Carbon Res.* **2019**, *5*, 60. [CrossRef]
3. Shi, W.; Song, S.; Zhang, H. Hydrothermal Synthetic Strategies of Inorganic Semiconducting Nanostructures. *Chem. Soc. Rev.* **2013**, *42*, 5714–5743. [CrossRef]
4. Li, L.; Dong, T. Photoluminescence Tuning in Carbon Dots: Surface Passivation or/and Functionalization, Heteroatom Doping. *J. Mater. Chem. C* **2018**, *6*, 7944–7970. [CrossRef]
5. Jorns, M.; Pappas, D. A Review of Fluorescent Carbon Dots, Their Synthesis, Physical and Chemical Characteristics, and Applications. *Nanomaterials* **2021**, *11*, 1448. [CrossRef]
6. Long, C.; Jiang, Z.; Shangguan, J.; Qing, T.; Zhang, P.; Feng, B. Applications of Carbon Dots in Environmental Pollution Control: A Review. *Chem. Eng. J.* **2021**, *406*, 126848. [CrossRef]
7. Sharma, V.; Tiwari, P.; Kaur, N.; Mobin, S.M. Optical Nanosensors Based on Fluorescent Carbon Dots for the Detection of Water Contaminants: A Review. *Environ. Chem. Lett.* **2021**, *19*, 3229–3241. [CrossRef]
8. Kurian, M.; Paul, A. Recent Trends in the Use of Green Sources for Carbon Dot Synthesis—A Short Review. *Carbon Trends* **2021**, *3*, 100032. [CrossRef]
9. Sahu, S.; Behera, B.; Maiti, T.K.; Mohapatra, S. Simple One-Step Synthesis of Highly Luminescent Carbon Dots from Orange Juice: Application as Excellent Bio-Imaging Agents. *Chem. Commun.* **2012**, *48*, 8835–8837. [CrossRef]
10. Zhou, J.; Sheng, Z.; Han, H.; Zou, M.; Li, C. Facile Synthesis of Fluorescent Carbon Dots Using Watermelon Peel as a Carbon Source. *Mater. Lett.* **2012**, *66*, 222–224. [CrossRef]
11. Du, F.; Zhang, M.; Li, X.; Li, J.; Jiang, X.; Li, Z.; Hua, Y.; Shao, G.; Jin, J.; Shao, Q.; et al. Economical and Green Synthesis of Bagasse-Derived Fluorescent Carbon Dots for Biomedical Applications. *Nanotechnology* **2014**, *25*, 315702. [CrossRef]
12. Tyagi, A.; Tripathi, K.M.; Singh, N.; Choudhary, S.; Gupta, R.K. Green Synthesis of Carbon Quantum Dots from Lemon Peel Waste: Applications in Sensing and Photocatalysis. *RSC Adv.* **2016**, *6*, 72423–72432. [CrossRef]
13. Edison, T.N.J.I.; Atchudan, R.; Shim, J.J.; Kalimuthu, S.; Ahn, B.C.; Lee, Y.R. Turn-off Fluorescence Sensor for the Detection of Ferric Ion in Water Using Green Synthesized N-Doped Carbon Dots and Its Bio-Imaging. *J. Photochem. Photobiol. B Biol.* **2016**, *158*, 235–242. [CrossRef]
14. Shi, J.; Ni, G.; Tu, J.; Jin, X.; Peng, J. Green Synthesis of Fluorescent Carbon Dots for Sensitive Detection of Fe^{2+} and Hydrogen Peroxide. *J. Nanopart. Res.* **2017**, *19*, 209. [CrossRef]
15. Zhao, J.; Huang, M.; Zhang, L.; Zou, M.; Chen, D.; Huang, Y.; Zhao, S. Unique Approach to Develop Carbon Dot-Based Nanohybrid Near-Infrared Ratiometric Fluorescent Sensor for the Detection of Mercury Ions. *Anal. Chem.* **2017**, *89*, 8044–8049. [CrossRef]
16. Su, A.; Wang, D.; Shu, X.; Zhong, Q.; Chen, Y.; Liu, J.; Wang, Y. Synthesis of Fluorescent Carbon Quantum Dots from Dried Lemon Peel for Determination of Carmine in Drinks. *Chem. Res. Chin. Univ.* **2018**, *34*, 164–168. [CrossRef]
17. Ding, H.; Ji, Y.; Wei, J.S.; Gao, Q.Y.; Zhou, Z.Y.; Xiong, H.M. Facile Synthesis of Red-Emitting Carbon Dots from Pulp-Free Lemon Juice for Bioimaging. *J. Mater. Chem. B* **2017**, *5*, 5272–5277. [CrossRef]
18. Chatzimitakos, T.; Kasouni, A.; Sygellou, L.; Avgeropoulos, A.; Troganis, A.; Stalikas, C. Two of a Kind but Different: Luminescent Carbon Quantum Dots from Citrus Peels for Iron and Tartrazine Sensing and Cell Imaging. *Talanta* **2017**, *175*, 305–312. [CrossRef]
19. Gharat, P.M.; Pal, H.; Dutta Choudhury, S. Photophysics and Luminescence Quenching of Carbon Dots Derived from Lemon Juice and Glycerol. *Spectrochim. Acta Part A Mol. Biomol. Spectrosc.* **2019**, *209*, 14–21. [CrossRef]
20. Schneider, E.M.; Bärtsch, A.; Stark, W.J.; Grass, R.N. Safe One-Pot Synthesis of Fluorescent Carbon Quantum Dots from Lemon Juice for a Hands-On Experience of Nanotechnology. *J. Chem. Educ.* **2019**, *96*, 540–545. [CrossRef]
21. Tadesse, A.; RamaDevi, D.; Battu, G.; Basavaiah, K. Facile Green Synthesis of Fluorescent Carbon Quantum Dots from Citrus Lemon Juice for Live Cell Imaging. *Asian J. Nanosci. Mater.* **2018**, *1*, 36–46.
22. Lu, M.; Duan, Y.; Song, Y.; Tan, J.; Zhou, L. Green Preparation of Versatile Nitrogen-Doped Carbon Quantum Dots from Watermelon Juice for Cell Imaging, Detection of Fe^{3+} Ions and Cysteine, and Optical Thermometry. *J. Mol. Liq.* **2018**, *269*, 766–774. [CrossRef]
23. Rajendran, K.; Rajendiran, N. Bluish Green Emitting Carbon Quantum Dots Synthesized from Jackfruit (Artocarpus Heterophyllus) and Its Sensing Applications of Hg (II) and Cr (VI) Ions. *Mater. Res. Express* **2018**, *5*, 24008. [CrossRef]
24. Ahmadian-Fard-Fini, S.; Salavati-Niasari, M.; Ghanbari, D. Hydrothermal Green Synthesis of Magnetic Fe_3O_4-Carbon Dots by Lemon and Grape Fruit Extracts and as a Photoluminescence Sensor for Detecting of E. Coli Bacteria. *Spectrochim. Acta Part A Mol. Biomol. Spectrosc.* **2018**, *203*, 481–493. [CrossRef]

25. Anindita, F.; Darmawan, N.; Mas'Ud, Z.A. Fluorescence Carbon Dots from Durian as an Eco-Friendly Inhibitor for Copper Corrosion. *AIP Conf. Proc.* **2018**, *2014*, 020008. [CrossRef]
26. Carvalho, J.; Santos, L.R.; Germino, J.C.; Terezo, A.J.; Moreto, J.A.; Quites, F.J.; Freitas, R.G. Hydrothermal Synthesis to Water-Stable Luminescent Carbon Dots from Acerola Fruit for Photoluminescent Composites Preparation and Its Application as Sensors. *Mater. Res.* **2019**, *22*, 1–8. [CrossRef]
27. Fatahi, Z.; Esfandiari, N.; Ehtesabi, H.; Bagheri, Z.; Ranjbar, Z.; Latifi, H. Physicochemical and Cytotoxicity Analysis of Green Synthesis Carbon Dots for Cell Imaging. *EXCLI J.* **2019**, *18*, 454–466.
28. Tadesse, A.; Hagos, M.; Ramadevi, D.; Basavaiah, K.; Belachew, N. Fluorescent-Nitrogen-Doped Carbon Quantum Dots Derived from Citrus Lemon Juice: Green Synthesis, Mercury(II) Ion Sensing, and Live Cell Imaging. *ACS Omega* **2020**, *5*, 3889–3898. [CrossRef]
29. Monte-Filho, S.S.; Andrade, S.I.E.; Lima, M.B.; Araujo, M.C.U. Synthesis of Highly Fluorescent Carbon Dots from Lemon and Onion Juices for Determination of Riboflavin in Multivitamin/Mineral Supplements. *J. Pharm. Anal.* **2019**, *9*, 209–216. [CrossRef]
30. Hoan, B.T.; Tam, P.D.; Pham, V.H. Green Synthesis of Highly Luminescent Carbon Quantum Dots from Lemon Juice. *J. Nanotechnol.* **2019**, *2019*, 2852816. [CrossRef]
31. Jayaweera, S.; Yin, K.; Ng, W.J. Nitrogen-Doped Durian Shell Derived Carbon Dots for Inner Filter Effect Mediated Sensing of Tetracycline and Fluorescent Ink. *J. Fluoresc.* **2019**, *29*, 221–229. [CrossRef]
32. Hashemi, F.; Heidari, F.; Mohajeri, N.; Mahmoodzadeh, F.; Zarghami, N. Fluorescence Intensity Enhancement of Green Carbon Dots: Synthesis, Characterization and Cell Imaging. *Photochem. Photobiol.* **2020**, *96*, 1032–1040. [CrossRef]
33. Muktha, H.; Sharath, R.; Kottam, N.; Smrithi, S.P.; Samrat, K.; Ankitha, P. Green Synthesis of Carbon Dots and Evaluation of Its Pharmacological Activities. *Bionanoscience* **2020**, *10*, 731–744. [CrossRef]
34. Zhang, Q.; Liang, J.; Zhao, L.; Wang, Y.; Zheng, Y.; Wu, Y.; Jiang, L. Synthesis of Novel Fluorescent Carbon Quantum Dots From *Rosa roxburghii* for Rapid and Highly Selective Detection of O-Nitrophenol and Cellular Imaging. *Front. Chem.* **2020**, *8*, 1–9. [CrossRef]
35. Gudimella, K.K.; Appidi, T.; Wu, H.F.; Battula, V.; Jogdand, A.; Rengan, A.K.; Gedda, G. Sand Bath Assisted Green Synthesis of Carbon Dots from Citrus Fruit Peels for Free Radical Scavenging and Cell Imaging. *Colloids Surf. B Biointerfaces* **2021**, *197*, 111362. [CrossRef]
36. Atchudan, R.; Jebakumar Immanuel Edison, T.N.; Shanmugam, M.; Perumal, S.; Somanathan, T.; Lee, Y.R. Sustainable Synthesis of Carbon Quantum Dots from Banana Peel Waste Using Hydrothermal Process for in Vivo Bioimaging. *Phys. E Low-Dimens. Syst. Nanostruct.* **2021**, *126*, 114417. [CrossRef]
37. Ghereghlou, M.; Esmaeili, A.A.; Darroudi, M. Green Synthesis of Fluorescent Carbon Dots from *Elaeagnus angustifolia* and Its Application as Tartrazine Sensor. *J. Fluoresc.* **2021**, *31*, 185–193. [CrossRef]
38. Ashok Varman, G.; Kalanidhi, K.; Nagaraaj, P. Green Synthesis of Fluorescent Carbon Dots from Canon Ball Fruit for Sensitive Detection of Fe^{3+} and Catalytic Reduction of Textile Dyes. *Dyes Pigment.* **2022**, *199*, 110101. [CrossRef]
39. Vijeata, A.; Chaudhary, S.; Chaudhary, G.R. Fluorescent Carbon Dots from Indian Bael Patra as Effective Sensing Tool to Detect Perilous Food Colorant. *Food Chem.* **2022**, *373*, 131492. [CrossRef]
40. Atchudan, R.; Edison, T.N.J.I.; Perumal, S.; Vinodh, R.; Sundramoorthy, A.K.; Babu, R.S.; Lee, Y.R. Morus Nigra-Derived Hydrophilic Carbon Dots for the Highly Selective and Sensitive Detection of Ferric Ion in Aqueous Media and Human Colon Cancer Cell Imaging. *Colloids Surf. A Physicochem. Eng. Asp.* **2022**, *635*, 128073. [CrossRef]
41. Chandra, S.; Bano, D.; Sahoo, K.; Kumar, D.; Kumar, V.; Kumar Yadav, P.; Hadi Hasan, S. Synthesis of Fluorescent Carbon Quantum Dots from Jatropha Fruits and Their Application in Fluorometric Sensor for the Detection of Chlorpyrifos. *Microchem. J.* **2022**, *172*, 106953. [CrossRef]
42. Qu, Y.; Yu, L.; Zhu, B.; Chai, F.; Su, Z. Green Synthesis of Carbon Dots by Celery Leaves for Use as Fluorescent Paper Sensors for the Detection of Nitrophenols. *New J. Chem.* **2020**, *44*, 1500–1507. [CrossRef]
43. Yin, B.; Deng, J.; Peng, X.; Long, Q.; Zhao, J.; Lu, Q.; Chen, Q.; Li, H.; Tang, H.; Zhang, Y.; et al. Green Synthesis of Carbon Dots with Down- and up-Conversion Fluorescent Properties for Sensitive Detection of Hypochlorite with a Dual-Readout Assay. *Analyst* **2013**, *138*, 6551–6557. [CrossRef]
44. Thota, S.P.; Thota, S.M.; Bhagavatham, S.S.; Manoj, K.S.; Muthukumar, V.S.S.; Venketesh, S.; Vadlani, P.V.; Belliraj, S.K. Facile One-Pot Hydrothermal Synthesis of Stable and Biocompatible Fluorescent Carbon Dots from Lemon Grass Herb. *IET Nanobiotechnol.* **2018**, *12*, 127–132. [CrossRef]
45. Miao, H.; Wang, L.; Zhuo, Y.; Zhou, Z.; Yang, X. Label-Free Fluorimetric Detection of CEA Using Carbon Dots Derived from Tomato Juice. *Biosens. Bioelectron.* **2016**, *86*, 83–89. [CrossRef]
46. Liu, Y.; Liu, Y.; Park, M.; Park, S.J.; Zhang, Y.; Akanda, M.R.; Park, B.Y.; Kim, H.Y. Green Synthesis of Fluorescent Carbon Dots from Carrot Juice for in Vitro Cellular Imaging. *Carbon Lett.* **2017**, *21*, 61–67. [CrossRef]
47. Liu, W.; Diao, H.; Chang, H.; Wang, H.; Li, T.; Wei, W. Green Synthesis of Carbon Dots from Rose-Heart Radish and Application for Fe^{3+} Detection and Cell Imaging. *Sens. Actuators B Chem.* **2017**, *241*, 190–198. [CrossRef]
48. Vasimalai, N.; Vilas-Boas, V.; Gallo, J.; Cerqueira, M.d.F.; Menéndez-Miranda, M.; Costa-Fernández, J.M.; Diéguez, L.; Espiña, B.; Fernández-Argüelles, M.T. Green Synthesis of Fluorescent Carbon Dots from Spices for in Vitro Imaging and Tumour Cell Growth Inhibition. *Beilstein J. Nanotechnol.* **2018**, *9*, 530–544. [CrossRef]

49. Li, L.S.; Jiao, X.Y.; Zhang, Y.; Cheng, C.; Huang, K.; Xu, L. Green Synthesis of Fluorescent Carbon Dots from Hongcaitai for Selective Detection of Hypochlorite and Mercuric Ions and Cell Imaging. *Sens. Actuators B Chem.* **2018**, *263*, 426–435. [CrossRef]
50. Tafreshi, F.A.; Fatahi, Z.; Ghasemi, S.F.; Taherian, A.; Esfandiari, N. Ultrasensitive Fluorescent Detection of Pesticides in Real Sample by Using Green Carbon Dots. *PLoS ONE* **2020**, *15*, 1–17. [CrossRef]
51. Zhao, C.; Li, X.; Cheng, C.; Yang, Y. Green and Microwave-Assisted Synthesis of Carbon Dots and Application for Visual Detection of Cobalt(II) Ions and PH Sensing. *Microchem. J.* **2019**, *147*, 183–190. [CrossRef]
52. Kailasa, S.K.; Ha, S.; Baek, S.H.; Phan, L.M.T.; Kim, S.; Kwak, K.; Park, T.J. Tuning of Carbon Dots Emission Color for Sensing of Fe^{3+} Ion and Bioimaging Applications. *Mater. Sci. Eng. C* **2019**, *98*, 834–842. [CrossRef] [PubMed]
53. Xiao-Yan, W.; Xue-Yan, H.; Tian-Qi, W.; Xu-Cheng, F. Crown Daisy Leaf Waste–Derived Carbon Dots: A Simple and Green Fluorescent Probe for Copper Ion. *Surf. Interface Anal.* **2020**, *52*, 148–155. [CrossRef]
54. Long, R.; Tang, C.; Li, T.; Tong, X.; Tong, C.; Guo, Y.; Gao, Q.; Wu, L.; Shi, S. Dual-Emissive Carbon Dots for Dual-Channel Ratiometric Fluorometric Determination of PH and Mercury Ion and Intracellular Imaging. *Microchim. Acta* **2020**, *187*, 307. [CrossRef]
55. Lai, Z.; Guo, X.; Cheng, Z.; Ruan, G.; Du, F. Green Synthesis of Fluorescent Carbon Dots from Cherry Tomatoes for Highly Effective Detection of Trifluralin Herbicide in Soil Samples. *ChemistrySelect* **2020**, *5*, 1956–1960. [CrossRef]
56. Zhang, Z.; Hu, B.; Zhuang, Q.; Wang, Y.; Luo, X.; Xie, Y.; Zhou, D. Green Synthesis of Fluorescent Nitrogen–Sulfur Co-Doped Carbon Dots from Scallion Leaves for Hemin Sensing. *Anal. Lett.* **2020**, *53*, 1704–1718. [CrossRef]
57. Rodríguez-Varillas, S.; Fontanil, T.; Obaya, Á.J.; Fernández-González, A.; Murru, C.; Badía-Laíño, R. Biocompatibility and Antioxidant Capabilities of Carbon Dots Obtained from Tomato (*Solanum lycopersicum*). *Appl. Sci.* **2022**, *12*, 773. [CrossRef]
58. Cao, Y.; Wang, X.; Bai, H.; Jia, P.; Zhao, Y.; Liu, Y.; Wang, L.; Zhuang, Y.; Yue, T. Fluorescent Detection of Tetracycline in Foods Based on Carbon Dots Derived from Natural Red Beet Pigment. *LWT* **2022**, *157*, 113100. [CrossRef]
59. Sun, R.; Liu, S. Synthesis of Photoluminescent Carbon Dots and Its Effect on Chondrocytes for Knee Joint Therapy Applications. *Artif. Cells Nanomed. Biotechnol.* **2019**, *47*, 1321–1325. [CrossRef]
60. Deka, M.J.; Dutta, P.; Sarma, S.; Medhi, O.K.; Talukdar, N.C.; Chowdhury, D. Carbon Dots Derived from Water Hyacinth and Their Application as a Sensor for Pretilachlor. *Heliyon* **2019**, *5*, e01985. [CrossRef]
61. Wang, M.; Wan, Y.; Zhang, K.; Fu, Q.; Wang, L.; Zeng, J.; Xia, Z.; Gao, D. Green Synthesis of Carbon Dots Using the Flowers of *Osmanthus fragrans* (Thunb.) Lour. as Precursors: Application in Fe^{3+} and Ascorbic Acid Determination and Cell Imaging. *Anal. Bioanal. Chem.* **2019**, *411*, 2715–2727. [CrossRef] [PubMed]
62. Shekarbeygi, Z.; Farhadian, N.; Khani, S.; Moradi, S.; Shahlaei, M. The Effects of Rose Pigments Extracted by Different Methods on the Optical Properties of Carbon Quantum Dots and Its Efficacy in the Determination of Diazinon. *Microchem. J.* **2020**, *158*, 105232. [CrossRef]
63. Ghosh, S.; Gul, A.R.; Park, C.Y.; Kim, M.W.; Xu, P.; Baek, S.H.; Bhamore, J.R.; Kailasa, S.K.; Park, T.J. Facile Synthesis of Carbon Dots from *Tagetes erecta* as a Precursor for Determination of Chlorpyrifos via Fluorescence Turn-off and Quinalphos via Fluorescence Turn-on Mechanisms. *Chemosphere* **2021**, *279*, 130515. [CrossRef] [PubMed]
64. Gu, D.; Shang, S.; Yu, Q.; Shen, J. Green Synthesis of Nitrogen-Doped Carbon Dots from Lotus Root for Hg(II) Ions Detection and Cell Imaging. *Appl. Surf. Sci.* **2016**, *390*, 38–42. [CrossRef]
65. Kumar, A.; Chowdhuri, A.R.; Laha, D.; Mahto, T.K.; Karmakar, P.; Sahu, S.K. Green Synthesis of Carbon Dots from *Ocimum sanctum* for Effective Fluorescent Sensing of Pb^{2+} Ions and Live Cell Imaging. *Sens. Actuators B Chem.* **2017**, *242*, 679–686. [CrossRef]
66. Bhamore, J.R.; Jha, S.; Park, T.J.; Kailasa, S.K. Fluorescence Sensing of Cu^{2+} Ion and Imaging of Fungal Cell by Ultra-Small Fluorescent Carbon Dots Derived from *Acacia concinna* Seeds. *Sens. Actuators B Chem.* **2018**, *277*, 47–54. [CrossRef]
67. Fahmi, M.Z.; Haris, A.; Permana, A.J.; Nor Wibowo, D.L.; Purwanto, B.; Nikmah, Y.L.; Idris, A. Bamboo Leaf-Based Carbon Dots for Efficient Tumor Imaging and Therapy. *RSC Adv.* **2018**, *8*, 38376–38383. [CrossRef]
68. Li, W.; Liu, Y.; Wu, M.; Feng, X.; Redfern, S.A.T.; Shang, Y.; Yong, X.; Feng, T.; Wu, K.; Liu, Z.; et al. Carbon-Quantum-Dots-Loaded Ruthenium Nanoparticles as an Efficient Electrocatalyst for Hydrogen Production in Alkaline Media. *Adv. Mater.* **2018**, *30*, 1800676. [CrossRef]
69. Wei, X.; Li, L.; Liu, J.; Yu, L.; Li, H.; Cheng, F.; Yi, X.; He, J.; Li, B. Green Synthesis of Fluorescent Carbon Dots from *Gynostemma* for Bioimaging and Antioxidant in Zebrafish. *ACS Appl. Mater. Interfaces* **2019**, *11*, 9832–9840. [CrossRef]
70. Dager, A.; Uchida, T.; Maekawa, T.; Tachibana, M. Synthesis and Characterization of Mono-Disperse Carbon Quantum Dots from Fennel Seeds: Photoluminescence Analysis Using Machine Learning. *Sci. Rep.* **2019**, *9*, 14004. [CrossRef]
71. Yang, X.; Wang, D.; Luo, N.; Feng, M.; Peng, X.; Liao, X. Green Synthesis of Fluorescent N,S-Carbon Dots from Bamboo Leaf and the Interaction with Nitrophenol Compounds. *Spectrochim. Acta Part A Mol. Biomol. Spectrosc.* **2020**, *239*, 118462. [CrossRef] f
72. Kalanidhi, K.; Nagaraaj, P. Facile and Green Synthesis of Fluorescent N-Doped Carbon Dots from Betel Leaves for Sensitive Detection of Picric Acid and Iron Ion. *J. Photochem. Photobiol. A Chem.* **2021**, *418*, 113369. [CrossRef]
73. Ghosh, S.; Gul, A.R.; Park, C.Y.; Xu, P.; Baek, S.H.; Bhamore, J.R.; Kim, M.W.; Lee, M.; Kailasa, S.K.; Park, T.J. Green Synthesis of Carbon Dots from *Calotropis procera* Leaves for Trace Level Identification of Isoprothiolane. *Microchem. J.* **2021**, *167*, 106272. [CrossRef]
74. Zaib, M.; Akhtar, A.; Maqsood, F.; Shahzadi, T. Green Synthesis of Carbon Dots and Their Application as Photocatalyst in Dye Degradation Studies. *Arab. J. Sci. Eng.* **2021**, *46*, 437–446. [CrossRef]

75. Chauhan, P.; Chaudhary, S.; Kumar, R. Biogenic Approach for Fabricating Biocompatible Carbon Dots and Their Application in Colorimetric and Fluorometric Sensing of Lead Ion. *J. Clean. Prod.* **2021**, *279*, 123639. [CrossRef]
76. Wang, C.; Xu, J.; Zhang, R.; Zhao, W. Facile and Low-Energy-Consumption Synthesis of Dual-Functional Carbon Dots from Cornus Walteri Leaves for Detection of p-Nitrophenol and Photocatalytic Degradation of Dyes. *Colloids Surf. A Physicochem. Eng. Asp.* **2022**, *640*, 128351. [CrossRef]
77. Ge, G.; Li, L.; Chen, M.; Wu, X.; Yang, Y.; Wang, D.; Zuo, S.; Zeng, Z.; Xiong, W.; Guo, C. Green Synthesis of Nitrogen–Doped Carbon Dots from Fresh Tea Leaves for Selective Fe^{3+} Ions Detection and Cellular Imaging. *Nanomaterials* **2022**, *12*, 986. [CrossRef]
78. Krishnaiah, P.; Atchudan, R.; Perumal, S.; Salama, E.S.; Lee, Y.R.; Jeon, B.H. Utilization of Waste Biomass of Poa Pratensis for Green Synthesis of N-Doped Carbon Dots and Its Application in Detection of Mn^{2+} and Fe^{3+}. *Chemosphere* **2022**, *286*, 131764. [CrossRef]
79. Tan, X.W.; Romainor, A.N.B.; Chin, S.F.; Ng, S.M. Carbon Dots Production via Pyrolysis of Sago Waste as Potential Probe for Metal Ions Sensing. *J. Anal. Appl. Pyrolysis* **2014**, *105*, 157–165. [CrossRef]
80. Ang, W.L.; Boon Mee, C.A.L.; Sambudi, N.S.; Mohammad, A.W.; Leo, C.P.; Mahmoudi, E.; Ba-Abbad, M.; Benamor, A. Microwave-Assisted Conversion of Palm Kernel Shell Biomass Waste to Photoluminescent Carbon Dots. *Sci. Rep.* **2020**, *10*, 21199. [CrossRef]
81. Monday, Y.N.; Abdullah, J.; Yusof, N.A.; Rashid, S.A.; Shueb, R.H. Facile Hydrothermal and Solvothermal Synthesis and Characterization of Nitrogen-Doped Carbon Dots from Palm Kernel Shell Precursor. *Appl. Sci.* **2021**, *11*, 1630. [CrossRef]
82. Liu, S.; Liu, Z.; Li, Q.; Xia, H.; Yang, W.; Wang, R.; Li, Y.; Zhao, H.; Tian, B. Facile Synthesis of Carbon Dots from Wheat Straw for Colorimetric and Fluorescent Detection of Fluoride and Cellular Imaging. *Spectrochim. Acta Part A Mol. Biomol. Spectrosc.* **2021**, *246*, 118964. [CrossRef] [PubMed]
83. Ramanan, V.; Thiyagarajan, S.K.; Raji, K.; Suresh, R.; Sekar, R.; Ramamurthy, P. Outright Green Synthesis of Fluorescent Carbon Dots from Eutrophic Algal Blooms for in Vitro Imaging. *ACS Sustain. Chem. Eng.* **2016**, *4*, 4724–4731. [CrossRef]
84. Moonrinta, S.; Jamnongsong, S.; Sampattavanich, S.; Kladsomboon, S.; Sajomsang, W.; Paoprasert, P. Synthesis of Biocompatible Carbon Dots from Yogurt and Gas Vapor Sensing. *IOP Conf. Ser. Mater. Sci. Eng.* **2018**, *378*, 012005. [CrossRef]
85. Pacquiao, M.R.; de Luna, M.D.G.; Thongsai, N.; Kladsomboon, S.; Paoprasert, P. Highly Fluorescent Carbon Dots from Enokitake Mushroom as Multi-Faceted Optical Nanomaterials for Cr^{6+} and VOC Detection and Imaging Applications. *Appl. Surf. Sci.* **2018**, *453*, 192–203. [CrossRef]
86. Plácido, J.; Bustamante-López, S.; Meissner, K.E.; Kelly, D.E.; Kelly, S.L. Microalgae Biochar-Derived Carbon Dots and Their Application in Heavy Metal Sensing in Aqueous Systems. *Sci. Total Environ.* **2019**, *656*, 531–539. [CrossRef]
87. Zulfajri, M.; Liu, K.C.; Pu, Y.H.; Rasool, A.; Dayalan, S.; Huang, G.G. Utilization of Carbon Dots Derived from Volvariella Volvacea Mushroom for a Highly Sensitive Detection of Fe^{3+} and Pb^{2+} Ions in Aqueous Solutions. *Chemosensors* **2020**, *8*, 47. [CrossRef]
88. Chauhan, P.; Saini, J.; Chaudhary, S.; Bhasin, K.K. Sustainable Synthesis of Carbon Dots from Agarose Waste and Prospective Application in Sensing of L-Aspartic Acid. *Mater. Res. Bull.* **2021**, *134*, 111113. [CrossRef]
89. Shen, C.; Dong, C.; Cheng, L.; Shi, X.; Bi, H. Fluorescent Carbon Dots from *Shewanella oneidensis* MR–1 for Hg^{2+} and Tetracycline Detection and Selective Fluorescence Imaging of Gram–Positive Bacteria. *J. Environ. Chem. Eng.* **2022**, *10*, 107020. [CrossRef]
90. Hu, Y.; Yang, J.; Tian, J.; Jia, L.; Yu, J.S. Waste Frying Oil as a Precursor for One-Step Synthesis of Sulfur-Doped Carbon Dots with PH-Sensitive Photoluminescence. *Carbon* **2014**, *77*, 775–782. [CrossRef]
91. Zhang, C.; Xiao, Y.; Ma, Y.; Li, B.; Liu, Z.; Lu, C.; Liu, X.; Wei, Y.; Zhu, Z.; Zhang, Y. Algae Biomass as a Precursor for Synthesis of Nitrogen-and Sulfur-Co-Doped Carbon Dots: A Better Probe in Arabidopsis Guard Cells and Root Tissues. *J. Photochem. Photobiol. B Biol.* **2017**, *174*, 315–322. [CrossRef] [PubMed]
92. Ramanan, V.; Siddaiah, B.; Raji, K.; Ramamurthy, P. Green Synthesis of Multifunctionalized, Nitrogen-Doped, Highly Fluorescent Carbon Dots from Waste Expanded Polystyrene and Its Application in the Fluorimetric Detection of Au^{3+} Ions in Aqueous Media. *ACS Sustain. Chem. Eng.* **2018**, *6*, 1627–1638. [CrossRef]
93. Konwar, A.; Baruah, U.; Deka, M.J.; Hussain, A.A.; Haque, S.R.; Pal, A.R.; Chowdhury, D. Tea-Carbon Dots-Reduced Graphene Oxide: An Efficient Conducting Coating Material for Fabrication of an E-Textile. *ACS Sustain. Chem. Eng.* **2017**, *5*, 11645–11651. [CrossRef]
94. Su, R.; Wang, D.; Liu, M.; Yan, J.; Wang, J.X.; Zhan, Q.; Pu, Y.; Foster, N.R.; Chen, J.F. Subgram-Scale Synthesis of Biomass Waste-Derived Fluorescent Carbon Dots in Subcritical Water for Bioimaging, Sensing, and Solid-State Patterning. *ACS Omega* **2018**, *3*, 13211–13218. [CrossRef]
95. Xue, H.; Yan, Y.; Hou, Y.; Li, G.; Hao, C. Novel Carbon Quantum Dots for Fluorescent Detection of Phenol and Insights into the Mechanism. *New J. Chem.* **2018**, *42*, 11485–11492. [CrossRef]
96. Lin, B.; Yan, Y.; Guo, M.; Cao, Y.; Yu, Y.; Zhang, T.; Huang, Y.; Wu, D. Modification-Free Carbon Dots as Turn-on Fluorescence Probe for Detection of Organophosphorus Pesticides. *Food Chem.* **2018**, *245*, 1176–1182. [CrossRef]
97. Kumari, A.; Kumar, A.; Sahu, S.K.; Kumar, S. Synthesis of Green Fluorescent Carbon Quantum Dots Using Waste Polyolefins Residue for Cu^{2+} Ion Sensing and Live Cell Imaging. *Sens. Actuators B Chem.* **2018**, *254*, 197–205. [CrossRef]
98. Aji, M.P.; Wati, A.L.; Priyanto, A.; Karunawan, J.; Nuryadin, B.W.; Wibowo, E.; Marwoto, P. Sulhadi Polymer Carbon Dots from Plastics Waste Upcycling. *Environ. Nanotechnol. Monit. Manag.* **2018**, *9*, 136–140. [CrossRef]
99. Devi, S.; Gupta, R.K.; Paul, A.K.; Kumar, V.; Sachdev, A.; Gopinath, P.; Tyagi, S. Ethylenediamine Mediated Luminescence Enhancement of Pollutant Derivatized Carbon Quantum Dots for Intracellular Trinitrotoluene Detection: Soot to Shine. *RSC Adv.* **2018**, *8*, 32684–32694. [CrossRef]

100. Feng, X.; Zhang, Y. A Simple and Green Synthesis of Carbon Quantum Dots from Coke for White Light-Emitting Devices. *RSC Adv.* **2019**, *9*, 33789–33793. [CrossRef]
101. Hu, Y.; Gao, Z.; Yang, J.; Chen, H.; Han, L. Environmentally Benign Conversion of Waste Polyethylene Terephthalate to Fluorescent Carbon Dots for "on-off-on" Sensing of Ferric and Pyrophosphate Ions. *J. Colloid Interface Sci.* **2019**, *538*, 481–488. [CrossRef] [PubMed]
102. Gunjal, D.B.; Gurav, Y.M.; Gore, A.H.; Naik, V.M.; Waghmare, R.D.; Patil, C.S.; Sohn, D.; Anbhule, P.V.; Shejwal, R.V.; Kolekar, G.B. Nitrogen Doped Waste Tea Residue Derived Carbon Dots for Selective Quantification of Tetracycline in Urine and Pharmaceutical Samples and Yeast Cell Imaging Application. *Opt. Mater.* **2019**, *98*, 109484. [CrossRef]
103. Gunjal, D.B.; Naik, V.M.; Waghmare, R.D.; Patil, C.S.; Shejwal, R.V.; Gore, A.H.; Kolekar, G.B. Sustainable Carbon Nanodots Synthesised from Kitchen Derived Waste Tea Residue for Highly Selective Fluorimetric Recognition of Free Chlorine in Acidic Water: A Waste Utilization Approach. *J. Taiwan Inst. Chem. Eng.* **2019**, *95*, 147–154. [CrossRef]
104. Irmania, N.; Dehvari, K.; Gedda, G.; Tseng, P.J.; Chang, J.Y. Manganese-Doped Green Tea-Derived Carbon Quantum Dots as a Targeted Dual Imaging and Photodynamic Therapy Platform. *J. Biomed. Mater. Res. Part B Appl. Biomater.* **2020**, *108*, 1616–1625. [CrossRef] [PubMed]
105. Zhu, J.; Zhu, F.; Yue, X.; Chen, P.; Sun, Y.; Zhang, L.; Mu, D.; Ke, F. Waste Utilization of Synthetic Carbon Quantum Dots Based on Tea and Peanut Shell. *J. Nanomater.* **2019**, *2019*, 7965756. [CrossRef]
106. Venkatesan, S.; Mariadoss, A.J.; Kathiravan, A.; Muthupandian, A. Fuel Waste to Fluorescent Carbon Dots and Its Multifarious Applications. *Sens. Actuators B Chem.* **2019**, *282*, 972–983. [CrossRef]
107. Park, S.J.; Park, J.Y.; Chung, J.W.; Yang, H.K.; Moon, B.K.; Yi, S.S. Color Tunable Carbon Quantum Dots from Wasted Paper by Different Solvents for Anti-Counterfeiting and Fluorescent Flexible Film. *Chem. Eng. J.* **2020**, *383*, 123200. [CrossRef]
108. Chaudhary, S.; Kumari, M.; Chauhan, P.; Ram Chaudhary, G. Upcycling of Plastic Waste into Fluorescent Carbon Dots: An Environmentally Viable Transformation to Biocompatible C-Dots with Potential Prospective in Analytical Applications. *Waste Manag.* **2021**, *120*, 675–686. [CrossRef]
109. Lauria, A.; Lizundia, E. Luminescent Carbon Dots Obtained from Polymeric Waste. *J. Clean. Prod.* **2020**, *262*, 121288. [CrossRef]
110. Ma, J.; Zhang, L.; Chen, X.; Su, R.; Shi, Q.; Zhao, S.; Xu, Q.; Xu, C. Mass Production of Highly Fluorescent Full Color Carbon Dots from the Petroleum Coke. *Chin. Chem. Lett.* **2020**, *32*, 1532–1536. [CrossRef]
111. Liang, Y.M.; Yang, H.; Zhou, B.; Chen, Y.; Yang, M.; Wei, K.S.; Yan, X.F.; Kang, C. Waste Tobacco Leaves Derived Carbon Dots for Tetracycline Detection: Improving Quantitative Accuracy with the Aid of Chemometric Model. *Anal. Chim. Acta* **2022**, *1191*, 339269. [CrossRef]
112. Chen, B.B.; Liu, Z.X.; Zou, H.Y.; Huang, C.Z. Highly Selective Detection of 2,4,6-Trinitrophenol by Using Newly Developed Terbium-Doped Blue Carbon Dots. *Analyst* **2013**, *141*, 2676–2681. [CrossRef]
113. Dong, Y.; Pang, H.; Yang, H.B.; Guo, C.; Shao, J.; Chi, Y.; Li, C.M.; Yu, T. Carbon-Based Dots Co-Doped with Nitrogen and Sulfur for High Quantum Yield and Excitation-Independent Emission. *Angew. Chem. Int. Ed.* **2013**, *52*, 7800–7804. [CrossRef] [PubMed]
114. Niu, Q.; Gao, K.; Lin, Z.; Wu, W. Amine-Capped Carbon Dots as a Nanosensor for Sensitive and Selective Detection of Picric Acid in Aqueous Solution via Electrostatic Interaction. *Anal. Methods* **2013**, *5*, 6228–6233. [CrossRef]
115. Ahmed, G.H.G.; Laíño, R.B.; Calzón, J.A.G.; García, M.E.D. Highly Fluorescent Carbon Dots as Nanoprobes for Sensitive and Selective Determination of 4-Nitrophenol in Surface Waters. *Microchim. Acta* **2015**, *182*, 51–59. [CrossRef]
116. Zhang, H.; Chen, Y.; Liang, M.; Xu, L.; Qi, S.; Chen, H.; Chen, X. Solid-Phase Synthesis of Highly Fluorescent Nitrogen-Doped Carbon Dots for Sensitive and Selective Probing Ferric Ions in Living Cells. *Anal. Chem.* **2014**, *86*, 9846–9852. [CrossRef] [PubMed]
117. Zhao, L.; Geng, F.; Di, F.; Guo, L.H.; Wan, B.; Yang, Y.; Zhang, H.; Sun, G. Polyamine-Functionalized Carbon Nanodots: A Novel Chemiluminescence Probe for Selective Detection of Iron(Iii) Ions. *RSC Adv.* **2014**, *4*, 45768–45771. [CrossRef]
118. Zhang, R.; Chen, W. Nitrogen-Doped Carbon Quantum Dots: Facile Synthesis and Application as a "Turn-off" Fluorescent Probe for Detection of Hg^{2+} Ions. *Biosens. Bioelectron.* **2013**, *55*, 83–90. [CrossRef]
119. Zhang, P.; Xue, Z.; Luo, D.; Yu, W.; Guo, Z.; Wang, T. Dual-Peak Electrogenerated Chemiluminescence of Carbon Dots for Iron Ions Detection. *Anal. Chem.* **2014**, *86*, 5620–5623. [CrossRef]
120. Zhang, L.; Han, Y.; Zhu, J.; Zhai, Y.; Dong, S. Simple and Sensitive Fluorescent and Electrochemical Trinitrotoluene Sensors Based on Aqueous Carbon Dots. *Anal. Chem.* **2015**, *87*, 2033–2036. [CrossRef]
121. Hou, J.; Dong, J.; Zhu, H.; Teng, X.; Ai, S.; Mang, M. A Simple and Sensitive Fluorescent Sensor for Methyl Parathion Based on L-Tyrosine Methyl Ester Functionalized Carbon Dots. *Biosens. Bioelectron.* **2015**, *68*, 20–26. [CrossRef] [PubMed]
122. Cui, X.; Zhu, L.; Wu, J.; Hou, Y.; Wang, P.; Wang, Z.; Yang, M. A Fluorescent Biosensor Based on Carbon Dots-Labeled Oligodeoxyribonucleotide and Graphene Oxide for Mercury (II) Detection. *Biosens. Bioelectron.* **2015**, *63*, 506–512. [CrossRef] [PubMed]
123. Wang, B.; Song, A.; Feng, L.; Ruan, H.; Li, H.; Dong, S.; Hao, J. Tunable Amphiphilicity and Multifunctional Applications of Ionic-Liquid-Modified Carbon Quantum Dots. *ACS Appl. Mater. Interfaces* **2015**, *7*, 6919–6925. [CrossRef] [PubMed]
124. Liu, L.; Feng, F.; Paau, M.C.; Hu, Q.; Liu, Y.; Chen, Z.; Choic, M.M.F. Carbon Dots Isolated from Chromatographic Fractions for Sensing Applications. *RSC Adv.* **2015**, *5*, 106838–106847. [CrossRef]
125. Li, L.; Yu, B.; You, T. Nitrogen and Sulfur Co-Doped Carbon Dots for Highly Selective and Sensitive Detection of Hg (II) Ions. *Biosens. Bioelectron.* **2015**, *74*, 263–269. [CrossRef]

126. Wang, Y.; Kim, S.H.; Feng, L. Highly Luminescent N, S- Co-Doped Carbon Dots and Their Direct Use as Mercury(II) Sensor. *Anal. Chim. Acta* **2015**, *890*, 134–142. [CrossRef]
127. Liu, Y.; Liao, M.; He, X.; Liu, X.; Kou, X.; Xiao, D. One-Step Synthesis of Highly Luminescent Nitrogen-Doped Carbon Dots for Selective and Sensitive Detection of Mercury(Ii) Ions and Cellular Imaging. *Anal. Sci.* **2015**, *31*, 971–977. [CrossRef]
128. Hou, Y.; Lu, Q.; Deng, J.; Li, H.; Zhang, Y. One-Pot Electrochemical Synthesis of Functionalized Fluorescent Carbon Dots and Their Selective Sensing for Mercury Ion. *Anal. Chim. Acta* **2015**, *866*, 69–74. [CrossRef]
129. Wang, J.; Zhang, P.; Huang, C.; Liu, G.; Leung, K.C.F.; Wáng, Y.X.J. High Performance Photoluminescent Carbon Dots for in Vitro and in Vivo Bioimaging: Effect of Nitrogen Doping Ratios. *Langmuir* **2015**, *31*, 8063–8073. [CrossRef]
130. Schneider, J.; Reckmeier, C.J.; Xiong, Y.; Von Seckendorff, M.; Susha, A.S.; Kasak, P.; Rogach, A.L. Molecular Fluorescence in Citric Acid-Based Carbon Dots. *J. Phys. Chem. C* **2016**, *121*, 2014–2022. [CrossRef]
131. Xu, S.; Lu, H. Mesoporous Structured MIPs@CDs Fluorescence Sensor for Highly Sensitive Detection of TNT. *Biosens. Bioelectron.* **2016**, *85*, 950–956. [CrossRef] [PubMed]
132. Dai, J.; Zambrana, M.; Fidalgo, M.; Dai, J.; Zambrana, M. Amino-Functionalized Fluorescent Carbon Dots for Chemical Sensing Jingjing. *MRS Adv.* **2016**, *1*, 1365–1370. [CrossRef]
133. He, J.; Zhang, H.; Zou, J.; Liu, Y.; Zhuang, J.; Xiao, Y.; Lei, B. Carbon Dots-Based Fluorescent Probe for "off-on" Sensing of Hg(II) and I-. *Biosens. Bioelectron.* **2016**, *79*, 531–535. [CrossRef] [PubMed]
134. Zhao, Z.; Zhang, J.; Wang, Y.; Chen, L.; Zhang, Y. Hydrothermal Synthesis of Fluorescent Nitrogen-Doped Carbon Quantum Dots from Ascorbic Acid and Valine for Selective Determination of Picric Acid in Water Samples. *Int. J. Environ. Anal. Chem.* **2016**, *96*, 1402–1413. [CrossRef]
135. He, G.; Xu, M.; Shu, M.; Li, X.; Yang, Z.; Zhang, L.; Su, Y.; Hu, N.; Zhang, Y. Rapid Solid-Phase Microwave Synthesis of Highly Photoluminescent Nitrogen-Doped Carbon Dots for Fe^{3+} Detection and Cellular Bioimaging. *Nanotechnology* **2016**, *27*, 395706. [CrossRef]
136. Fan, Y.Z.; Zhang, Y.; Li, N.; Liu, S.G.; Liu, T.; Li, N.B.; Luo, H.Q. A Facile Synthesis of Water-Soluble Carbon Dots as a Label-Free Fluorescent Probe for Rapid, Selective and Sensitive Detection of Picric Acid. *Sens. Actuators B Chem.* **2017**, *240*, 949–955. [CrossRef]
137. Chang, M.M.F.; Ginjom, I.R.; Ng, S.M. Single-Shot 'Turn-off' Optical Probe for Rapid Detection of Paraoxon-Ethyl Pesticide on Vegetable Utilising Fluorescence Carbon Dots. *Sens. Actuators B Chem.* **2017**, *242*, 1050–1056. [CrossRef]
138. Song, W.; Zhang, H.J.; Liu, Y.H.; Ren, C.L.; Chen, H.L. A New Fluorescence Probing Strategy for the Detection of Parathion-Methyl Based on N-Doped Carbon Dots and Methyl Parathion Hydrolase. *Chin. Chem. Lett.* **2017**, *28*, 1675–1680. [CrossRef]
139. Tian, X.; Peng, H.; Li, Y.; Yang, C.; Zhou, Z.; Wang, Y. Highly Sensitive and Selective Paper Sensor Based on Carbon Quantum Dots for Visual Detection of TNT Residues in Groundwater. *Sens. Actuators B Chem.* **2017**, *243*, 1002–1009. [CrossRef]
140. Liu, T.; Cui, Z.W.; Zhou, J.; Wang, Y.; Zou, Z.G. Synthesis of Pyridinic-Rich N, S Co-Doped Carbon Quantum Dots as Effective Enzyme Mimics. *Nanoscale Res. Lett.* **2017**, *12*, 375. [CrossRef]
141. Liu, H.; Zhang, Y.; Liu, J.H.; Hou, P.; Zhou, J.; Huang, C.Z. Preparation of Nitrogen-Doped Carbon Dots with High Quantum Yield from: Bombyx Mori Silk for Fe(III) Ions Detection. *RSC Adv.* **2017**, *7*, 50584–50590. [CrossRef]
142. Liu, Y.; Liu, Y.; Lee, J.; Lee, J.H.; Park, M.; Kim, H.Y. Rational Designed Strategy to Dispel Mutual Interference of Mercuric and Ferric Ions towards Robust, PH-Stable Fluorescent Carbon Nanodots. *Analyst* **2017**, *142*, 1149–1156. [CrossRef] [PubMed]
143. Huang, H.; Weng, Y.; Zheng, L.; Yao, B.; Weng, W.; Lin, X. Nitrogen-Doped Carbon Quantum Dots as Fluorescent Probe for "off-on" Detection of Mercury Ions, L-Cysteine and Iodide Ions. *J. Colloid Interface Sci.* **2017**, *506*, 373–378. [CrossRef] [PubMed]
144. Tian, Z.; Zhang, X.; Li, D.; Zhou, D.; Jing, P.; Shen, D.; Qu, S.; Zboril, R.; Rogach, A.L. Full-Color Inorganic Carbon Dot Phosphors for White-Light-Emitting Diodes. *Adv. Opt. Mater.* **2017**, *5*, 1700416. [CrossRef]
145. Thongsai, N.; Nagae, Y.; Hirai, T.; Takahara, A.; Uchiyama, T.; Kamitani, K.; Paoprasert, P. Multifunctional Nitrogen-Doped Carbon Dots from Maleic Anhydride and Tetraethylenepentamine via Pyrolysis for Sensing, Adsorbance, and Imaging Applications. *Sens. Actuators B Chem.* **2017**, *253*, 1026–1033. [CrossRef]
146. Huang, Y.; Cheng, Z. Simple and Green Synthesis of Boron-, Sulfur-, and Nitrogen-Co-Doped Carbon Dots as Fluorescent Probe for Selective and Sensitive Detection of Sunset Yellow. *Nano* **2017**, *12*, 1750123. [CrossRef]
147. Du, Q.; Zheng, J.; Wang, J.; Yang, Y.; Liu, X. The Synthesis of Green Fluorescent Carbon Dots for Warm White LEDs. *RSC Adv.* **2018**, *8*, 19585–19595. [CrossRef]
148. Chen, L.; Zhang, J. Carbon Dots with Tunable Photoluminescence Properties. In Proceedings of the 2nd International Conference of Theoretical and Applied Nanoscience and Nanotechnology, Niagara Falls, ON, Canada, 10–12 June 2018; pp. 1–6. [CrossRef]
149. Yu, T.; Wang, H.; Guo, C.; Zhai, Y.; Yang, J.; Yuan, J. A Rapid Microwave Synthesis of Green-Emissive Carbon Dots with Solid-State Fluorescence and PH-Sensitive Properties. *R. Soc. Open Sci.* **2018**, *5*, 180245. [CrossRef]
150. Ren, G.; Yu, L.; Zhu, B.; Tang, M.; Chai, F.; Wang, C.; Su, Z. Orange Emissive Carbon Dots for Colorimetric and Fluorescent Sensing of 2,4,6-Trinitrophenol by Fluorescence Conversion. *RSC Adv.* **2018**, *8*, 16095–16102. [CrossRef]
151. Zhang, L.; Chang, J.; Su, R.; Huang, R.; Qi, W.; He, Z. Carbon Dots and Quantum Dots-Based Nanohybrid as a Ratiometric Fluorescent Probe for Fe^{3+} and Phytic Acid Sensing. *Chem. Eng. Trans.* **2018**, *70*, 2065–2070. [CrossRef]
152. Ma, Y.; Mei, J.; Bai, J.; Chen, X.; Ren, L. Ratiometric Fluorescent Nanosensor Based on Carbon Dots for the Detection of Mercury Ion. *Mater. Res. Express* **2018**, *5*, 055605. [CrossRef]

153. Tabaraki, R.; Abdi, O. Green and Simple Turn off/on Fluorescence Sensor for Mercury (II), Cysteine and Histidine. *J. Mol. Liq.* **2018**, *251*, 77–82. [CrossRef]
154. Li, H.; Yan, X.; Lu, G.; Su, X. Carbon Dot-Based Bioplatform for Dual Colorimetric and Fluorometric Sensing of Organophosphate Pesticides. *Sens. Actuators B Chem.* **2018**, *260*, 563–570. [CrossRef]
155. Yan, X.; Song, Y.; Zhu, C.; Li, H.; Du, D.; Su, X.; Lin, Y. MnO_2 Nanosheet-Carbon Dots Sensing Platform for Sensitive Detection of Organophosphorus Pesticides. *Anal. Chem.* **2018**, *90*, 2618–2624. [CrossRef]
156. Prathumsuwan, T.; Jamnongsong, S.; Sampattavanich, S.; Paoprasert, P. Preparation of Carbon Dots from Succinic Acid and Glycerol as Ferrous Ion and Hydrogen Peroxide Dual-Mode Sensors and for Cell Imaging. *Opt. Mater.* **2018**, *86*, 517–529. [CrossRef]
157. Jiang, K.; Wang, Y.; Cai, C.; Lin, H. Conversion of Carbon Dots from Fluorescence to Ultralong Room-Temperature Phosphorescence by Heating for Security Applications. *Adv. Mater.* **2018**, *30*, e1800783. [CrossRef]
158. Jiang, K.; Wang, Y.; Gao, X.; Cai, C.; Lin, H. Facile, Quick, and Gram-Scale Synthesis of Ultralong-Lifetime Room-Temperature-Phosphorescent Carbon Dots by Microwave Irradiation. *Angew. Chem. Int. Ed.* **2018**, *57*, 6216–6220. [CrossRef]
159. Shamsipur, M.; Molaei, K.; Molaabasi, F.; Alipour, M.; Alizadeh, N.; Hosseinkhani, S.; Hosseini, M. Facile Preparation and Characterization of New Green Emitting Carbon Dots for Sensitive and Selective off/on Detection of Fe^{3+} Ion and Ascorbic Acid in Water and Urine Samples and Intracellular Imaging in Living Cells. *Talanta* **2018**, *183*, 122–130. [CrossRef]
160. Ren, G.; Meng, Y.; Zhang, Q.; Tang, M.; Zhu, B.; Chai, F.; Wang, C.; Su, Z. Nitrogen-Doped Carbon Dots for the Detection of Mercury Ions in Living Cells and Visualization of Latent Fingerprints. *New J. Chem.* **2018**, *42*, 6824–6830. [CrossRef]
161. Ludmerczki, R.; Mura, S.; Carbonaro, C.M.; Mandity, I.M.; Carraro, M.; Senes, N.; Garroni, S.; Granozzi, G.; Calvillo, L.; Marras, S.; et al. Carbon Dots from Citric Acid and Its Intermediates Formed by Thermal Decomposition. *Chem.-A Eur. J.* **2019**, *25*, 11963–11974. [CrossRef]
162. Hu, G.; Lei, B.; Jiao, X.; Wu, S.; Zhang, X.; Zhuang, J.; Liu, X.; Hu, C.; Liu, Y. Synthesis of Modified Carbon Dots with Performance of Ultraviolet Absorption Used in Sunscreen. *Opt. Express* **2019**, *27*, 7629. [CrossRef] [PubMed]
163. Zhao, Y.Y.; Qu, S.N.; Feng, X.Y.; Xu, J.C.; Yang, Y.; Su, S.C.; Wang, S.P.; Ng, K.W. Tailoring the Photoluminescence Excitation Dependence of the Carbon Dots via an Alkali Treatment. *J. Phys. Chem. Lett.* **2019**, *10*, 4596–4602. [CrossRef] [PubMed]
164. Zhao, X.; Qi, T.; Yang, M.; Zhang, W.; Kong, C.; Hao, M.; Wang, Y.; Zhang, H.; Yang, B.; Yang, J.; et al. Synthesis of Dual Functional Procaine-Derived Carbon Dots for Bioimaging and Anticancer Therapy. *Nanomedicine* **2020**, *15*, 677–689. [CrossRef] [PubMed]
165. Wang, M.; Gao, M.; Deng, L.; Kang, X.; Yang, L.; Quan, T.; Xia, Z.; Gao, D. Composite Material Based on Carbon Dots and Molecularly Imprinted Polymers: A Facile Probe for Fluorescent Detection of 4-Nitrophenol. *Nano* **2020**, *15*, 2050105. [CrossRef]
166. Chan, K.K.; Yap, S.H.K.; Yong, K.T. Solid State Carbon Dots-Based Sensor Using Optical Microfiber for Ferric Ion Detection. In Proceedings of the 2019 IEEE International Conference on Sensors and Nanotechnology, Penang, Malaysia, 24–25 July 2019; pp. 1–4. [CrossRef]
167. Yang, H.; He, L.; Pan, S.; Liu, H.; Hu, X. Nitrogen-Doped Fluorescent Carbon Dots for Highly Sensitive and Selective Detection of Tannic Acid. *Spectrochim. Acta Part A Mol. Biomol. Spectrosc.* **2019**, *210*, 111–119. [CrossRef]
168. Sahiner, N.; Suner, S.S.; Sahiner, M.; Silan, C. Nitrogen and Sulfur Doped Carbon Dots from Amino Acids for Potential Biomedical Applications. *J. Fluoresc.* **2019**, *29*, 1191–1200. [CrossRef]
169. Pu, Z.F.; Wen, Q.L.; Yang, Y.J.; Cui, X.M.; Ling, J.; Liu, P.; Cao, Q.E. Fluorescent Carbon Quantum Dots Synthesized Using Phenylalanine and Citric Acid for Selective Detection of Fe^{3+} Ions. *Spectrochim. Acta Part A Mol. Biomol. Spectrosc.* **2020**, *229*, 117944. [CrossRef]
170. Wang, X.; Liu, Y.; Zhou, Q.; Sheng, X.; Sun, Y.; Zhou, B.; Zhao, J.; Guo, J. A Reliable and Facile Fluorescent Sensor from Carbon Dots for Sensing 2,4,6-Trinitrophenol Based on Inner Filter Effect. *Sci. Total Environ.* **2020**, *720*, 137680. [CrossRef]
171. Gu, S.; Hsieh, C.T.; Yuan, C.Y.; Gandomi, Y.A.; Chang, J.K.; Fu, C.C.; Yang, J.W.; Juang, R.S. Fluorescence of Functionalized Graphene Quantum Dots Prepared from Infrared-Assisted Pyrolysis of Citric Acid and Urea. *J. Lumin.* **2020**, *217*, 116774. [CrossRef]
172. Strauss, V.; Wang, H.; Delacroix, S.; Ledendecker, M.; Wessig, P. Carbon Nanodots Revised: The Thermal Citric Acid/Urea Reaction. *Chem. Sci.* **2020**, *11*, 8256–8266. [CrossRef]
173. Li, Y.; Yang, Y.; Jiang, Y.; Han, S. Detection of Tannic Acid Exploiting Carbon Dots Enhanced Hydrogen Peroxide/Potassium Ferricyanide Chemiluminescence. *Microchem. J.* **2020**, *157*, 105113. [CrossRef]
174. Sutanto, H.; Alkian, I.; Romanda, N.; Lewa, I.W.L.; Marhaendrajaya, I.; Triadyaksa, P. High Green-Emission Carbon Dots and Its Optical Properties: Microwave Power Effect. *AIP Adv.* **2020**, *10*, 055008. [CrossRef]
175. Chahal, S.; Yousefi, N.; Tufenkji, N. Green Synthesis of High Quantum Yield Carbon Dots from Phenylalanine and Citric Acid: Role of Stoichiometry and Nitrogen Doping. *ACS Sustain. Chem. Eng.* **2020**, *8*, 5566–5575. [CrossRef]
176. Arab, S.; Masoum, S.; Seyed Hosseini, E. Engineering the Synthesis of Luminescent Carbon Dots with Ultra High-Quantum Yield Using Experimental Design Approach in Order to Develop Sensing Applications. *IEEE Sens. J.* **2020**, *20*, 1705–1711. [CrossRef]
177. He, X.; Li, Y.; Yang, C.; Lu, L.; Nie, Y.; Tian, X. Carbon Dots–MnO_2 Nanocomposites for As(Iii) Detection in Groundwater with High Sensitivity and Selectivity. *Anal. Methods* **2020**, *12*, 5572–5580. [CrossRef]
178. Bhatt, M.; Bhatt, S.; Vyas, G.; Raval, I.H.; Haldar, S.; Paul, P. Water-Dispersible Fluorescent Carbon Dots as Bioimaging Agents and Probes for Hg^{2+} and Cu^{2+} Ions. *ACS Appl. Nano Mater.* **2020**, *3*, 7096–7104. [CrossRef]

179. Sun, Y.; Zheng, S.; Liu, L.; Kong, Y.; Zhang, A.; Xu, K.; Han, C. The Cost-Effective Preparation of Green Fluorescent Carbon Dots for Bioimaging and Enhanced Intracellular Drug Delivery. *Nanoscale Res. Lett.* **2020**, *15*, 55. [CrossRef]
180. Luo, M.; Wei, J.; Zhao, Y.; Sun, Y.; Liang, H.; Wang, S.; Li, P. Fluorescent and Visual Detection of Methyl-Paraoxon by Using Boron-and Nitrogen-Doped Carbon Dots. *Microchem. J.* **2020**, *154*, 104547. [CrossRef]
181. Li, D.; Chen, C.; Guo, X.; Liu, C.; Yang, W. A Simple Electrochemiluminesecence Aptasenor Using a GCE/NCQDs/Aptamers for Detection of Pb. *Environ. Technol.* **2021**, *43*, 2270–2277. [CrossRef]
182. Supchocksoonthorn, P.; Hanchaina, R.; Sinoy, M.C.A.; de Luna, M.D.G.; Kangsamaksin, T.; Paoprasert, P. Novel Solution- and Paper-Based Sensors Based on Label-Free Fluorescent Carbon Dots for the Selective Detection of Pyrimethanil. *Appl. Surf. Sci.* **2021**, *564*, 150372. [CrossRef]
183. Wang, S.; Chen, H.; Xie, H.; Wei, L.; Xu, L.; Zhang, L.; Lan, W.; Zhou, C.; She, Y.; Fu, H. A Novel Thioctic Acid-Carbon Dots Fluorescence Sensor for the Detection of Hg^{2+} and Thiophanate Methyl via S-Hg Affinity. *Food Chem.* **2021**, *346*, 128923. [CrossRef] [PubMed]
184. Liu, Q.; Dong, Z.; Hao, A.; Guo, X.; Dong, W. Synthesis of Highly Fluorescent Carbon Dots as a Dual-Excitation Rationmetric Fluorescent Probe for the Fast Detection of Chlorogenic Acid. *Talanta* **2021**, *221*, 121372. [CrossRef] [PubMed]
185. Tang, X.; Yu, H.; Bui, B.; Wang, L.; Xing, C.; Wang, S.; Chen, M.; Hu, Z.; Chen, W. Nitrogen-Doped Fluorescence Carbon Dots as Multi-Mechanism Detection for Iodide and Curcumin in Biological and Food Samples. *Bioact. Mater.* **2021**, *6*, 1541–1554. [CrossRef] [PubMed]
186. Vidya, T.; Anupama, M.; Muhammed, S.; Joseph, J.; Anappara, A.A. Multi-Functional Carbon Dots for Visual Detection of Picric Acid and White-Light Emission. *Mater. Res. Bull.* **2021**, *138*, 111223. [CrossRef]
187. Mu, X.; Wu, M.; Zhang, B.; Liu, X.; Xu, S.; Huang, Y.; Wang, X.; Song, D.; Ma, P.; Sun, Y. A Sensitive "off-on" Carbon Dots-Ag Nanoparticles Fluorescent Probe for Cysteamine Detection via the Inner Filter Effect. *Talanta* **2021**, *221*, 121463. [CrossRef]
188. Zairov, R.R.; Dovzhenko, A.P.; Sarkanich, K.A.; Nizameev, I.R.; Luzhetskiy, A.V.; Sudakova, S.N.; Podyachev, S.N.; Burilov, V.A.; Vatsouro, I.M.; Vomiero, A.; et al. Single Excited Dual Band Luminescent Hybrid Carbon Dots-Terbium Chelate Nanothermometer. *Nanomaterials* **2021**, *11*, 3080. [CrossRef]
189. Yi, Z.; Li, X.; Zhang, H.; Ji, X.; Sun, W.; Yu, Y.; Liu, Y.; Huang, J.; Sarshar, Z.; Sain, M. High Quantum Yield Photoluminescent N-Doped Carbon Dots for Switch Sensing and Imaging. *Talanta* **2021**, *222*, 121663. [CrossRef]
190. Ge, M.; Huang, X.; Ni, J.; Han, Y.; Zhang, C.; Li, S.; Cao, J.; Li, J.; Chen, Z.; Han, S. One-Step Synthesis of Self-Quenching-Resistant Biomass-Based Solid-State Fluorescent Carbon Dots with High Yield for White Lighting Emitting Diodes. *Dye. Pigment.* **2021**, *185*, 108953. [CrossRef]
191. Ma, W.; Wang, B.; Yang, Y.; Li, J. Photoluminescent Chiral Carbon Dots Derived from Glutamine. *Chin. Chem. Lett.* **2021**, *32*, 3916–3920. [CrossRef]
192. Xu, X.; Mo, L.; Li, W.; Li, Y.; Lei, B.; Zhang, X.; Zhuang, J.; Hu, C.; Liu, Y. Red, Green and Blue Aggregation-Induced Emissive Carbon Dots. *Chin. Chem. Lett.* **2021**, *32*, 3927–3930. [CrossRef]
193. Ji, Y.; Zou, X.; Wang, W.; Wang, T.; Zhang, S.; Gong, Z. Co-Doped S, N-Carbon Dots and Its Fluorescent Film Sensors for Rapid Detection of Cr (VI) and Ascorbic Acid. *Microchem. J.* **2021**, *167*, 106284. [CrossRef]
194. Liu, Y.; Chen, P.; Yu, K.; Wu, Z.; Wang, N.; Yu, X. Nitrogen and Sulfur Co-Doped Carbon Dots: Facile Synthesis and Multifunctional Applications for PH Sensing, Temperature Sensing and RNA-Selective Imaging. *Microchem. J.* **2021**, *168*, 106248. [CrossRef]
195. Yang, Z.; Liu, Y.; Lu, C.; Yue, G.; Wang, Y.; Rao, H.; Zhang, W.; Lu, Z.; Wang, X. One-Pot Synthesis of CeO_2-Carbon Dots with Enhanced Peroxidase-like Activity and Carbon Dots for Ratiometric Fluorescence Detection of H_2O_2 and Cholesterol. *J. Alloys Compd.* **2021**, *862*, 158323. [CrossRef]
196. Şen, F.B.; Beğiç, N.; Bener, M.; Apak, R. Fluorescence Turn-off Sensing of TNT by Polyethylenimine Capped Carbon Quantum Dots. *Spectrochim. Acta Part A Mol. Biomol. Spectrosc.* **2022**, *271*, 120884. [CrossRef] [PubMed]
197. Huo, X.; Shen, H.; Xu, Y.; Shao, J.; Liu, R.; Zhang, Z. Fluorescence Properties of Carbon Dots Synthesized by Different Solvents for PH Detector. *Opt. Mater.* **2022**, *123*, 111889. [CrossRef]
198. Wang, Q.; Zheng, H.; Long, Y.; Zhang, L.; Gao, M.; Bai, W. Microwave-Hydrothermal Synthesis of Fluorescent Carbon Dots from Graphite Oxide. *Carbon* **2011**, *49*, 3134–3140. [CrossRef]
199. Liu, R.; Li, H.; Kong, W.; Liu, J.; Liu, Y.; Tong, C.; Zhang, X.; Kang, Z. Ultra-Sensitive and Selective Hg^{2+} Detection Based on Fluorescent Carbon Dots. *Mater. Res. Bull.* **2013**, *48*, 2529–2534. [CrossRef]
200. Shi, J.; Lu, C.; Yan, D.; Ma, L. High Selectivity Sensing of Cobalt in HepG2 Cells Based on Necklace Model Microenvironment-Modulated Carbon Dot-Improved Chemiluminescence in Fenton-like System. *Biosens. Bioelectron.* **2013**, *45*, 58–64. [CrossRef]
201. Xu, Y.; Wu, M.; Feng, X.Z.; Yin, X.B.; He, X.W.; Zhang, Y.K. Reduced Carbon Dots versus Oxidized Carbon Dots: Photo- and Electrochemiluminescence Investigations for Selected Applications. *Chem.-A Eur. J.* **2013**, *19*, 6282–6288. [CrossRef]
202. Dong, X.; Su, Y.; Geng, H.; Li, Z.; Yang, C.; Li, X.; Zhang, Y. Fast One-Step Synthesis of N-Doped Carbon Dots by Pyrolyzing Ethanolamine. *J. Mater. Chem. C* **2014**, *2*, 7477–7481. [CrossRef]
203. Huang, L.; Yang, S.; Chen, L.; Chen, S. Hydrothermal Synthesis of Fluorescent Carbon Dots towards Ion Response and Silk Screen Patterns. *Chem. Lett.* **2015**, *44*, 1251–1253. [CrossRef]
204. Ahmed, G.H.G.; Laíño, R.B.; Calzón, J.A.G.; García, M.E.D. Fluorescent Carbon Nanodots for Sensitive and Selective Detection of Tannic Acid in Wines. *Talanta* **2015**, *132*, 252–257. [CrossRef]

205. Hu, Y.; Yang, J.; Jia, L.; Yu, J.S. Ethanol in Aqueous Hydrogen Peroxide Solution: Hydrothermal Synthesis of Highly Photoluminescent Carbon Dots as Multifunctional Nanosensors. *Carbon* **2015**, *93*, 999–1007. [CrossRef]
206. Zou, W.S.; Ji, Y.J.; Wang, X.F.; Zhao, Q.C.; Zhang, J.; Shao, Q.; Liu, J.; Wang, F.; Wang, Y.Q. Insecticide as a Precursor to Prepare Highly Bright Carbon Dots for Patterns Printing and Bioimaging: A New Pathway for Making Poison Profitable. *Chem. Eng. J.* **2016**, *294*, 323–332. [CrossRef]
207. Wu, Z.; Feng, M.; Chen, X.; Tang, X. N-Dots as a Photoluminescent Probe for the Rapid and Selective Detection of Hg^{2+} and Ag^{+} in Aqueous Solution. *J. Mater. Chem. B* **2016**, *4*, 2086–2089. [CrossRef]
208. Campos, B.B.; Contreras-Cáceres, R.; Bandosz, T.J.; Jiménez-Jiménez, J.; Rodríguez-Castellón, E.; Esteves da Silva, J.C.G.; Algarra, M. Carbon Dots as Fluorescent Sensor for Detection of Explosive Nitrocompounds. *Carbon* **2016**, *106*, 171–178. [CrossRef]
209. Li, H.; Sun, C.; Vijayaraghavan, R.; Zhou, F.; Zhang, X.; MacFarlane, D.R. Long Lifetime Photoluminescence in N, S Co-Doped Carbon Quantum Dots from an Ionic Liquid and Their Applications in Ultrasensitive Detection of Pesticides. *Carbon* **2016**, *104*, 33–39. [CrossRef]
210. Liu, X.; Pang, J.; Xu, F.; Zhang, X. Simple Approach to Synthesize Amino-Functionalized Carbon Dots by Carbonization of Chitosan. *Sci. Rep.* **2016**, *6*, 31100. [CrossRef]
211. Wu, X.; Song, Y.; Yan, X.; Zhu, C.; Ma, Y.; Du, D.; Lin, Y. Carbon Quantum Dots as Fluorescence Resonance Energy Transfer Sensors for Organophosphate Pesticides Determination. *Biosens. Bioelectron.* **2017**, *94*, 292–297. [CrossRef]
212. Wu, P.; Li, W.; Wu, Q.; Liu, Y.; Liu, S. Hydrothermal Synthesis of Nitrogen-Doped Carbon Quantum Dots from Microcrystalline Cellulose for the Detection of Fe^{3+} Ions in an Acidic Environment. *RSC Adv.* **2017**, *7*, 44144–44153. [CrossRef]
213. Mohapatra, S.; Bera, M.K.; Das, R.K. Rapid "Turn-on" Detection of Atrazine Using Highly Luminescent N-Doped Carbon Quantum Dot. *Sens. Actuators B Chem.* **2018**, *263*, 459–468. [CrossRef]
214. Devi, S.; Gupta, R.K.; Paul, A.K.; Tyagi, S. Waste Carbon Paper Derivatized Carbon Quantum Dots/(3- Aminopropyl)Triethoxysilane Based Fluorescent Probe for Trinitrotoluene Detection. *Mater. Res. Express* **2019**, *6*, 1–12. [CrossRef]
215. Feng, Y.; Tan, L.; Tang, Q.; Zhong, W.; Yang, X. Synthesis of Carbon Dots from PEG6000 and Papain for Fluorescent and Doxycycline Sensing. *Nano* **2018**, *13*, 1–9. [CrossRef]
216. Siddique, A.B.; Pramanick, A.K.; Chatterjee, S.; Ray, M. Amorphous Carbon Dots and Their Remarkable Ability to Detect 2,4,6-Trinitrophenol. *Sci. Rep.* **2018**, *8*, 9770. [CrossRef]
217. Zhao, D.; Liu, X.; Wei, C.; Qu, Y.; Xiao, X.; Cheng, H. One-Step Synthesis of Red-Emitting Carbon Dots: Via a Solvothermal Method and Its Application in the Detection of Methylene Blue. *RSC Adv.* **2019**, *9*, 29533–29540. [CrossRef]
218. Fang, J.; Zhuo, S.; Zhu, C. Fluorescent Sensing Platform for the Detection of P-Nitrophenol Based on Cu-Doped Carbon Dots. *Opt. Mater.* **2019**, *97*, 109396. [CrossRef]
219. Xu, Y.; Yan, L.; Yue, M.; Yu, Y. Green Hydrothermal Synthesis of Fluorescent Carbon Dots from Glucose and Taurine for Fe^{3+} and PH Sensing. *Nano* **2019**, *14*, 1950014. [CrossRef]
220. Gogoi, J.; Chowdhury, D. Calcium-Modified Carbon Dots Derived from Polyethylene Glycol: Fluorescence-Based Detection of Trifluralin Herbicide. *J. Mater. Sci.* **2020**, *55*, 11597–11608. [CrossRef]
221. Saravanan, A.; Maruthapandi, M.; Das, P.; Ganguly, S.; Margel, S.; Luong, J.H.T.; Gedanken, A. Applications of N-Doped Carbon Dots as Antimicrobial Agents, Antibiotic Carriers, and Selective Fluorescent Probes for Nitro Explosives. *ACS Appl. Bio Mater.* **2020**, *3*, 8023–8031. [CrossRef]
222. Tammina, S.K.; Yang, Y. Highly Sensitive and Selective Detection of 4-Nitrophenol, and on-off-on Fluorescence Sensor for Cr (VI) and Ascorbic Acid Detection by Glucosamine Derived n-Doped Carbon Dots. *J. Photochem. Photobiol. A Chem.* **2020**, *387*, 112134. [CrossRef]
223. Houdová, D.; Soto, J.; Castro, R.; Rodrigues, J.; Soledad Pino-González, M.; Petković, M.; Bandosz, T.J.; Algarra, M. Chemically Heterogeneous Carbon Dots Enhanced Cholesterol Detection by MALDI TOF Mass Spectrometry. *J. Colloid Interface Sci.* **2021**, *591*, 373–383. [CrossRef] [PubMed]
224. Hu, Y.; Gao, Z.; Luo, J. Fluorescence Detection of Malachite Green in Fish Tissue Using Red Emissive Se,N,Cl-Doped Carbon Dots. *Food Chem.* **2021**, *335*, 127677. [CrossRef] [PubMed]
225. Mohammadi, S.; Mohammadi, S.; Salimi, A. A 3D Hydrogel Based on Chitosan and Carbon Dots for Sensitive Fluorescence Detection of MicroRNA-21 in Breast Cancer Cells. *Talanta* **2021**, *224*, 121895. [CrossRef] [PubMed]
226. Liu, Q.; Zhao, F.; Shi, B.; Changli, L. Mussel-Inspired Polydopamine-Encapsulated Carbon Dots with Dual Emission for Detection of 4-Nitrophenol and Fe^{3+}. *Luminescence* **2021**, *36*, 431–442. [CrossRef]
227. Bisauriya, R.; Antonaroli, S.; Ardini, M.; Angelucci, F.; Ricci, A.; Pizzoferrato, R. Tuning the Sensing Properties of N and S Co-Doped Carbon Dots for Colorimetric Detection of Copper and Cobalt in Water. *Sensors* **2022**, *22*, 2487. [CrossRef]
228. Ezati, P.; Rhim, J.W.; Molaei, R.; Priyadarshi, R.; Roy, S.; Min, S.; Kim, Y.H.; Lee, S.G.; Han, S. Preparation and Characterization of B, S, and N-Doped Glucose Carbon Dots: Antibacterial, Antifungal, and Antioxidant Activity. *Sustain. Mater. Technol.* **2022**, *32*, e00397. [CrossRef]
229. Kong, B.; Yang, T.; Cheng, F.; Qian, Y.; Li, C.; Zhan, L.; Li, Y.; Zou, H.; Huang, C. Carbon Dots as Nanocatalytic Medicine for Anti-Inflammation Therapy. *J. Colloid Interface Sci.* **2022**, *611*, 545–553. [CrossRef]
230. Zhu, X.; Han, L.; Liu, H.; Sun, B. A Smartphone-Based Ratiometric Fluorescent Sensing System for on-Site Detection of Pyrethroids by Using Blue-Green Dual-Emission Carbon Dots. *Food Chem.* **2022**, *379*, 132154. [CrossRef]

231. Fen, Y.W.; Yunus, W.M.M.; Yusof, N.A. Surface Plasmon Resonance Optical Sensor for Detection of Pb^{2+} Based on Immobilized P-Tert-Butylcalix[4]Arene-Tetrakis in Chitosan Thin Film as an Active Layer. *Sens. Actuators B Chem.* **2012**, *171*, 287–293. [CrossRef]
232. Daniyal, W.M.E.M.M.; Fen, Y.W.; Abdullah, J.; Sadrolhosseini, A.R.; Saleviter, S.; Omar, N.A.S. Exploration of Surface Plasmon Resonance for Sensing Copper Ion Based on Nanocrystalline Cellulose-Modified Thin Film. *Opt. Express* **2018**, *26*, 34880. [CrossRef]
233. Anas, N.A.A.; Fen, Y.W.; Omar, N.A.S.; Ramdzan, N.S.M.; Daniyal, W.M.E.M.M.; Saleviter, S.; Zainudin, A.A. Optical Properties of Chitosan/Hydroxyl-Functionalized Graphene Quantum Dots Thin Film for Potential Optical Detection of Ferric (III) Ion. *Opt. Laser Technol.* **2019**, *120*, 105724. [CrossRef]
234. Daniyal, W.M.E.M.M.; Fen, Y.W.; Anas, N.A.A.; Omar, N.A.S.; Ramdzan, N.S.M.; Nakajima, H.; Mahdi, M.A. Enhancing the Sensitivity of a Surface Plasmon Resonance-Based Optical Sensor for Zinc Ion Detection by the Modification of a Gold Thin Film. *RSC Adv.* **2019**, *9*, 41729–41736. [CrossRef] [PubMed]
235. Ramdzan, N.S.M.; Fen, Y.W.; Omar, N.A.S.; Anas, N.A.A.; Liew, J.Y.C.; Daniyal, W.M.E.M.M.; Hashim, H.S. Detection of Mercury Ion Using Surface Plasmon Resonance Spectroscopy Based on Nanocrystalline Cellulose/Poly(3,4-Ethylenedioxythiophene) Thin Film. *Measurement* **2021**, *182*, 109728. [CrossRef]
236. Omar, N.A.S.; Irmawati, R.; Fen, Y.W.; Abdullah, J.; Daud, N.F.M.; Daniyal, W.M.E.M.M.; Mahdi, M.A. A Sensing Approach for Manganese Ion Detection by Carbon Dots Nanocomposite Thin Film-based Surface Plasmon Resonance Sensor. *Optik* **2021**, *243*, 167435. [CrossRef]
237. Mustapha Kamil, Y.; Al-Rekabi, S.H.; Abu Bakar, M.H.; Fen, Y.W.; Mohammed, H.A.; Halip, N.H.M.; Alresheedi, M.T.; Mahdi, M.A. Arsenic Detection Using Surface Plasmon Resonance Sensor with Hydrous Ferric Oxide Layer. *Photonic Sens.* **2021**, *12*, 220306. [CrossRef]
238. Gonçalves, H.M.R.; Duarte, A.J.; Esteves da Silva, J.C.G. Optical Fiber Sensor for Hg(II) Based on Carbon Dots. *Biosens. Bioelectron.* **2010**, *26*, 1302–1306. [CrossRef]
239. Sun, X.; Li, G.; Yin, Y.; Zhang, Y.; Li, H. Carbon Quantum Dot-Based Fluorescent Vesicles and Chiral Hydrogels with Biosurfactant and Biocompatible Small Molecule. *Soft Matter* **2018**, *14*, 6983–6993. [CrossRef]
240. Wang, X.; Guo, H.; Wu, N.; Xu, M.; Zhang, L.; Yang, W. A Dual-Emission Fluorescence Sensor Constructed by Encapsulating Double Carbon Dots in Zeolite Imidazole Frameworks for Sensing Pb^{2+}. *Colloids Surf. A Physicochem. Eng. Asp.* **2021**, *615*, 126218. [CrossRef]
241. Jia, M.; Peng, L.; Yang, M.; Wei, H.; Zhang, M.; Wang, Y. Carbon Dots with Dual Emission: A Versatile Sensing Platform for Rapid Assay of Cr (VI). *Carbon* **2021**, *182*, 42–50. [CrossRef]
242. Hashim, H.S.; Fen, Y.W.; Omar, N.A.S.; Fauzi, N.I.M.; Daniyal, W.M.E.M.M. Recent Advances of Priority Phenolic Compounds Detection Using Phenol Oxidases-Based Electrochemical and Optical Sensors. *Meas. J. Int. Meas. Confed.* **2021**, *184*, 109855. [CrossRef]
243. Babar, D.G.; Garje, S.S. Nitrogen and Phosphorus Co-Doped Carbon Dots for Selective Detection of Nitro Explosives. *ACS Omega* **2020**, *5*, 2710–2717. [CrossRef] [PubMed]
244. Fauzi, N.I.M.; Fen, Y.W.; Omar, N.A.S.; Hashim, H.S. Recent Advances on Detection of Insecticides Using Optical Sensors. *Sensors* **2021**, *21*, 3856. [CrossRef] [PubMed]
245. Hou, J.; Dong, G.; Tian, Z.; Lu, J.; Wang, Q.; Ai, S.; Wang, M. A Sensitive Fluorescent Sensor for Selective Determination of Dichlorvos Based on the Recovered Fluorescence of Carbon Dots-Cu(II) System. *Food Chem.* **2016**, *202*, 81–87. [CrossRef] [PubMed]
246. Mandal, P.; Sahoo, D.; Sarkar, P.; Chakraborty, K.; Das, S. Fluorescence Turn-on and Turn-off Sensing of Pesticides by Carbon Dot-Based Sensor. *New J. Chem.* **2019**, *43*, 12137–12151. [CrossRef]
247. Bera, M.K.; Behera, L.; Mohapatra, S. A Fluorescence Turn-down-up Detection of Cu^{2+} and Pesticide Quinalphos Using Carbon Quantum Dot Integrated UiO-66-NH_2. *Colloids Surf. A Physicochem. Eng. Asp.* **2021**, *624*, 126792. [CrossRef]
248. Liu, Y.; Zhou, Q.; Wu, Y.; Li, S.; Sun, Y.; Sheng, X.; Zhan, Y.; Zhao, J.; Guo, J.; Zhou, B. Sensitive Detection of 2,4,6-Trinitrotoluene Utilizing Fluorescent Sensor from Carbon Dots and Reusable Magnetic Core-Shell Nanomaterial. *Talanta* **2021**, *233*, 122498. [CrossRef]